Scientific report; WR 2004-01

KNMI

Seismic hazard due to small shallow induced earthquakes

Torild van Eck, Femke Goutbeek, Hein Haak and Bernard Dost

Koninklijk Nederlands Meteorologisch Instituut

De Bilt, 2004

Scientific report = wetenschappelijk rapport; WR 2004-01

De Bilt, 2004

PO Box 201
3730 AE De Bilt
Wilhelminalaan 10
De Bilt
The Netherlands
http://www.knmi.nl
Telephone +31(0)30-220 69 11
Telefax +31(0)30-221 04 07

Authors: Torild van Eck, Femke Goutbeek,Hein Haak and Bernard Dost

UDC: 550.34

ISSN: 0169-1651

ISBN: 90-369-2248-8

Seismic hazard due to small shallow induced earthquakes

Torild van Eck, Femke Goutbeek, Hein Haak, Bernard Dost

Seismology Division KNMI

Content:

Summary

We present the basic methodology for a Probabilistic Seismic Hazard Analysis (PSHA) applied to small and shallow earthquakes, i.e. $1.5 < M_L < 3.9$ and depth < 4 km, in The Netherlands. Such small shallow earthquakes occur as induced events due to gas exploitation, mainly in the north of The Netherlands. Few studies have applied a PSHA for small and shallow events and we indicate some specific complications. Most important is that relatively high Peak Ground Accelerations (PGA) are predicted and observed. PGA above 0.2g is not unusual, but damage is mostly restricted to cracks in masonry. The Peak Ground Velocity (PGV) is a more appropriate hazard parameter. Observed response spectra show a fairly stable peak around 10 Hz and are, consequently, used in the specified velocity hazard parameter. We predict that, for response spectra with 50% damping, peak values up to 20 and 30 mm/sec may be exceeded with an annual probability of 0.1 and 0.01 respectively above the Groningen field. In some small areas (about 3-4 km^2) above the Roswinkel and Bergermeer field values around 35 and 60 mm/sec may be exceeded with an annual probability of 0.1 and 0.01 respectively. For response spectra with 5% damping, the corresponding peak values may reach 50 and 80 mm/sec, and 85 and 140 mm/sec. These values, which do not include possible site-specific effects, can be related to the existing vibration guidelines in use in The Netherlands.

For the three regions, where regular induced seismicity is observed, we have computed tentative hazard maps for return periods of 10 and 100 years, i.e. around Roswinkel, Bergermeer and Groningen. These hazard maps do not include the influence of specific site responses. Also a more general model has been computed under the assumption that seismicity is an inevitable consequence of gas exploitation, but that additional models, explaining the physical relation between gas extraction and seismicity, are lacking. In all our hazard models we find significant uncertainties. Some of these uncertainties may be constrained with additional information, like for example: refining local attenuation relations, relating seismicity to specific faults, including exploitation-seismicity relations, a priory focal mechanism information, etc. Other uncertainties, mostly related to the attenuation will remain. The inherent non-stationary character of induced seismicity can yet not been modeled.

Continuous monitoring of seismic activity shows that the seismic hazard due to induced seismicity remained stable during the last five years. The introduction of a systematic hazard estimation methodology may be appropriate for fields with clearly defined seismicity, but in other cases it requires additional information in order to be valuable for pragmatic purposes. However, the systematic quantitative methodology of a PSHA is an excellent tool to clarify crucial knowledge gaps and helps, consequently, to define additional research priorities. Hereby the continuous and improved monitoring provides, with the geophysical data from the exploited reservoirs, the essential database. Improved hazard estimates may be obtained by investigating statistical correlation of mechanical parameters with seismicity, attenuation and site response models, possible favored earthquake mechanism and, for the long-term, microearthquakes ($M < -3$) and their relation to small earthquakes ($1.5 < M < 3.9$).

1. Introduction

Earthquakes in the north of The Netherlands induced by the exploitation of gas fields have occasionally caused damage (Dost and Haak, 1997; Haak et al., 2001). This has been of concern to the regional population and the Dutch government. As a consequence, the new mining legislation requires from January 1, 2004 a hazard analysis for each new exploitation license (Staatsblad, 2002).

In this report we present a pragmatic approach to the analysis of seismic hazard due to small and shallow earthquakes ($1.5 < M < 3.5$) as a guideline for meeting the requirements of the new legislation. The rapid enforcement of the new legislation leaves little time to test new hypotheses that may improve our hazard estimates. Therefore, our report is based on our current knowledge, but indicates promising research directions for improving current hazard estimates. We have chosen an approach that uses internationally established robust methods and assumes, in lack of better evidence, the simplest models. More complex models, although tantalizing, are at present not realistic due to the high degree of uncertainties that are still involved. We would like to emphasize that a hazard analysis for induced seismicity in the north of The Netherlands, i.e. small and shallow events, poses some interesting new problems that are not usually considered in general seismic hazard analysis. Obviously, characterizing non-stationary seismicity related to gas exploitation is one of these problems.

We aim at a clear and transparent logic for estimating the seismic hazard and use suitable analytical tools to accomplish this. Specifically, we follow the intention of the new legislation. Therefore, intensive discussions with all directly involved parties have accompanied our study. However, we clearly emphasize that this report does not attempt at a cost-benefit analysis. Such a comprehensive risk analysis requires a much broader treatment of the problem. In fact, specific risk concerns (economical and/or social) may very well influence the fundamental assumptions used in estimating the seismic hazard.

Finally, a short note on the terminology used. We follow the international terminology for seismic hazard and seismic risk. *Seismic hazard* is the probability that a certain level of (strong/weak) ground motion due to earthquakes will be exceeded within a specific time period at a specific site. *Seismic risk* is the combination of the seismic hazard and the vulnerability of a construction, economical consequences, etc and quantifies the probability of the financial and/or social consequences. In other words:

*Seismic risk = seismic hazard * vulnerability [* cost* exposure]*

Cost can be defined in the broadest sense of the word including both economical and social concerns. A cost-benefit analysis can, for example, only be done on the basis of seismic risk, not on the basis of seismic hazard alone. We restrict ourselves to the general approach of a seismic hazard analysis and only when relevant do we include some risk elements. Terminology is further summarized in a glossary (Appendix 1). For further details we refer to Reiter (1990), which gives a clear and broad overview of seismic hazard analysis, Lomnitz (1974), which presents the involved statistical models more in depth, and Chen and Scawthorn (2003), who provide an extensive overview of the engineering aspects.

2. Basic approach

The hazard analysis we present is based on some basic constraints and assumptions summarized below:

Model constraints.
We put the following constraints on our methodology:

1. It should not deviate much from internationally accepted practices and
2. It should reflect, as accurately as possible, the state-of-the-art knowledge for induced earthquakes in the north of The Netherlands

Fundamental assumption.
We start out with some fundamental assumptions:

- Seismicity in the north of The Netherlands as observed since 1986 can be classified as induced seismicity due to gas exploitation (BOA, 1993) and is not related to tectonic movements.
- We know there is a probability of seismicity due to hydrocarbon exploitation (BOA, 1993; De Crook et al., 1997). Currently, however, we have neither a physical model explaining why we observe induced earthquakes at some fields and not at others, nor a general validated quantitative physical model for the causal relation between exploitation and seismicity.

The last assumption deserves some explanation. Induced seismicity, as observed in The Netherlands, is extensively studied in order to find one or more causal relations between exploitation and the occurrence of seismicity. Consequently a number of hypothesis relating to specific fields have been presented (Alkmaar field, Logan and Rudnicki, 1994; Bergermeer field, Logan et al., 1997, Roest and Mulder, 2000; Eleveld, Roest and Kuilman, 1993,1994; Roswinkel, van Eijs, 1999; Norg field, Nagelhout and Roest, 1997). So far we are unable to obtain quantitative models that predict the occurrence or non-occurrence of seismic events in a field, given specific physical conditions like reservoir pressure or pressure gradients. Segall et al. (1994), however, suggested that this may be possible. They show a correlation between the predicted seismicity and the observed seismicity using a poroelastic stressing model for the Lacq gas field in France. A more general, but preliminary, study of van Eijs and Scheffers (2000) comparing exploitation data with the occurrence of seismicity suggests some qualitative relations.

We further assume, as Grasso and Sornette (1998), that induced seismicity behaves as natural seismicity, i.e. most probably as chaotic phenomena (Main, 1996).

These assumptions may be too stringent or too conservative. Therefore we also discuss the uncertainties introduced by our lack of knowledge of the modeling parameters in the seismic hazard due to induced seismicity or the so-called epistemic uncertainty.

Applied basic seismicity model.
With the above constraints and assumptions the most plausible hypothesis is a simple seismicity model in which induced earthquakes occur as a stationary process randomly distributed over an area equal to the surface projection of all gas fields in production in the north of The Netherlands. The frequency-magnitude relation obtained from the observed seismicity in the period December 1986 – mid-October 2003 serves as our model characterizing future seismicity. When possible we consider more local information to characterize our models. Therefore, a few areas are discussed in more detail.

As we anticipate to obtain new knowledge about the induced seismicity, its statistics, ground motion characteristics and the causal relations between exploitation and the occurrence of earthquakes, we propose a systematic approach for making the appropriate improvements in the seismic hazard analysis.

3. Methodology

A seismic hazard analysis assumes models that describe where the seismicity occurs, i.e. seismicity zonation, the statistical description of this seismicity, i.e. seismicity characteristics, and the ground motion damping between source and site. The ground motion effect can be divided up in a general attenuation relation and a specific site response effect. The site response describes specifically the damping and/or amplification of the uppermost 10-30 meters at a site and may be significant at places where low seismic velocities are combined with high seismic velocity contrasts specifically in the upper 10-30 meters. The attenuation, or ground motion prediction equation, is an empirical relation describing the wave amplitude damping from source to usually an average surface condition.

Out of the several approaches (see Bommer, 2002 for a recent discussion on the subject) we have chosen a probabilistic seismic hazard analysis (PSHA) where we estimate the combined probabilistic hazard, i.e. ground motion at the surface due to the occurrence of earthquakes in the range between $2.5 < M_L < 3.5$.

We also include an additional step, the response spectrum (Gupta, 1990). A response spectrum translates the ground motion to a motion of a one-degree-of-freedom damped system and provides a first order estimate of the ground motion effect on surface structures and building elements. In Figure 1 we illustrate these different elements in the seismic hazard analysis together with one possible way of presenting the results; the seismic hazard as the annual probability that a specific peak ground acceleration, or velocity, will be exceeded at a specific site.

The general methodology of a probabilistic seismic hazard is presented below.

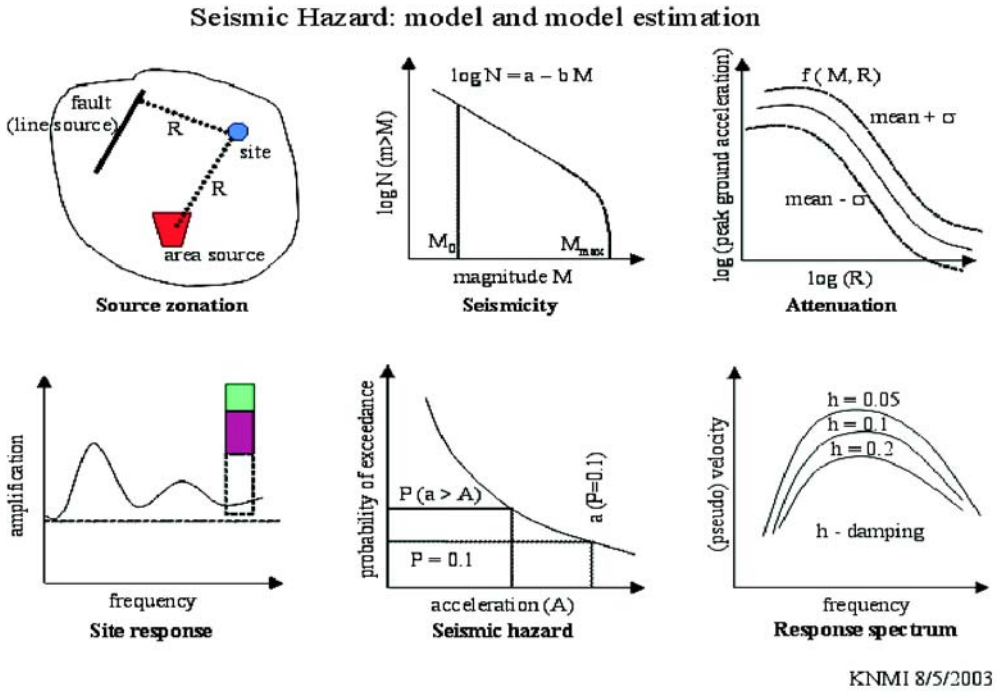

Figure 1. *Schematic overview describing the different elements in the Probabilistic Seismic Hazard Analysis as proposed. From left to right and top to bottom: The seismic zonation models, the statistic seismicity model, the empirical attenuation function, the site response and the seismic hazard expressed as the probability that a certain peak ground acceleration, or alternatively peak ground velocity, will be exceeded, finally an alternative way of providing more details on the expected ground motion using the "response spectrum".*

3.1 Point source probabilistic hazard model

A point source approach assumes that all seismicity occurs at one point. The probabilistic hazard can then be expressed as the integration of two distributions: 1) the magnitude-frequency distribution, *f (M)* describing the frequency of occurrence of events with magnitude M, and 2) the conditional probability function, *P (A>a | m,r)*, i.e. the probability that for a given magnitude *m* and distance *r* the acceleration *a* will be exceeded. Then, *P* [*A* > *a*|*r*] gives the probability that the ground acceleration, *A* at distance *r*, will exceed a specific value *a* due to any earthquake in the given point source or:

$$P[A > a|r] = \lambda \int_{M_0}^{M_{\max}} f(m) \cdot P(A > a|m,r) dm \qquad \text{eq. 1}$$

Here λ is a scaling factor representing the mean seismicity rate. We assume here implicitly that the seismicity is stationary. *M* is the local magnitude, M_L (De Crook et al., 1998), except when specifically defined otherwise.

3.2 Probabilistic Seismic Hazard model

The more general approach originally, proposed by Cornell and Merz (1975) and described in detail in Cornell (1968), is the Probabilistic Seismic Hazard Analysis (PSHA). Now we assume that all earthquakes do not occur only at one point, but are randomly distributed in a specified seismic zone. Consequently, we integrate over the area. The probability that a ground acceleration *a* will be exceeded, i.e. *P [A > a]*, can than be expressed as:

$$P[A > a] = \sum_{i=1}^{N} \lambda_i \int_0^{\infty M_{\max}} \int_{M_0} f_i(m) \cdot g_i(r) \cdot P(A > a \mid m,r) dm dr \qquad \text{eq. 2}$$

We added a third probability density function, $g_i(r)$, characterizing the probability that an event occurs at a distance, r, from the site. Equation 2 gives then for one specific site the probability, *P* [*A* > *a*], obtained by summing the hazard due to all different seismogenic zones, *i*.

The frequency-magnitude distribution.
For a specific region the empirical frequency-magnitude relation, log N(M) = a – bM , which describes the number of earthquakes N(M) that occur above a certain magnitude M, as decreasing exponentially with magnitude. This empirical relation may be slightly modified into a truncated exponential distribution to obtain a useful statistical frequency-magnitude description.

An exponential cumulative distribution *F (M)*,

$$F(M) = \int_{M}^{M_{\max}} f(m) dm \qquad \text{eq. 3}$$

may be found with an exponential density distribution *f(M)*,

$$f(M) = \alpha e^{-\beta M}$$

where both α and β are constants. The exponential decrease of the number of events, β, is related to the b-value as $\beta = b \ln 10$, where *ln 10* is the natural logarithm of 10.

Earthquake hazard is only relevant for earthquakes with magnitudes exceeding a certain minimum magnitude, M_0. For each region also an upper magnitude limit exists, i.e. M_{max}. Consequently, we consider an exponential distribution valid only for earthquakes within the magnitude range $M_0 \leq M \leq M_{max}$. The normalized frequency-magnitude distribution, *f (M)*, can then be written as:

$$f(M) = \left(\frac{\beta}{1 - e^{-\beta(M_{max} - M_0)}} \right) e^{-\beta(M - M_0)} \qquad \text{eq. 4}$$

The first term in equation 4 is a constant, normalizing the density distribution.

Substituting equation 4 in equation 3 we obtain the truncated cumulative frequency-magnitude distribution:

$$F(M) = \frac{e^{\beta M_0}}{1 - e^{-\beta(M_{max} - M_0)}} \left(e^{-\beta M} - e^{-\beta M_{max}} \right) \qquad \text{eq. 5}$$

For magnitudes reaching small values as compared to M_{max} , the upper bound truncation effect becomes negligible. Equation 5 approaches then the exponential distribution which, scaled with the average rate of seismicity λ, can be written as the empirical cumulative frequency-magnitude relation: log N(M) = a – bM. Here $N(M) = \lambda F(M)$.

The average seismicity rate.
The average seismicity rate, λ, is the annual rate of occurrence of events with magnitude $M > M_o$, that is $N (M = M_o)$. In our model we assume that earthquakes behave as a Poisson process, i.e. the earthquakes occur sequentially and independently from each other, and λ is stationary. Then the number of events, n, that are expected to occur within a unit of time (say a year) is:

$$g(n) = \frac{\lambda^n}{n!} e^{-\lambda} \qquad \text{eq. 6}$$

The spatial distribution of seismicity.
The distance distribution function, $g (r)$, depends on each site and source combination. We assume that the seismicity is uniformly distributed over a defined (areal) source zone and at a constant depth level of about 2.5 km, about the level where exploitation occurs.

The attenuation relation.
The conditional probability, $P(A > a \mid m,r)$, is the attenuation relation or ground motion prediction equation. Usually this is an empirical relation obtained for the specific ground motion parameter one is interested, often the Peak Ground Acceleration (PGA) or the Peak Ground Velocity (PGV), but also amplitudes at specific frequencies of the Response Spectra can be predicted in this form.

Site response.
The empirical attenuation relation generally provides an average ground motion estimate without a specific site response. Consequently, sites with significant damping or resonance require a (site) specific correction. Usually this concerns sites underlain by shallow low velocity layers with sharp contrasts in seismic velocities in the upper 10-30 meters. This correction is not included in the equations 1 and 2, but is treated separately by Wassing et al. (2003, 2004).

Frequency dependent ground motion amplitude.
The ground motion as observed at the surface due to earthquakes varies with frequency. In general terms, the PGA represents mostly the high-frequency part of the signal, while the PGV represent mostly the medium range frequency part of the signal. A more complete characterization is given by the (response) spectra.

This is used in the standard Eurocode-8 (CEN, 2002), which is mainly based on the ground motion characterization in terms of acceleration and which is mainly used for earthquake engineering design. The code is internationally accepted in both Europe and America (Dobry et al., 2000). It provides standardized site correction factors in which different soils are defined according to their seismic velocities and the underlying harder rock. An advantage of this method is that it is standardized and internationally used. An important disadvantage is that damage and accelerations due to small and shallow induced events do not compare well with those due to large earthquakes. Van Staalduinen and Geurts (1998) proposed local modifications of the Eurocode-8 with specific response spectra designed for induced earthquakes in the north of The Netherlands. This solution disregards the advantage of

international standardization and does not make the Eurocode-8 more appropriate to describe hazard due to small and shallow earthquakes.

An alternative is to use ground velocity characterization of the ground motion. The advantage of this method is that the results can be related to the Dutch SBR-guidelines for damage to buildings due to vibrations (SBR, 2002). Consequently, other local practices can be more easily related to ground motion due to small and shallow earthquakes. A disadvantage may be its international diversity of excepted codes (Van Staalduinen and Geurts, 1998). Also the SBR-guidelines are frequency specific. We prefer the velocity characterization of the ground motion due to small and shallow earthquakes.

Seismic hazard calculations

Equation 2 estimates the seismic hazard as the probability that a ground motion A at site S will be exceeded during a time period, i.e. return period, T (years). This gives an annual probability of 1/T. Seismic hazard due to natural earthquakes is generally presented as the probability that a PGA will be exceeded in 475 years. An alternative interpretation is a 10% probability that this PGA will be exceeded in 50 years (GSHAP, 2001).

As the duration of the gas production is usually much less then 475 or even 50 years we have chosen for this report to consider T = 100 years and T = 10 years, or 10% probability of exceedance in 10 years and 10% probability of exceedance in one year respectively.

The hazard for a specific site is then estimated by a numerical integration of the integral in equation 2. **A** number of programs have been developed over time to do this. EQRISK (McGuire, 1976), FRISK (McGuire, 1978), SEISRISK (Bender and Perkins, 1987) are some examples. Our calculations have been done with a modified version of EQRISK. A detailed description of the methodology and its algorithm can be found in Cornell (1968) and McGuire (1976).

3.3 Specifics for small and shallow earthquakes

The current KNMI monitoring network, consisting of borehole seismometers, surface installed seismometers and accelerometers has been recording induced events with magnitudes $-0.8 < M < 3.5$ (Dost and Haak, 2004) in the north of The Netherlands. The observations can be considered complete for $M \geq 1.5$ since 1996 (De Crook et al., 1998). The observed induced seismicity has specific characteristics, which make a seismic hazard analysis for these events distinctly different from a seismic hazard analysis for natural, i.e. tectonic, events. Here we discuss these differences and its implications on our work.

First, all observed seismicity in the north of The Netherlands (Figure 2) that has been recorded with the instrumentation installed after 1986 occurs at a 'shallow' depth as compared to tectonic events. Most events are located around a depth of 2.5 km ± 0.5 km and no events have occurred at depths larger then 4 km (De Crook et al., 1998 and Appendix 4). All events, with very few exceptions, have so far been located in or around exploited gasfields and we have no evidence of seismicity in the region from the time before the gas exploitation started. Therefore, we assume that the seismicity is induced due to gas exploitation. Others corroborate the existence of induced seismicity due to gas exploitation (Grasso, 1992; Grasso et al., 1994; Segall and Fitzgerald, 1998).

Second, these shallow, but small events cause relatively large peak ground accelerations (PGA) as predicted by McGarr (1984). On February 19, 1997, for example, we recorded a PGA of 0.31g (Figure 3) for a $M_L = 3.4$ event at around 3 km hypocentral distance from the source in the Roswinkel exploitation field in northeastern Netherlands. Up till the end of 2003 the KNMI recorded 22 events ($0.8 < M_L < 3.4$) on accelerometers installed in the north The Netherlands with PGA ranging from 2 cm/sec^2 – 304cm/sec^2 (0.31g) at hypocentral distances $2.0 < r < 2.8$ km (Dost et al., 2004). Large PGA's for small, shallow earthquakes are also observed elsewhere (Fletcher et al., 1983; McGarr and Bicknell, 1990; Ahorner, 1997 personal communication, Wu et al., 2003). Although a PGA of 0.31g is large, it is also of a short duration, essentially only one cycle. This is significant for engineering applications: a short strong pulse has different engineering implications as an acceleration sequence of several cycles duration. Schenk et al. (1990), van Staalduinen and Geurts (1998) and others found that in such cases the PGV correlates better with damage statistics than the PGA.

Third, induced events have, most probably, a maximum size. As the seismicity is related to the exploitation and existing faults it seems plausible that the maximum probable earthquake will also be related to the maximum possible rupture plane. Using this argumentation Logan et al. (1997) found a maximum $M_w = 3.8$ or, with less conservative assumptions, $M_w = 3.6$, as De Crook et al. (1995), for the Bergermeer field. For the Groningen field De Crook et al. (1995) estimated $M_w = 3.5$ as the maximum. So far the largest observed event in the north of The Netherlands, $M_L = 3.5$, occurred in the Bergermeer field 9/9/2001. De Crook et al. (1998) also estimated M_{max} using the statistics of the observed seismicity up till 1998. Assuming uncertainties in both the magnitude estimate and the numbers of observed events they found a maximum (with about 84% probability) size event of $M_L = 3.8$.

Fourth, implicitly we assume that exploitation is not triggering existing tectonic fault instabilities. This last assumption is very likely, as a) there is no historical evidence of tectonic earthquakes in north of The Netherlands (Houtgast, 1992), b) no faults in the north of The Netherlands seem connected to active faults and c) so far, observed earthquakes in the region occur at the top of the seismogenic zone of the crust and are therefore unlikely to trigger larger events that rupture deeper parts of the seismogenic zone (Scholtz, 2002).

In summary, in the north of The Netherlands only small ($M < 3.5$), shallow (< 4 km) induced earthquakes have been observed causing relatively large accelerations (up to 0.31g) and light damage, mostly cracks in masonry. The maximum observed intensity of VI occurred in the direct vicinity of the epicenter of a few events (Dost and Haak, 1997; Haak et al., 2001). For this kind of seismicity the PGV correlates most probably better with damage statistics than the PGA.

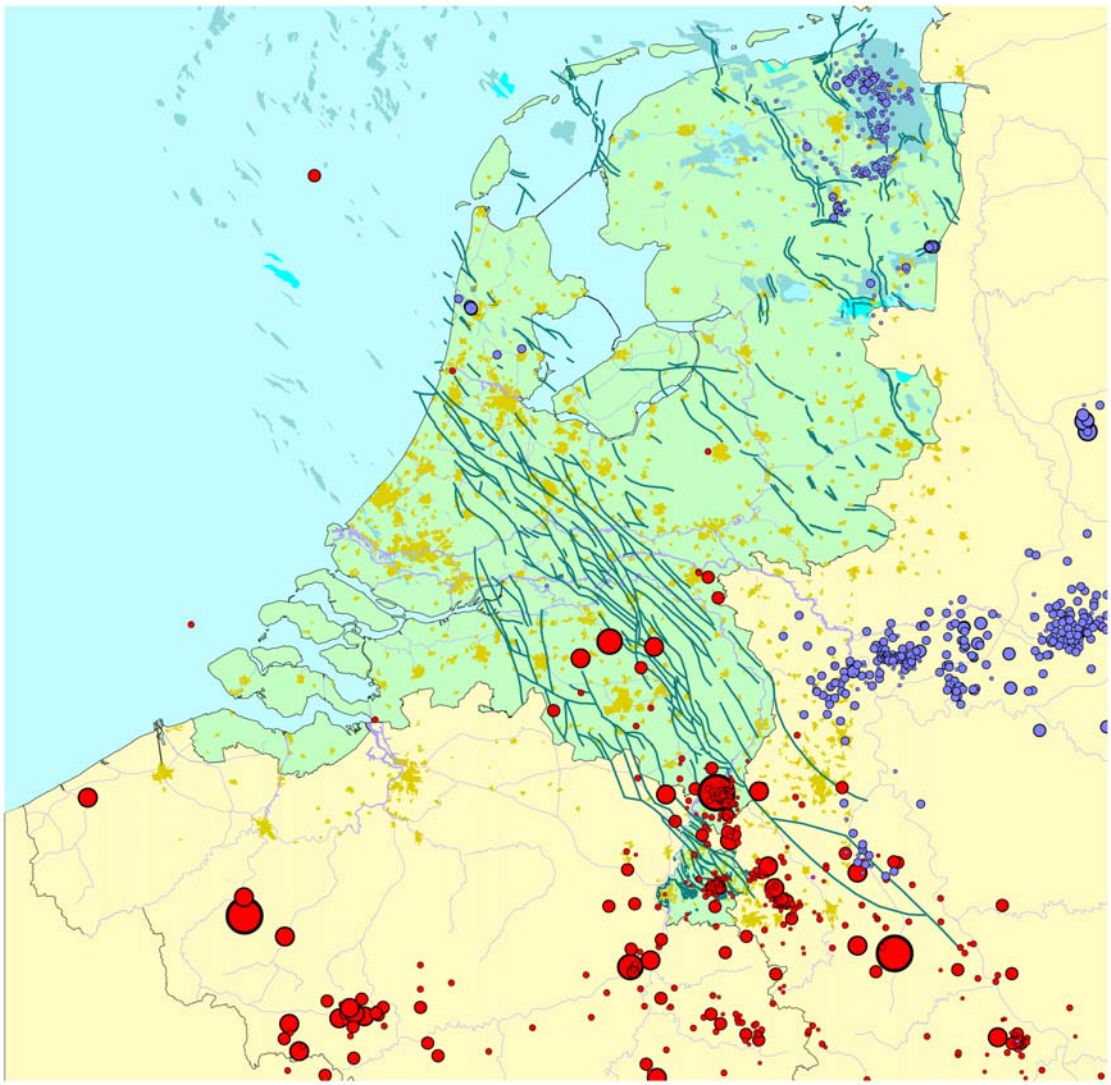

***Figure 2**. General overview over the seismicity in The Netherlands and its immediate surroundings since 1900 (source: KNMI). Red circles indicate earthquakes due to inherent movements in the crust. Blue circles indicate earthquakes caused by man-made activities, as classified by the KNMI, usually mining or gas exploitation. The earthquakes are scaled according to magnitude. Darkgreen solid lines indicate mapped faults in the upper-north-sea according to the NITG.*

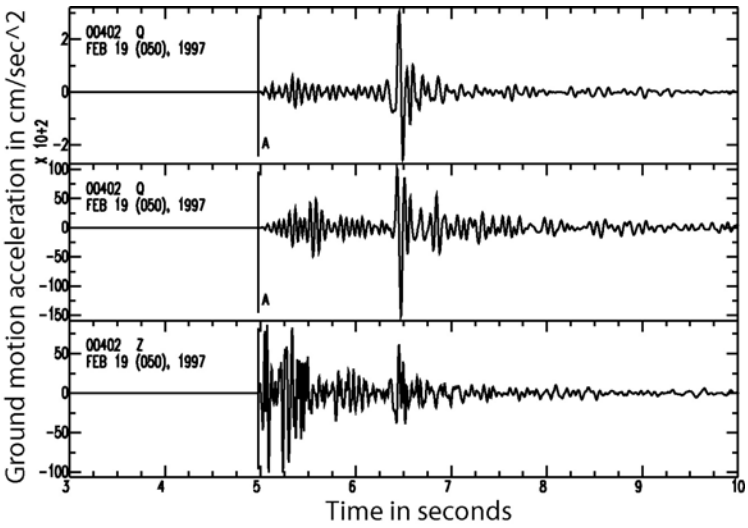

Figure 3. *The ground acceleration as observed by the KNMI at about 2 km epicentral distance of an M_L = 3.4 earthquake near Roswinkel on 19/2/1997. The figure depicts the radial(top), transverse(bottom) and vertical component (Z) respectively. The time is given in seconds, the ground acceleration amplitude in cm/sec^2 this is approximately equal to 1/1000 of g (gravity, g = 9,8 m/s^2). Note specifically the large S-wave pulse in the radial and transverse components. This registration is typical for shallow, small (induced) earthquakes. The vertical component with relatively high frequency and no S-waves, the horizontal components with essentially one large peak representing one cycle of an 8-10 Hz pulse.*

4. PSHA model parameters and the Logic Tree Approach

In this section we introduce the specific model parameters used in the probabilistic seismic hazard analysis.

4.1 Seismicity

In and around The Netherlands we observe seismicity of tectonic origin, related to the Roer Valley graben, mostly in the southeast, induced seismicity mostly in the north (Figure 2) and significant mining related seismicity in Germany. Here we discuss the seismicity in the north of The Netherlands.

De Crook et al. (1998) and Dost and Haak (2004) summarized the characteristics of the induced seismicity in the north of The Netherlands. No significance changes have been observed between 1998 and 2003. Since 1986 and up till the end of 2003 the KNMI has observed more than 330 induced events and only nine events with $M \geq 3.0$ (Appendix 4**)**. The observed frequency-magnitude distribution for all these events fit well a general exponential distribution, although local variations can be identified. No events with $M_L > 3.5$ and no Intensities larger than VI have been observed. Below we update the magnitude-frequency relation and the M_{max} estimates.

De Crook et al. (1995; 1998) estimated M_{max} using two statistical interpretation of the observed seismicity and one physical model:
a) The cumulative seismic energy release provides an idea of the regularity with which the seismic energy is released and therefore a rough estimate of the possible M_{max}. The seismic energy is estimated using the magnitude-energy relation of Ahorner and Pelzing (1985).
b) A finite magnitude-frequency distribution, like the truncated exponential distribution in equation 4, includes an M_{max} parameter. De Crook et al. (1998) used a Bayesian approach to estimate M_{max} from the observed seismicity. They repeatedly estimated the parameters of the truncated exponential distribution assuming errors in the magnitude estimates (Normal distribution) and the average number of events for a certain magnitude (Poisson distribution). They added the a priory constraint that the distribution fits the strictly exponential model of the data in the magnitude range $1.5 < M_L < 2.7$. Using a Monte Carlo approach they obtained then a mean, $M_{max} = 3.5$, and a mean plus one standard deviation, i.e. 84% confidence limit, $M_{max} = 3.8$.
c) Assuming a maximum possible rupture fault plane on an existing fault in or near the exploitation fault De Crook et al. (1995) obtained $M_{max} = 3.5$ for the Groningen field and $M_{max} = 3.6$ for the Bergermeer field. The M_{max} estimate for Bergermeer has been corroborated by Logan et al. (1997). They obtained $M_{max} = 3.6$, and $M_{max} = 3.8$ for the worst-case scenario.

The updated cumulative frequency-magnitude relation for all earthquakes based on events with $1.5 \leq M_L \leq 2.7$ in the northern part of The Netherlands for the period 1986 –2003 is (see also Figure 4):

$$log\ N = 2.16 \pm 0.15 - 0.80 \pm 0.08\ M \qquad \text{eq. 7}$$

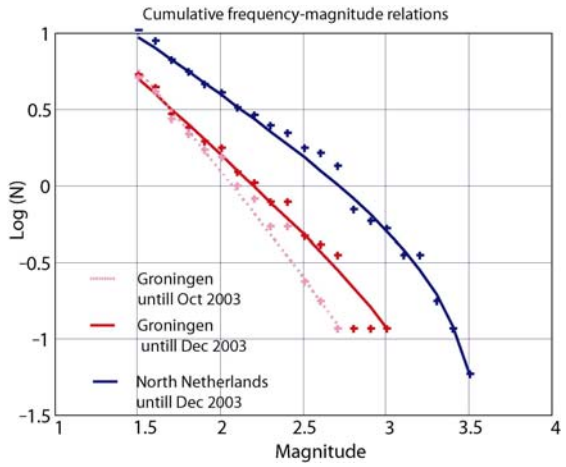

Figure 4. *Cumulative annual frequency-magnitude relation obtained for all induced seismicity in the north of The Netherlands for the period 1986 - 2003 (blue curve) and observations (blue crosses). Also is shown the same frequency-magnitude relation for all earthquakes in the Groningen field. However, for this selection we have shown the relation excluding (purple broken curve) and including (red curve) the three $2.7 < M < 3.0$ events that occurred October-November 2003. This shows that the slope (b-value) of the frequency-magnitude relation for a subset of 179 events has a tendency to approach the b-value of the frequency-magnitude relation for all earthquakes (340 events).*

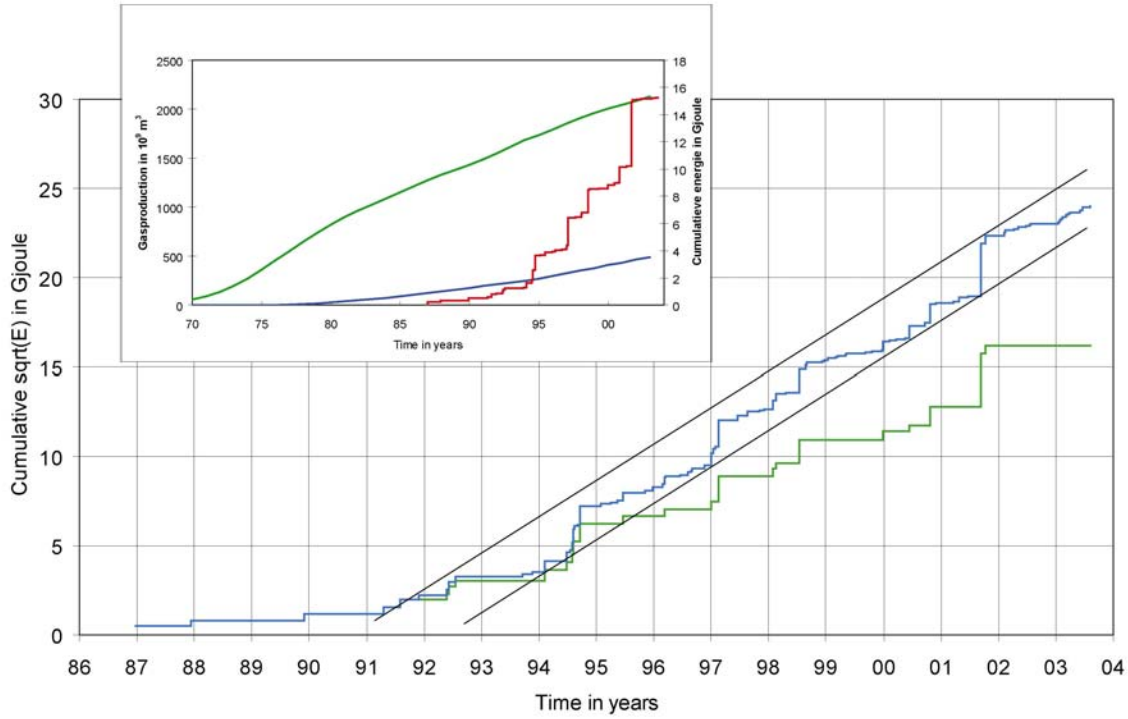

Figure 5. *Cumulative of the square root of the earthquake energy in Gjoule (blue curve) of all earthquakes with ML ≥ 1.5 as a function of time. Here we used the magnitude-energy relation of Ahorner and Pelzing (1985). The black straight lines indicate the upper and lower boundaries and provide an estimate of the maximum magnitude (M_{max} = 3.8) assuming that the energy release is and remains stationary. The cumulative curve (green line) only for all earthquakes with ML ≥ 2.5 illustrate the significance of including also the smaller earthquakes in the total energy release. The inlay figure compares the cumulative seismic energy release (red curve) with cumulative gas production on land (green curve) and on the continental shelf (blue curve). (source gas production numbers: NITG)*

Table 1*. Estimated M_{max} using a Bayesian approach.*

mean	median	84%	Comments
3.5	3.5	3.8	Earthquake data 1986-1997
3.7	3.6	3.9	Earthquake data 1986-2003

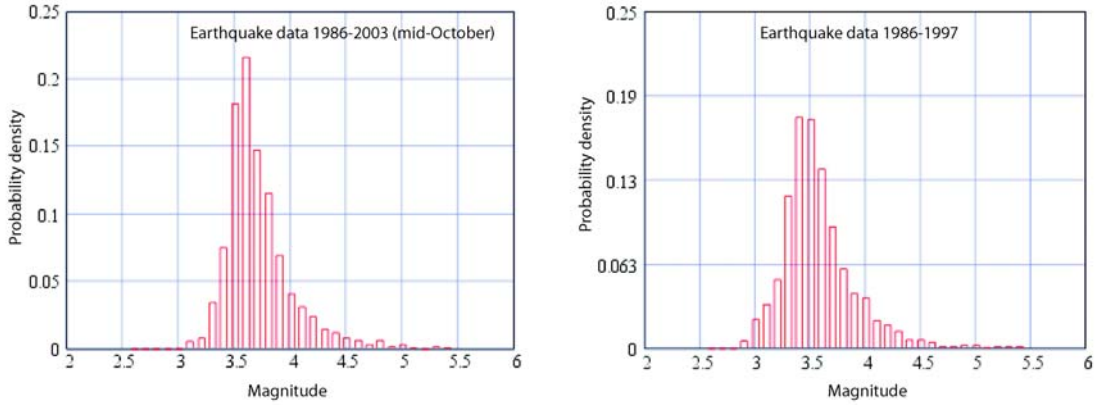

Figure 6. *Estimating the maximum possible magnitude based on the observed seismicity using a Bayesian approach. The left figure shows the most recent estimate based on earthquake data up to October 2003. Right figure shows an estimate based on the data up to 1997 and is consequently similar to that obtained by De Crook et al. (1998). The results of this analysis are summarized in Table 1.*

The M_{max} estimates obtained by De Crook et al. (1998) have now been updated for all earthquake data up to mid-October 2003. The seismic energy release method (Figure 5**)** gives an M_{max} = 3.7 and the Bayesian method of De Crook et al. (1998) for all earthquakes up to October 2003 (Figure 6 and Appendix 4) gives a mean, M_{max} = 3.6, and an 84% confidence limit at M_{max} = 3.9.

In summary, the statistics of the induced seismicity, i.e. magnitude-frequency relation and M_{max}, in the north of The Netherlands have remained fairly stable since 1998. This implies that the main conclusions in the evaluation of De Crook et al. (1998) remain valid.

4.2 Attenuation relation

The ground motion prediction equations or attenuation relations are usually empirical relation and show a large variability due to many factors like focal mechanism, rupture process, site response, unknown details of the 3D crustal structure etc. A review can be found, among others, in Campbell (2003).

For The Netherlands we have as yet insufficient data to obtain a reliable regional attenuation relation. Therefore, Dost et al. (2004) tested a number of existing relations for PGA and PGV (Campbell 1997, 2000, 2001; Ambraseys 1995; Sabetta and Pugliese 1987; Campbell and Bozorgnia, 2003) on their fit to the existing instrumental data in The Netherlands since 1997. Their conclusion was that the Campbell's (1997) equations provide a reasonable ground motion prediction for small and shallow earthquakes, as considered in this study, in spite of the fact that the relation was originally based on data from larger earthquakes ($M_w \geq 5$) and has been revised in 2003 (Campbell and Bozorgnia, 2003).

Consequently, we adopted the following attenuation relation for PGA and PGV from Campbell (1997):

$$\ln PGA = -2.896 + 0.812M - 1.318\ln\sqrt{r^2 + (0.187e^{0.616M})^2}$$

$$\ln PGV = \ln PGA + 0.26 + 0.29M - 1.44\ln(r + 0.0203e^{0.958M}) + 1.89\ln(r + 0.361e^{0.576M}) \quad \text{eq. 8}$$

$$+ (0.0001 - 0.000565M)r$$

In these equations r is the closest distance from site to earthquake rupture plane, which implies for small earthquakes the hypocentral distance. *ln* represents the natural logarithm. *PGA* is given in units of g (gravity) and *PGV* in cm/sec. Both PGA and PGV refer to S-waves amplitudes. Although Campbell (1997) also proposes different corrections for local site conditions and type of faulting, we present here only the equation relevant to our case. The predicted PGA (and PGV) are uncertain. This is described with a lognormal distribution in which the standard deviation, σ, for ln *PGA*, decreases from 0.55 and 0.39 with the size of the PGA as:

$$PGA < 0.068g : \sigma = 0.55$$

$$0.068g < PGA < 0.21g : \sigma = 0.173 - 0.140\ln PGA$$

$$PGA > 0.21g : \sigma = 0.39$$

The standard deviation, σ_v, for *ln PGV*, is related to σ as:

$$\sigma_v = \sqrt{\sigma^2 + 0.06^2} \quad \text{eq. 9}$$

Campbell defines the PGA and PGV in his publications (Campbell,1989; 1997; Campbell and Bozorgnia, 2003) as the geometric mean of the (horizontal) peak ground motion values of both horizontal components. These definitions are approximately 12% and 17% less than the largest horizontal component of PGA and PGV, respectively (Campbell, 1997). In Figure 7 we compare different attenuation relations for distances up to 20 km for M = 3.5 illustrating the large differences.

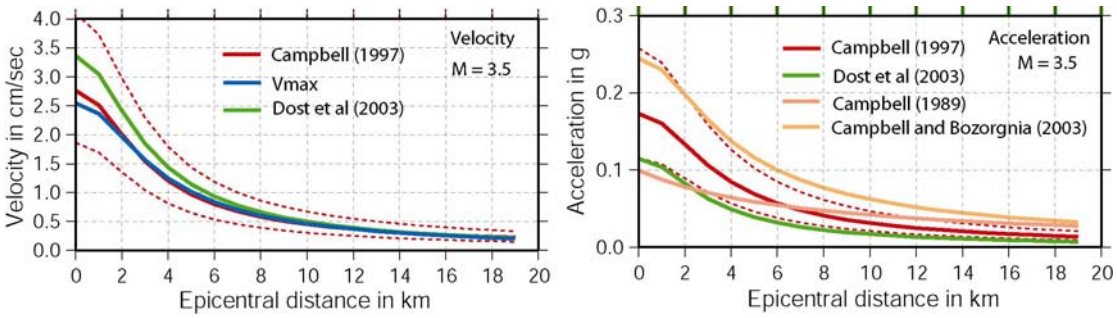

Figure 7. *Attenuation functions and standard deviations according to Campbell (1989; 1997), Campbell and Bozorgnia (2003) and Dost et al. (2004). Also shown is the V_{peak} estimate as presented in this paper (section 4.4). Right figure shows the PGA as a function of distance for M=3.5. The thicker curve shows the mean value, the thinner broken lines the median+1σ and median–1σ respectively. Left figure shows the same for PGV. An alternative interpretation of these figures is that this shows the 50% probability (median) and 84% probability (median + 1σ) of ground motion exceedance for an M=3.5 earthquake scenario for seismic hazard due to induced seismicity. In this case we have presented the hazard parameters PGA and PGV.*

4.3 Response Spectra

One pragmatic approach of presenting seismic hazard is to characterize the loading of structures as a result of ground motion in terms of the response spectra (Gupta, 1990; Reiter, 1990; Van Staalduinen and Geurts, 1998). A response spectrum provides the peak amplitudes of the response of a one-degree-of-freedom oscillator of different frequencies to the input ground motion (see also Figure 8). Such response spectra provide not only a good first approximation of the elastic response of a structure to the ground motion, it also displays the frequency content of this ground motion. This is one of the main reasons response spectra are used in both the European (Eurocode-8, CEN-2002) and American (2000 NEHRP recommended provisions, Dobry et al., 2000) building codes. A detailed presentation of response spectra can be found in Gupta (1990).

Horizontal ground motion is the most damaging and as mentioned in section 3.3 velocity can in our case be correlated better to possible damage and intensity. Therefore, in the north of The Netherlands specific response spectra for horizontal motion velocity need to be considered for seismic hazard. Van Staalduinen and Geurts (1998) showed that the standard response spectra as presented in the Eurocode-8 are not representative for the situation in the north of The Netherlands. They proposed a normalized averaged response spectra for 5 and 50% damping based on data obtained from the Roswinkel area in 1997.
For the case of 50% damping they obtained:

$A_{50}(f) = 1.2 \cdot PGA$ for $f > 10$ Hz and

$A_{50}(f) = 0.0895 \cdot PGA \cdot f^{1.0516}$ for $f < 10$ Hz.

In this equation $A_{50}(f)$ is the amplitude of the 50% damping acceleration response spectrum at frequency f.

For the case of 5% damping they found:

$A_5(f) = 2.9 \cdot PGA$ for f > 12 Hz and

$A_5(f) = 0.0138724 \cdot PGA \cdot f^{2.16241}$ for f < 12 Hz

In this equation $A_5(f)$ is the amplitude of the 5% damping acceleration response spectrum at frequency f.

The model spectra as proposed by Van Staalduinen and Geurts (1998) are shown in Figure 9 as relative velocity amplitude response spectra together with the Eurocode-8 definitions and the "observed" response spectrum of an additional, representative, Roswinkel event. While we observe clear spectral peaks around 10 Hz, also for the 50% damping case, the model of Van Staalduinen and Geurts (1998) does not.

We propose the peak of the velocity response spectra, V_{peak}, as a simple relevant parameter for seismic hazard analysis. Velocity correlates better with possible damage and observed Intensities than PGA values. We further find that observed ground motions due to induced events in the north of The Netherlands:

a) Have a short duration of strong acceleration (Figure 3), usually about 1 cycle in velocity,
b) Show PGA and V_{peak} occur usually at frequencies around 10 Hz (Figure 3, 9 and 10).

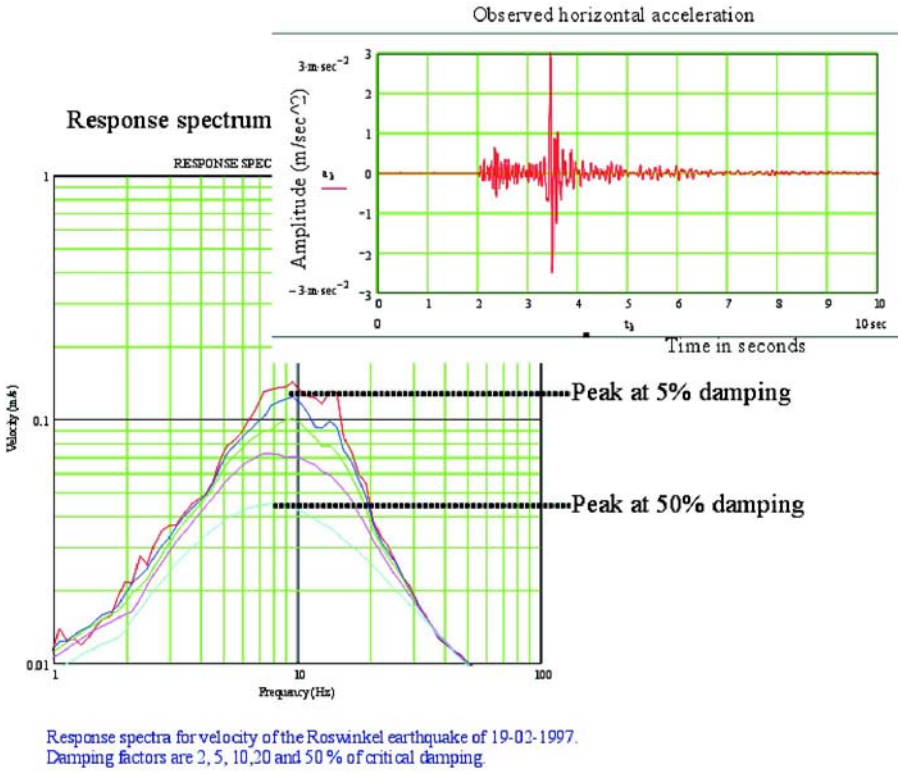

Figure 8. *Basic principle of the response spectrum approach illustrated on an actual example. The upper right inset shows a horizontal component of the19/2/1997 event near Roswinkel, as recorded on an accelerometer at about 2.5 km epicentral distance. Response spectra for 2, 5, 10, 20 and 50% damping respectively are shown. The hazard will be given as the peak value of the response spectra for 5% and 50% damping respectively.*

.

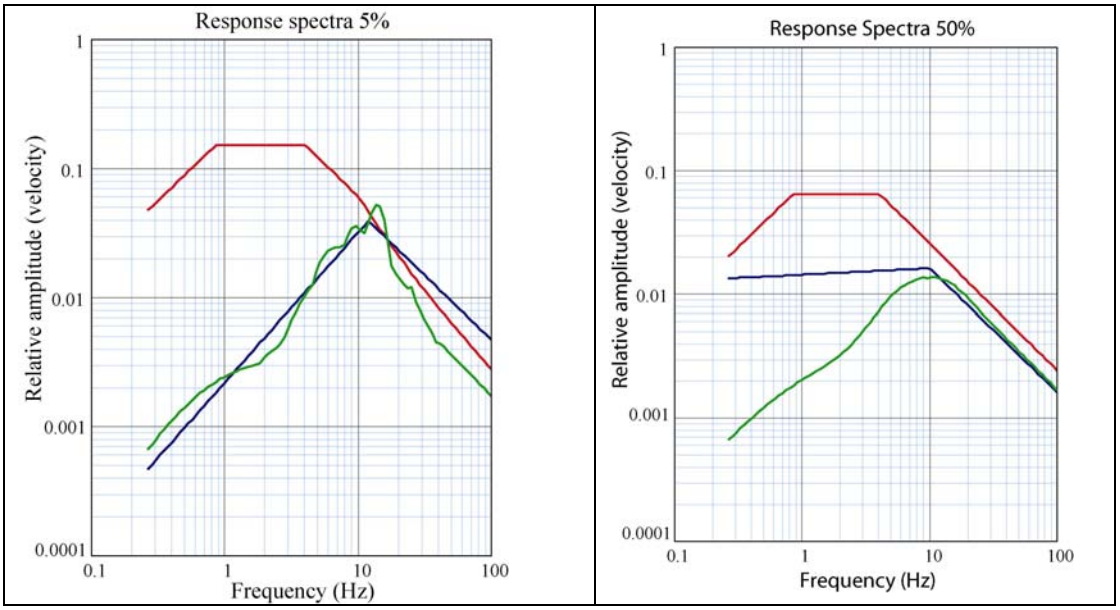

Figure 9. *Response spectra (velocity) according to the Eurocode-8Type 2 and ground type C (red), Van Staalduinen & Geurts (blue), as obtained for The Netherlands and an example as obtained from a horizontal component acceleration recording obtained at 2.5 km epicentral distance from the Roswinkel July 14, 1998 event (M=3.3) in the Roswinkel field (green). The 5% (left) and 50% (right) damping are given.*

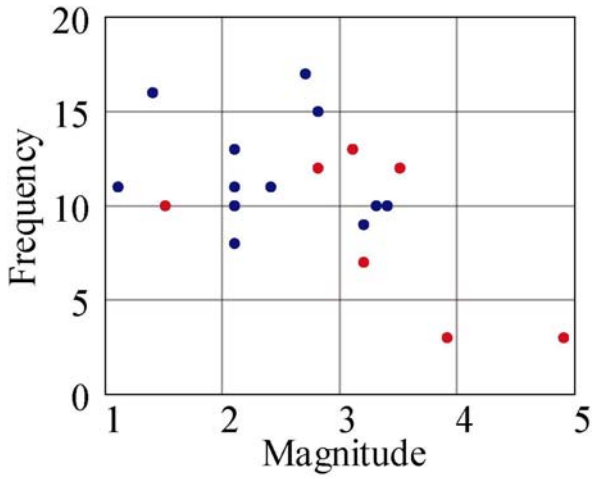

Figure 10. *Frequency at which the peak of the velocity response spectra occurs as a function of earthquake magnitude (M_L). The peak frequencies are measured at the horizontal components of recordings from 19 events. The measurements are made for 12 shallow induced events (blue) in the northern part of The Netherlands and 7 natural seismic events(red) in the southern part of The Netherlands.*

Assuming our observations are characteristic also for future events one can find a simple approximation of V_{peak} using the following formula:

$$V_{peak}(f) = PGA \cdot (2\pi f)^{-1} \cdot (1 - e^{-Nch2\pi}) \qquad \text{eq. 10}$$

Here N_c is the number of cycles and h the damping coefficient used in the response spectrum, i.e. 5 or 50% for example. PGA is given in cm/sec^2. With our assumptions $N_c = 1$, $h = 0.05$ and 0.5 for 5% and 50% damping respectively and the frequency $f = 10$ Hz. The procedure is presented schematically in Figure 8.

This simplification enables us to translate the PGA hazard maps directly into peak velocity maps or more accurately V_{peak} (f = 10 Hz) hazard maps which are directly comparable with the SBR provisions (SBR richtlijnen, 2002).

Interesting is that the V_{peak} as obtained with the above relation for 50% damping corresponds well with the PGV as obtained from the Campbell (1997) relation (Figure 7). An alternative engineering approach, in which the PGV is adapted as the input parameter, Van Staalduinen (1995) shows that this should be true for frequencies of 10 Hz or smaller. Consequently, our Campbell (1997) PGA - V_{max} approach and the Campbell (1997) PGV model are equivalent for frequencies around 10 Hz.

4.4 Site response

Steep gradients and lateral discontinuities of both velocity and Q in the near surface at a site may result in severe distortions of the earthquake signals. Serious frequency dependent amplifications and/or damping may occur that have a considerable impact on the response spectra as described above. This effect is usually modeled as site response (Borcherdt, 1994). Recently, more specific building codes require therefore also specific corrections on the response spectra (Borcherdt et al., 2000). The abundancy of different types of soil in The Netherlands suggest that site response effects may be important. Therefore Wassing et al. (2003, 2004) have performed a specific study combining our results with generalized site responses for relevant areas in The Netherlands.

4.5 Sensitivity analysis

We present a seismic hazard estimate based on a best judgment model. However, the model and input parameters contain uncertainties, either epistemic uncertainties, i.e. introduced by subjective judgments, or aleatory uncertainties, i.e. the inherent physical uncertainties. More discussions on these types of uncertainties can be found in Toro et al. (1997) and Bommer (2003). Some of the uncertainties, specifically aleatory uncertainty can be, and has been, included in the hazard analysis. Many of uncertainties, especially the epistemic uncertainties cannot be included in the analysis while at the same time keeping it reasonably transparent. An alternative approach is to show the impact of possible variations due to different model and parameter assumptions on the final hazard estimates. Both the logic/decision tree approach and the more general Bayesian Network approach provide a systematic methodology to perform such a sensitivity analysis. The first method has been extensively used in seismic hazard analysis (Reiter, 1990; Grünthal and Wahlström, 2001).

The sensitivity analysis is relevant to understand the relation between input parameters/models and the output for non-experts, and provide an insight in the most crucial model assumptions. Based on the elements in the analysis (Figure 10 and Table 2) we present a limited sensitivity analysis. With a number of different examples we provide an insight in the involved uncertainties and its relevance.

Table 2. *Tentative table of model parameters and how uncertainty is handled*

Model	**Function/ Parameter**	**Type of input**	**Comment**
Seismic zone	2D Area	subjective parameter	Difficult to model probabilistic
Seismicity:	$f(m\|\ \lambda, \beta, M_{max})$	pdf	Included in the probabilistic approach of the PSHA
Seismicity rate	Λ	(subjective) parameter	
Frequency-magnitude	β (b-value)	(subjective) parameter	
Maximum magnitude	M_{max}	(subjective) parameter (with pdf)	
Attenuation:			
Ground motion prediction function	$P(A>a\|\ m,r)$	conditional pdf	
Error distribution	$\sigma_{\ln A(m,r)}$	(subjective) parameter	
Site response:			Not included in the probabilistic approach
	$h(A_{out}/A_{in})$	deterministic function	
Response spectra			Not included in the probabilistic approach
	A(f)	deterministic function	

pdf – probability density function

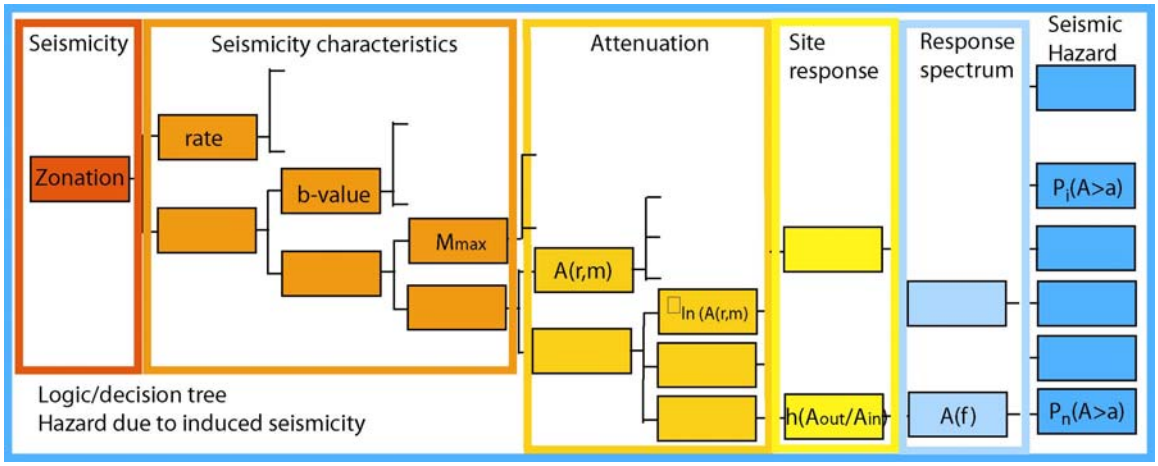

Figure 11. *Schematic logic tree (decision tree) describing the different model combinations, useful in performing a sensitivity analysis and indicating which parameters have the biggest influence on the uncertainty in the seismic hazard analysis. The functions are the same as in Table 2*

5. Seismic hazard due to induced seismicity in The Netherlands .

The seismic hazard, as probability of exceedance for T = 10 and T = 100, has been estimated for a specific site and the following three parameters:

- peak Ground Acceleration (PGA).
- peak velocity of the response spectrum, V_{max}, with 5% damping
- peak velocity of the response spectrum, V_{max}, with 50% damping

The seismic hazard, as presented in this report, includes all aspects except the specific site response, which depends more on local geology. This site response is reported in the accompanying report of Wassing et al. (2003, 2004).

We present essentially two situations. First we consider exploitation fields where we have observed seismicity and we believe we can characterize its seismicity on the basis of past information. This is the case for the Groningen field, the Roswinkel field and, assuming some similarity with the Roswinkel case, the Bergermeer field (see Figure 12) . Here we considered the Annerveen field and the Eleveld field to be similar to the Groningen field. Second, we consider exploitation fields for which we have little or no observed seismicity. This is applicable to many fields in Friesland and the south of The Netherlands. A quantitative analysis for these fields requires some additional basic assumptions.

The model and parameter choices have been kept as simple as possible. Consequently, the number of possible models and parameters are smaller then suggested in Figure 11.

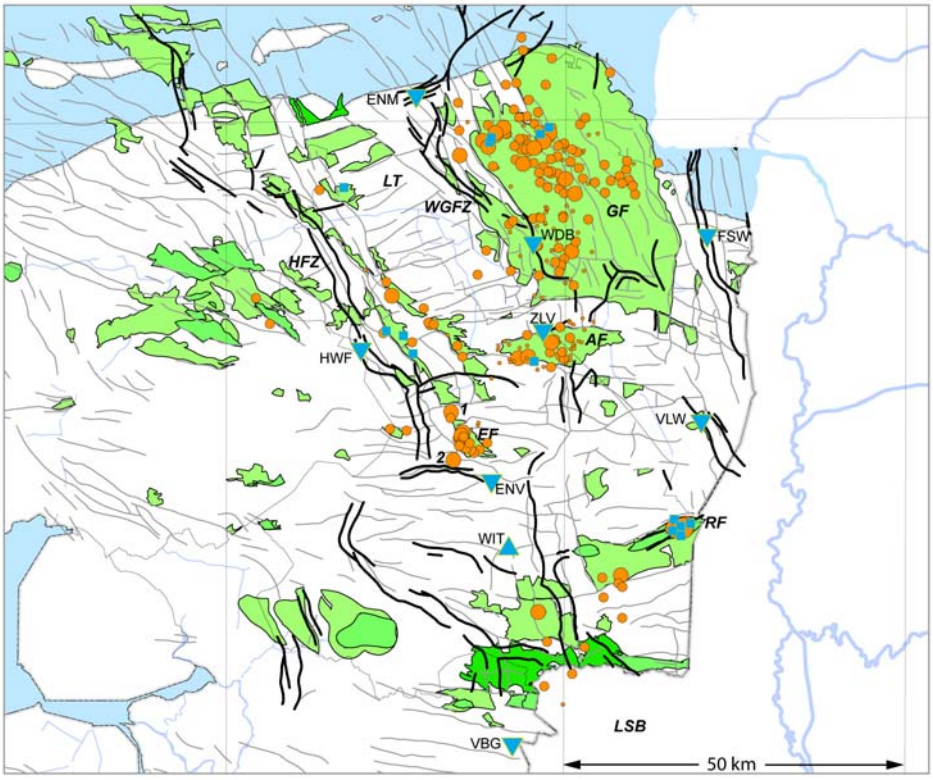

***Figure 12**. A schematic figure of the hydrocarbon (gas) exploitation fields (green), the major fault structures (source: NITG), the seismometer station WIT (blue triangle), borehole seismometers (blue inverted triangles), accelerometers (blue squares) and the seismicity (orange solid circles) in the north-eastern part of The Netherlands. Some of the gas fields discussed in this report are indicated: RF - Roswinkel Field; GF – Groningen Field, EF – Eleveld Field, AF – Annerveen Field. After Dost and Haak (2004)*

The general assumptions used in all seismic hazard estimates presented below are:

- The PGA (and PGV) attenuation are described in chapter 4.2
- The PGA attenuation variation has a fixed value; $\sigma = 0.4$.
- The maximum possible magnitude $M_{max} = 3.5$, unless specified differently.
- Seismic hazard for earthquakes $M < 1.5$ is not considered.
- The seismicity is uniformly distributed over the surface projection of the gas field.
- The rate of seismicity is assumed to be stationary (see Figure 13 and Table 3 for details)

The cases presented below differ from each other only with respect to the seismicity model used.

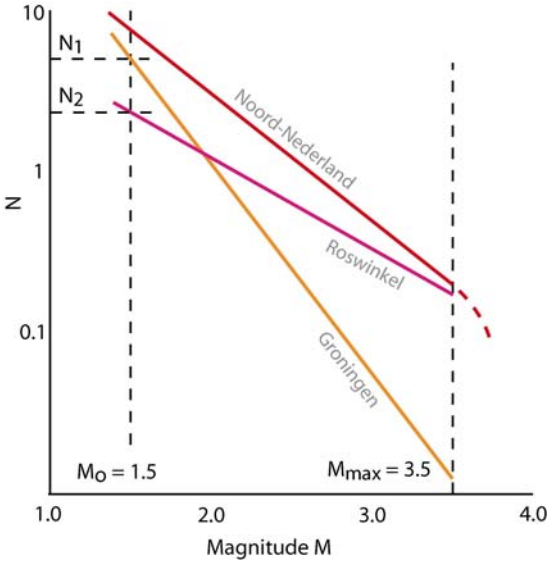

Figure 13. *Schematic overview of the seismicity models used. The seismicity is characterized as a stationary process with an exponential distribution of the cumulative number of events per magnitude, i.e. Log N = a – bM. Where N is the number of earthquakes with a magnitude larger then M per year. Three basic models for the seismicity are here presented. Model Noord-Nederland: A general model for all induced seismicity in the north of The Netherlands; Model Roswinkel: modeling the seismicity in and around Roswinkel; Model Groningen: modeling the seismicity in and around the Groningen gas field. N1 is the approximate number of earthquakes with magnitude larger than M = 1.5 for the Groningen field. N2 is the number of earthquakes with magnitude larger then M = 1.5 for the Roswinkel field. λ is in our case the number of events with magnitude larger than M = 1.5 or N (M≥1.5).*

Table 3. *Seismicity models used in the PSHA*

Region	***Seismicity model***	***λ***
Noord-Nederland	*log N = 2.1 – 0.8M*	*≈ 8*
Roswinkel/Bergermeer	*log N = 1.05 – 0.5M*	*≈ 2*
Groningen	*log N = 2.7 – 1.3M*	*≈ 6*

5.1 General case

We have established that the seismicity is induced. However, we are as yet unable to indicate why some fields are active and others not (yet?). Neither do we have an adequate induced seismicity model for hazard assessment. In this most simple model we assume that all observed seismicity could have occurred anywhere in an exploited hydrocarbon repository.

Based on the established magnitude-frequency relation for induced seismicity in The Netherlands the annual magnitude frequency relation has been modeled as log N = 2.1 – 0.8 M, characterizing the seismicity of all $M \geq 1.5$ events in all gas fields. That is, we observe about 8 induced events per year with magnitude larger than 1.5 in The Netherlands, mainly in the north. The total surface area projection of all these gasfields defines our seismic zone or "hypothetical field" comprising about 2500 km^2.

In Figure 14 we present the seismic hazard for one site situated in the middle of such a hypothetical field and different return periods, T (years), or annual probabilities, T^{-1} (per year). In all other figures throughout the report we will present the seismic hazard for a large number of sites in and around the hydrocarbon exploitation fields for the return periods T=10 and T=100 (Figures 16, 17, 23, 27, 29).

To illustrate the integration effect (equation 2) we also compared the seismic hazard for our large "hypothetical field" (L1 of 2400 km^2) with that of a small field (S1 of 10 km^2) with the same seismicity rate per unit area (Figure 17). The hazard within the larger zone reaches a higher value then the hazard in the center of a small field. The hazard maps in Figures 16 and 17 present the hazard at each individual site on the map.

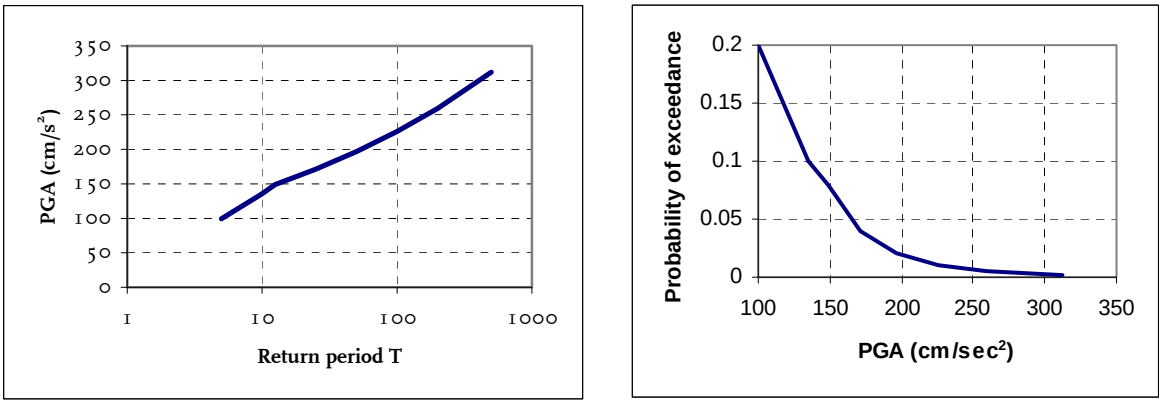

Figure 14. *Seismic hazard at one site above a hypothetical large gas field in the north of The Netherlands.*
The left figure presents the hazard as the probability that a certain PGA will be exceeded at least once within a certain return period T. Such a hazard curve will depend on where the site is situated in relation to the seismic source, i.e. the hydrocarbon exploitation field. The right figure presents the hazard as the annual probability that a specific PGA will be exceeded once. In the following figures we will show hazard maps that only present the hazard for T=10 and T=100 at each site. These maps can also be read as the isolines for the PGA that has an annual probability of being exceeded once of 0.1 and 0.01 respectively.

One can also consider the probability that one observes no seismicity in a specific sub-area with the above model, i.e. a stationary rate of seismicity, a simple uniform distribution of the possible earthquakes. For example, what is the probability that no seismicity is observed above a small hydrocarbon exploitation field (10 km^2 and 1/120 of the whole area) in a period of 20 years? This appears to be 50% (Figure 15). Hereby we assume inherently that all events with M ≥ 1.5, are detected by the existing monitoring network and all smaller events are not detected.

The presented hazard estimates provide a first order approximation for those exploitation fields where seismicity data or other relevant information on induced seismicity is lacking.

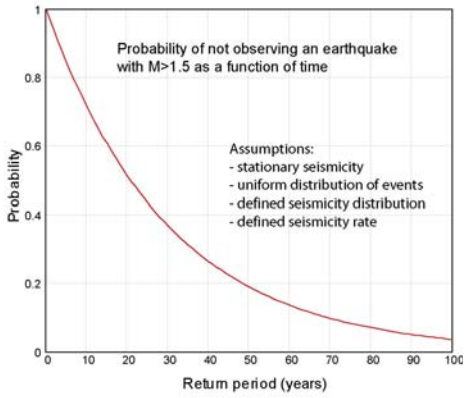

Figure 15. *Probability of occurrence of an event with M > 1.5 assuming a stationary seismicity modeled as a Poisson distribution and with uniform spatial distribution for a sub-area of 10 km^2, or 1/120 of the total area, exploitation field. The seismicity characteristics are taken from all observed seismicity in the north of The Netherlands and scaled according to the area (i.e. model "Noord-Nederland" in Table 3). After 20 years we have a 50% chance of observing an event with M > 1.5, alternatively a 50% chance of not observing an event with M > 1.5.*

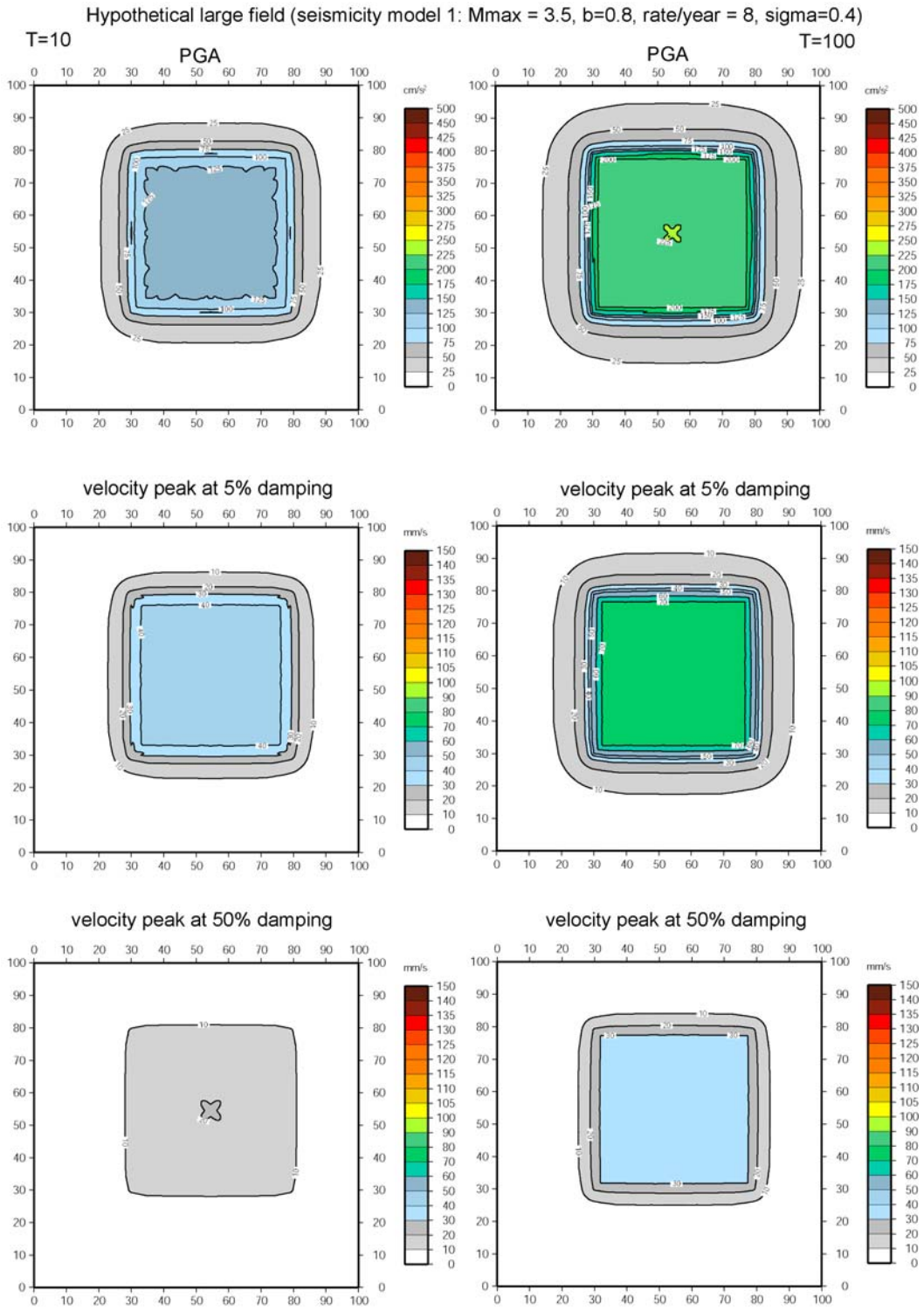

Figure 16. *Estimated hazard at sites in and around a hypothetical large field, L1 (total surface projection of all operating gasfields on land in The Netherlands, approximately 2400 km^2). This and the following hazard maps indicate the potential hazard at each individual site on this map. In the upper two frames the hazard is presented as the PGA that may be exceeded once in T=10 years (left) and once in T=100 years (right). The lower four frames present the hazard as the peak velocities that may be exceeded once in T=10 years and once in T = 100 years respectively. Alternatively, the hazard indicates a 10% probability that the peak values as indicated can be exceeded within 1 year (T=10), respectively within 10 years (T=100). The x- and y-axis indicate distance in kilometers.*

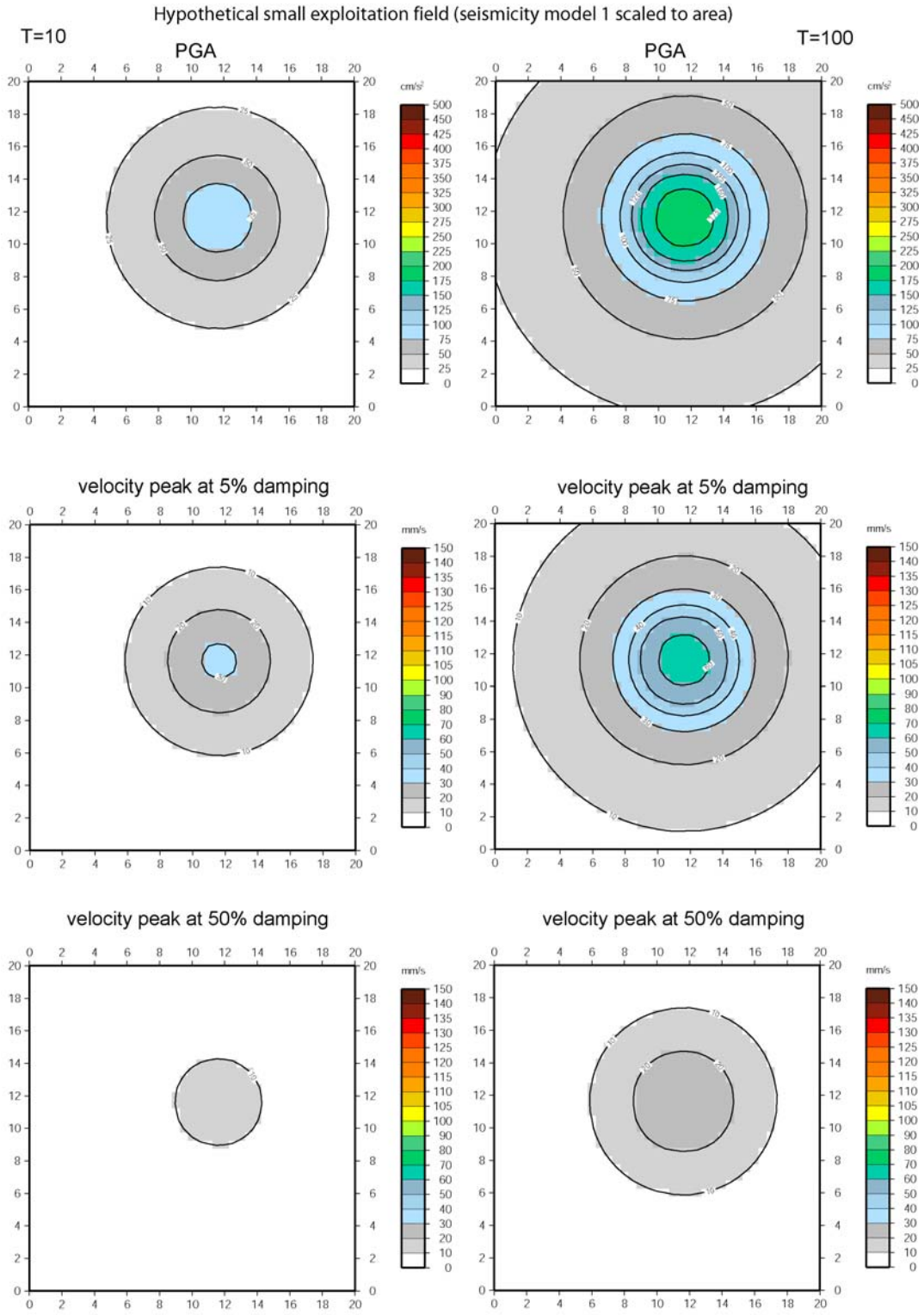

Figure 17. *Estimated hazard at and around, S1, a hypothetical small field (about 10.5 km^2). The hazard estimates are presented as in Figure* ***16****.*

5.2 Specific case: Roswinkel area

The Roswinkel gas reservoir is situated in the sandstones of the Bontzandsteen formation of the Trias in a synclinal structure due to salt tectonics at a depth varying from 2000 to about 2400 meters. Below this reservoir we find another gas reservoir, the Emmen field, at a depth of 3800 to 4300 meters in the Lutte subgroup of sandstones and claystones (Rijkers et al. 1999).

The Roswinkel field (see Figure 12) has, up till now, shown the highest concentration of induced earthquakes. The first recorded event occurred in 1992 when the pore pressure in the reservoir reached about 1/3 of its original value (Van Eijs, 1999). The largest magnitude, event M_L = 3.4, occurred five years later on 19 February 1997 and caused damage (Figure 19). In total the KNMI monitoring network recorded 36 events in the period 1992-2003. We judged this to be a sufficient basis for a specific hazard analysis. The seismicity in and around Roswinkel is characterized by relatively few small earthquakes, which can be seen by the low b-value estimate we have found for this region (Figure 18).

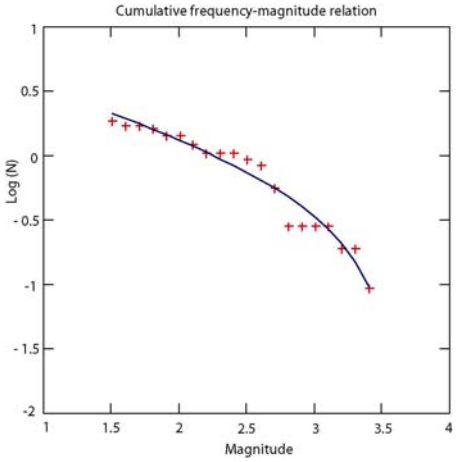

Figure 18. *Annual cumulative frequency-magnitude relation for all events associated with the Roswinkel gas field during the period 1992 – November 2003. In blue the best fit seismicity model for all available data using the function in equation 3. In the seismic hazard modeling we apply a modified model that fits better the magnitude range 2.5 ≤ M ≤ 3.4 (Table 3).*

The tectonics are characterized by Frikken (1999) as wrench faulting. A SW-NE striking anticline with a set of normal faults on top of the anticline with strike SW-NE, parallel to the structure, and faults with a strike SE-NW (Figure 20). These faults provide the outline of a small graben structure on top of the anticline. The seismicity seems to occur above the (highest) reservoir, however, without sensors at large depth near the source we have bad constraints on the depth estimates (± 500 m). This uncertainty is due to a combination of the 2D sensor location at the surface and the large uncertainties in the ray path estimation inherent to a heterogeneous upper crust. For a more detailed explanation see Moser et al. 1992 for example. The depth constraints from macroseismic observations are better. The macroseismic analysis of the 1997 event (Dost and Haak, 1997) shows a depth of 1.5 km with a possible error of 0.5 km, indicating a depth of at most 2 km, which is just above the highest (Roswinkel) reservoir (Figure 20). No seismicity has been observed at depths corresponding to the deeper reservoir, the Emmen field

The obtained focal mechanism as obtained for the 1997 event is generally consistent with those of most Roswinkel events. Initially, the seismic events were explained as earthquakes that re-activated the normal faults on top of the anticline (Rijkers et al. 1999). However, the obtained focal mechanism (representative for most Roswinkel events) provides two possible solutions: a) a reverse fault strike consistent with the strike of the anticline and b) a normal fault with a strike perpendicular to the anticline. The obtained relative locations may suggest two active normal faults with different dip directions, but this contradicts the consistent similarity of the focal mechanism. The normal fault focal mechanism solution has a strike, which does not correspond with those identified along the syncline axis. Consequently, from this circumstantial evidence we prefer the reverse mechanism solution as the most probable earthquake rupture mechanism. Recently the Shell/NAM group involved in the microearthquake experiments (Jupe et al. 2001) and the KNMI attempted a joint interpretation of the 3D microearthquake locations with the larger KNMI events. The possible existence of reverse fault structures on top of the gas field (Segall and Fitzgerald, 1998), the tentative joint locations and a reverse mechanism interpretation of the obtained focal mechanism solution, are three arguments that favor the model of a reactivated reverse fault on top of the gasfield.

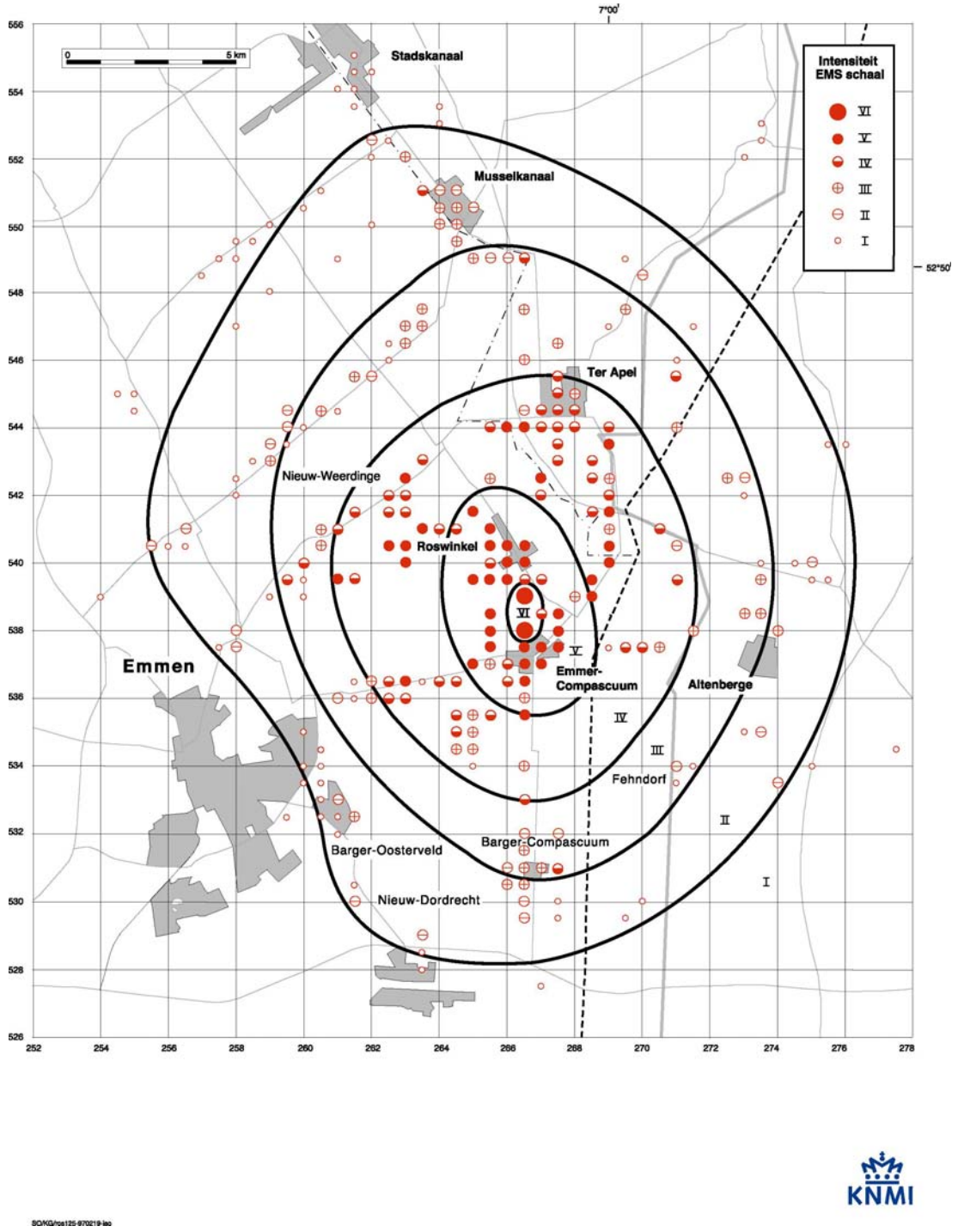

Figure 19. *Macroseismic map with the isoseisms for the M = 3.4 earthquake above the Roswinkel area on February 19, 1997 (from Dost and Haak, 1997). The data, 651 macroseismic inquiry forms, is interpreted in the EMS scale. The data circles on the map are averaged values of the observed intensities in a 0.25 km^2 area. This macroseismic map provides the basis for a depth estimate between 1 and 2 km for the observed event.*

.

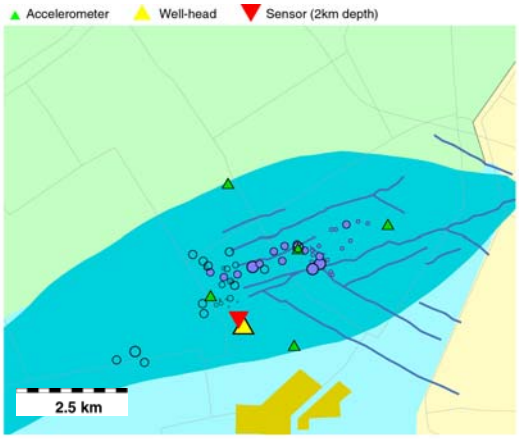

***Figure 20a**. Locations of earthquakes in and around Roswinkel. The earthquakes recorded by the KNMI network since 1992 are shown (solid purple circles). A number of events have similar focal mechanisms and therefore similar seismograms. These events have been located relative to a master event with accuracies around 100 meters. Installed and operating accelerometers at the surface are depicted. The 28 day microearthquake experiment as described in Jupe et al. (2001) used an experimental sensor placed at 2 km depth (red triangle) in a well (yellow triangle shows location at the surface). The locations of the recorded microearthquakes are (open circles) and identified faults (NITG) are also shown..*

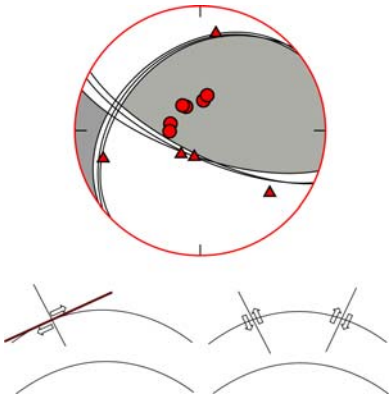

***Figure 20b.** Focal mechanism for the M = 3.4 event near Roswinkel on 19 February 1997. This is a lower hemisphere projection of the focal sphere, where the dark colored quadrangles represent compression and the white quadrangles extension. The red circles corresponds to the observed dilatational first motion in the seismogram, the red triangles correspond to the compressional first motion in the seismogram. This focal mechanism provides two possible fault plane solutions, i.e. a low angle reverse motion with strike NE-SW and dip towards the NW, shown schematically in the lower left corner, and a steep (reactivated normal fault?) reverse motion with strike WNW-ESE and dip SSW, shown schematically in the lower right corner.*

In order to get an impression of the total released energy we computed the magnitude that corresponds to the total sum of released seismic energy, E_s, using the empirical relation of Ahorner and Pelzing (1985):

$$\log E_s = 3.81 + 1.64 M_L \qquad \text{eq. 11}$$

E_s is here given in Joule. The result is summarized in Table 4.

***Table 4.** Roswinkel field M ≥ 3.0 earthquakes and cumulative seismic energy release as observed up to Nov 2003*

Date	M_L	M_w	comments
19-02-1997	3.4	-	
14-07-1998	3.3	-	
25-10-2000	3.2	-	
	3.6		Cumulative magnitude of all M ≥ 3.0 events
	3.7		Cumulative magnitude all 36 recorded events

Based on the observations and the estimated magnitude frequency relation for the Roswinkel area the annual magnitude frequency relation has been modeled as: log N = 1.05 – 0.5 M. This corresponds to about 2 induced events per year with M ≥ 1.5. The obtained hazard maps are shown in Figure 21.

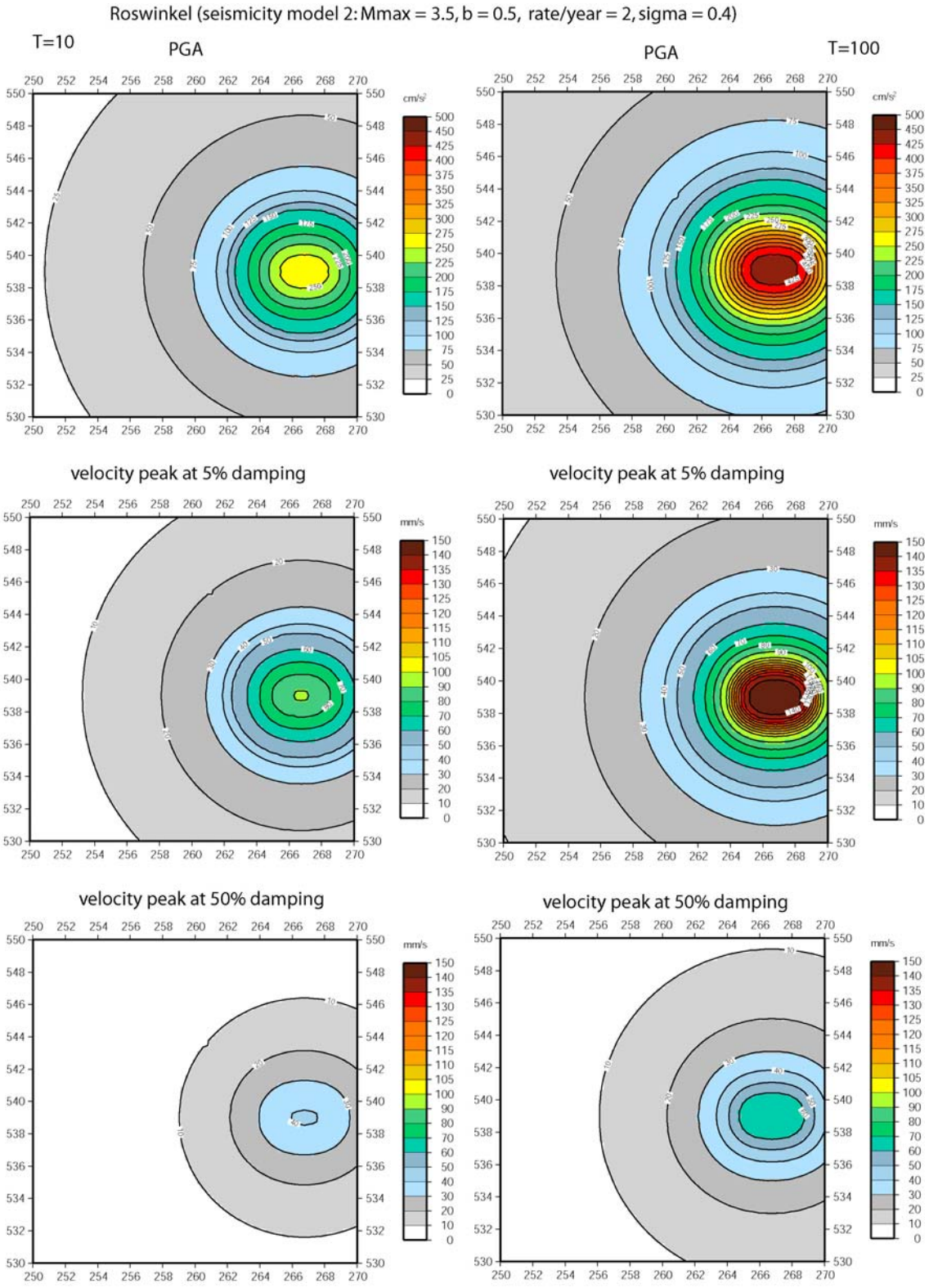

Figure 21. *Estimated hazard at and around the Roswinkel field. The hazard has been estimated for two return periods, i.e. T=10 years (left) and T=100 years (right). The hazard indicates a 10% probability that the peak values as indicated can be exceeded within 1 year (T=10), respectively within 10 years (T=100). Alternatively, the figures indicate an annual probability of 0.1 (T=10) or 0.01 (T=100) that the indicated peak values will be exceeded. The rate/year refers here to the to the average number of events per year with M ≥ 1.5. The x- and y-axis indicate distance in kilometers.*

5.3 Specific case: Bergermeer area

The Bergermeer reservoir is situated in the sandstones of the Rotliegend at a depth of about 2100 meters. Up till now the reservoir has experienced four earthquakes with magnitudes $3.0 \leq M \leq 3.5$, most probably situated along a major normal fault (see Figure 22). The seismicity is remarkable because of the lack of events smaller than 3.0. Till 1995 no monitoring seismograph stations have been operating in the region. Therefore smaller events, not felt by the population, may have occurred before that date, i.e. events with M smaller than approximately 2.0. Since 1995 three borehole seismometers and since 2002 three additional accelerometers have been operating around the Bergermeer area. Also since 1995 no events with $M \leq 3.2$ have been detected in and around the Bergermeer field. We estimate the detection level since 1995 to be around M = 0.5-1.0 (Dost and Haak, 2003: Appendix 3)

Logan et al. (1997) had difficulties in explaining why the 1994 earthquakes occurred in the middle of the field. However, the 1994 and 2001 events seem to indicate that all four events have relative locations that line up and probably coincide with the tip of a NW-SE striking normal fault in the reservoir (Figure 22). Their composite focal mechanism confirms the fault plane, but indicates a reverse fault suggesting a reverse re-activation of this normal fault. Hereby one should note that relative location is only possible if the event signals recorded from different events on the same sensor are highly correlated. This has been the case. This implies that their locations differ very little and all events have the same focal mechanism (Haak et al. 2001). The event location along this fault seem to favor the differential compaction hypothesis as proposed for Eleveld (Roest and Kuilman, 1994; Roest and Mulders, 2000) and seems to contradict the assumption by Logan et al. (1997) that fault-reservoir geometries would not have any significance in explaining the seismicity in the Bergermeer field.

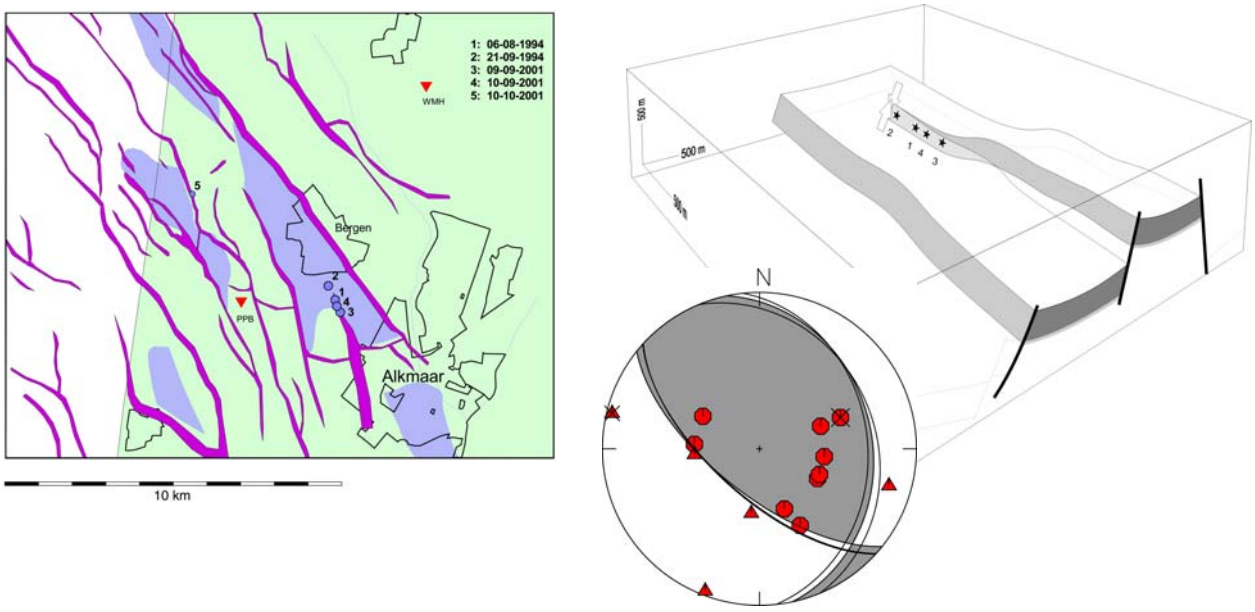

Figure 22. *From left to right; the locations of the earthquakes recorded in the Bergen and the Bergermeer field, the composite focal mechanism solution and a figure depicting the three dimensional schematic tectonics. The earthquake location, the obtained focal mechanism and the local tectonics (courtesy Amoco Netherlands BV) suggest reverse faulting on a reactivated (normal) fault (from Haak et al. 2001).*

Modelling the seismicity in Bergermeer is difficult with so few events. However, the seismic hazard seems to be of the same order as that for Roswinkel. Damage (cracks in masonry) has been reported for both the 1994 and the 2001 events (see also Figure 23). Applying the energy-magnitude relation of Ahorner and Pelzing (1985) in equation 11 we obtain for both fields of comparable size the same accumulated magnitude, i.e. 3.7 (Table 4 and 5). We have therefore used the Roswinkel seismicity model to estimate the seismic hazard; $\log N = 1.05 - 0.5\ M$. The obtained hazard maps are shown in Figure 24.

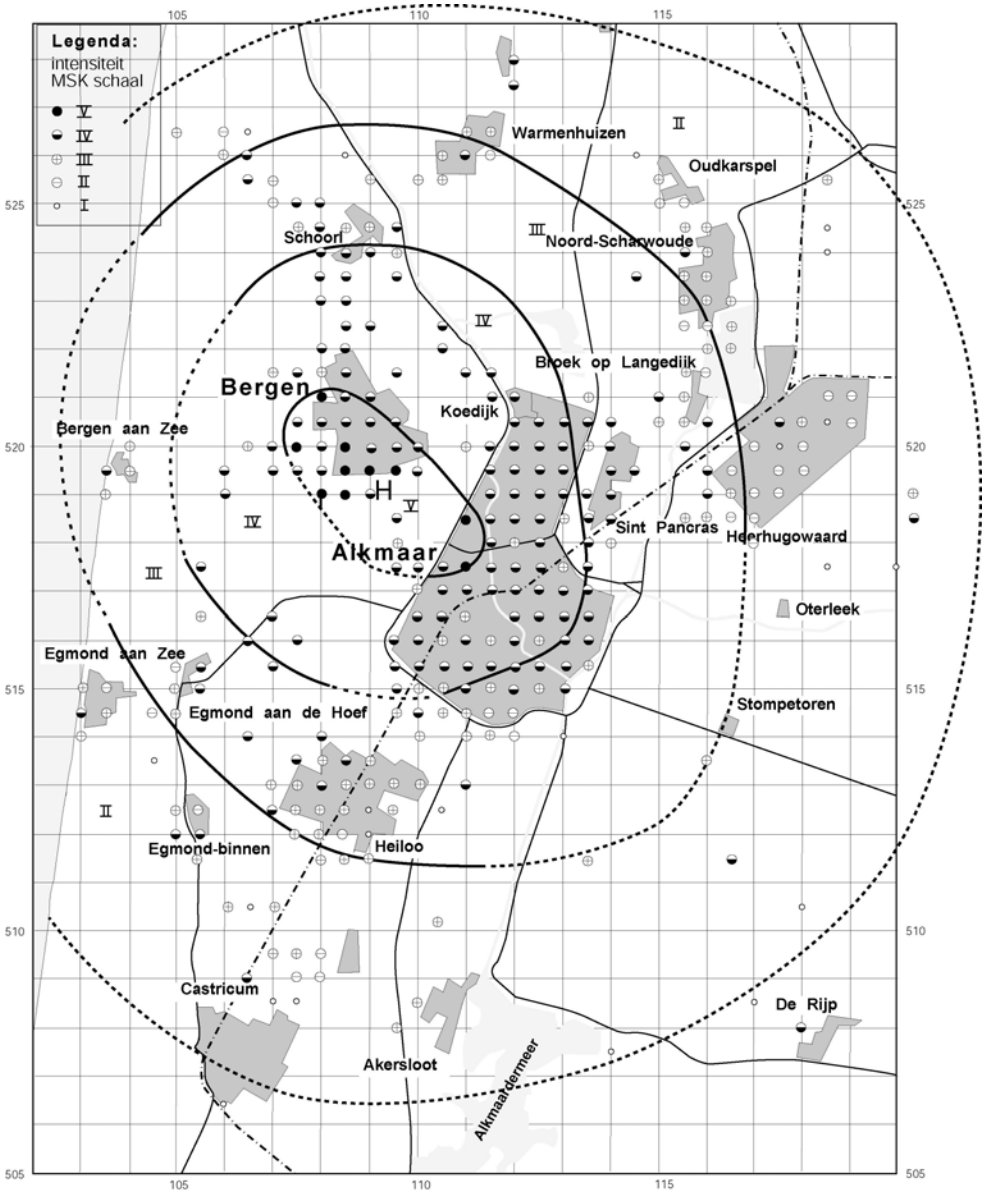

Figure 23. *Macroseismic map with the isoseisms for the M = 3.2 earthquake in the Bergermeer field on September 21, 1994 (from Haak, 1994b). The data, about 3500 macroseismic inquiry forms, is interpreted in the MKS scale. The data circles on the map are averaged values of the observed intensities in a 0.25 km^2 area. This macroseismic map provides the basis for a depth estimate between 1 and 2 km for the observed event (Haak, 1994b).*

Table 5. *Bergermeer field earthquakes and cumulative energy release as observed up to Nov 2003*

Date	M_L	M_w	Comments
06-08-1994	3.0	-	
21-09-1994	3.2	3.2*)	
09-09-2001	3.5	3.5**)	
10-09-2001	3.2	3.1**)	
	3.7		Cumulative magnitude

*) Haak (1994b); **) Haak et al. (2001)

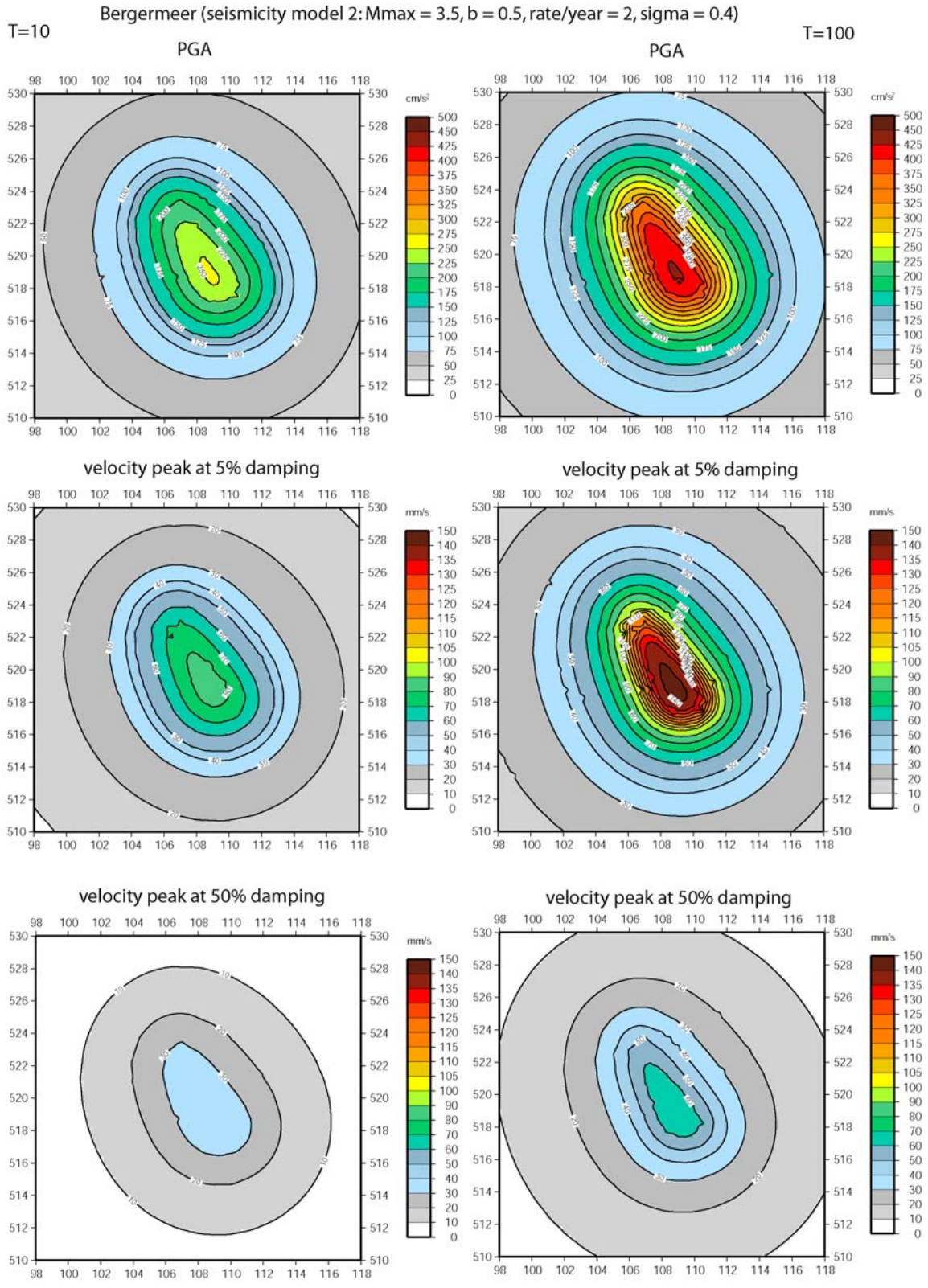

Figure 24. *Estimated hazard at and around the Bergermeer field. The hazard has been estimated for two return periods, i.e. T=10 years (left) and T=100 years (right). The hazard indicates a 10% probability that the peak values as indicated can be exceeded within 1 year (T=10), respectively within 10 years (T=100). Alternatively, the figures indicate an annual probability of 0.1 (T=10) or 0.01 (T=100) that the indicated peak values will be exceeded. The rate/year as in Figure 21.*

5.4 Specific case: Groningen area

The Groningen field represents the largest gas reservoir in The Netherlands and is situated in the sandstones of the Upper-Rotliegend of the Groninger High tectonic unit at varying depth ranging from about 3150 to 2600 meters (RGD, 1995). The first seismicity was observed in 1991, 28 years after the gas production in this field started. Since then the seismicity has been fairly stable at a rate of nearly 2 events per year with $M \geq 2.0$. The depth of the events recorded so far is estimated at around 3 km, but incorporates a large error, as explained in section 5.3. The recent events ($M_L = 3.0$ on October 24, 2003 and $M_L = 3.0$ on September 11) have been the largest events so far observed in the Groningen field area. Up till 2003 we have observed 179 events with magnitudes in the range $-0.2 \leq M \leq 3.0$. Many of the events seem to occur along NW-SE trending fault lines in the northwestern part of the gasfield, described in some more detail in Mulders (2003). As yet we have not been able to corroborate the hypothesis that the seismicity is related to specific fault zones.

The hazard studies have been performed based on the data until mid-October. The three events, $2.7 \leq M \leq 3.0$, that occurred in the period October-November 2003 changed the b-value estimate from b = 1.3 before, to b = 1.0 after that period (Figures 4 and 25). Although this will change little the current hazard estimates it is interesting to observe that the b = 1.0 approaches more the b-value as obtained by considering the seismicity in the whole of north of The Netherlands and can be interpreted as that larger events have been lacking up to autumn 2003.

Based on the observed seismicity up to mid-October 2003, the seismicity has been modeled as: $\log N = 2.7 - 1.3\,M$. This corresponds to nearly 6 earthquakes per year with $M \geq 1.5$.

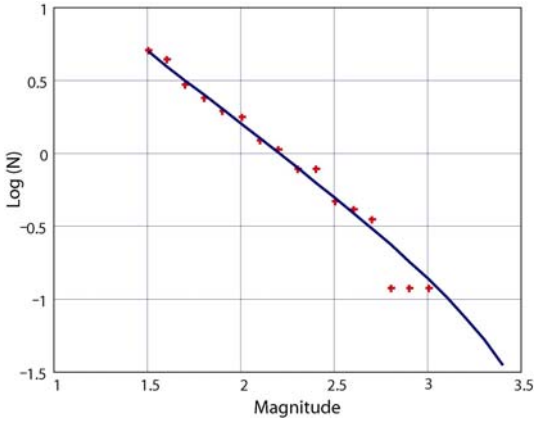

Figure 25. *Annual cumulative frequency-magnitude relation for all events associated with the Groningen field during the period 1986 – November 2003, and the best seismicity model fit characterized by the parameters a = 2.16 and b = 0.98.*

Two smaller gas reservoirs, close to the Groningen field, Annerveen and Eleveld, are also situated in the sandstones of the Upper-Rotliegend, and have been seen to cause significant induced seismicity. The Annerveen field has been discussed in Mulders (2003, chapter 7). The Eleveld field has its reservoir at a depth of 3300-3400 meters. Here the first event occurred in 1991, 16 years after the production started and when the pore pressure in the reservoir reached less than 1/3 of its original value (Roest and Kuilman, 1993). The movements in the Eleveld field have been modeled in detail by Roest and Kuilman (1993; 1994). They suggest a mechanism of differential compaction at opposite sides of a pre-existing normal fault. Unfortunately, the seismicity data for both the Annerveen and Eleveld fields are too limited to be analyzed separately. The seismicity rate is comparable to that of the Groningen field, therefore the obtained hazard estimates for the Groningen field (Figure 26) can also be applied to these fields.

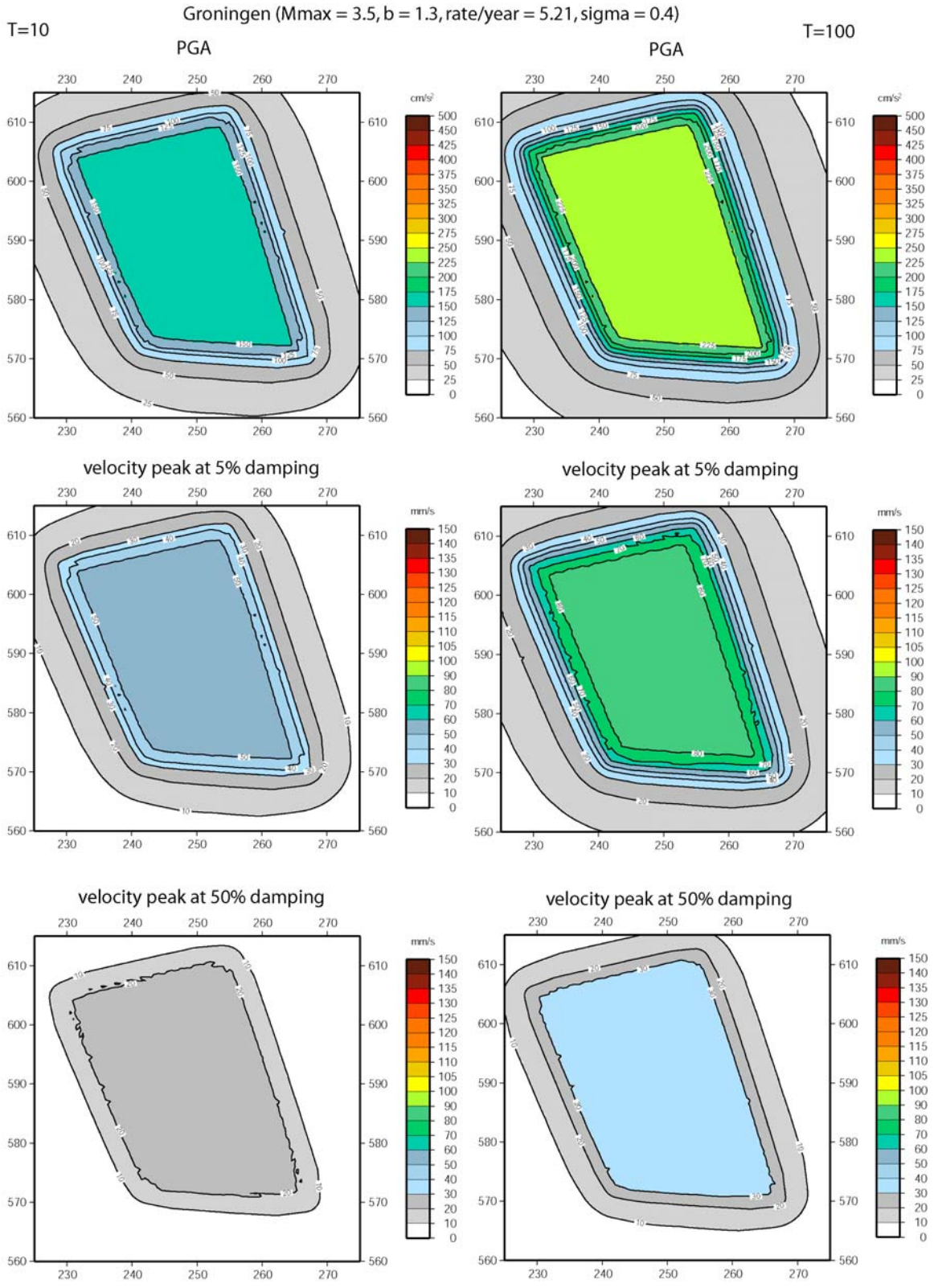

Figure 26. *Estimated hazard at and around a schematic Groningen field (about 945 km^2). The hazard estimates are presented as in Figure 16.*

5.5 Summary of the results

The results of the hazard analysis presented above can be summarized by simple hazard curves describing the hazard as a function of the distance to the border of an exploitation field (Figure 27). Three specific cases are presented: Roswinkel, Bergermeer and Groningen and essentially one generalized case, i.e. "hypothetical field". We also compared the hazard of this hypothetical field with one were we assume double seismicity rate per unit area (S2) to illustrate the influence of the rate of seismicity. The hazard curve of S2 is only marginally higher for T=100.

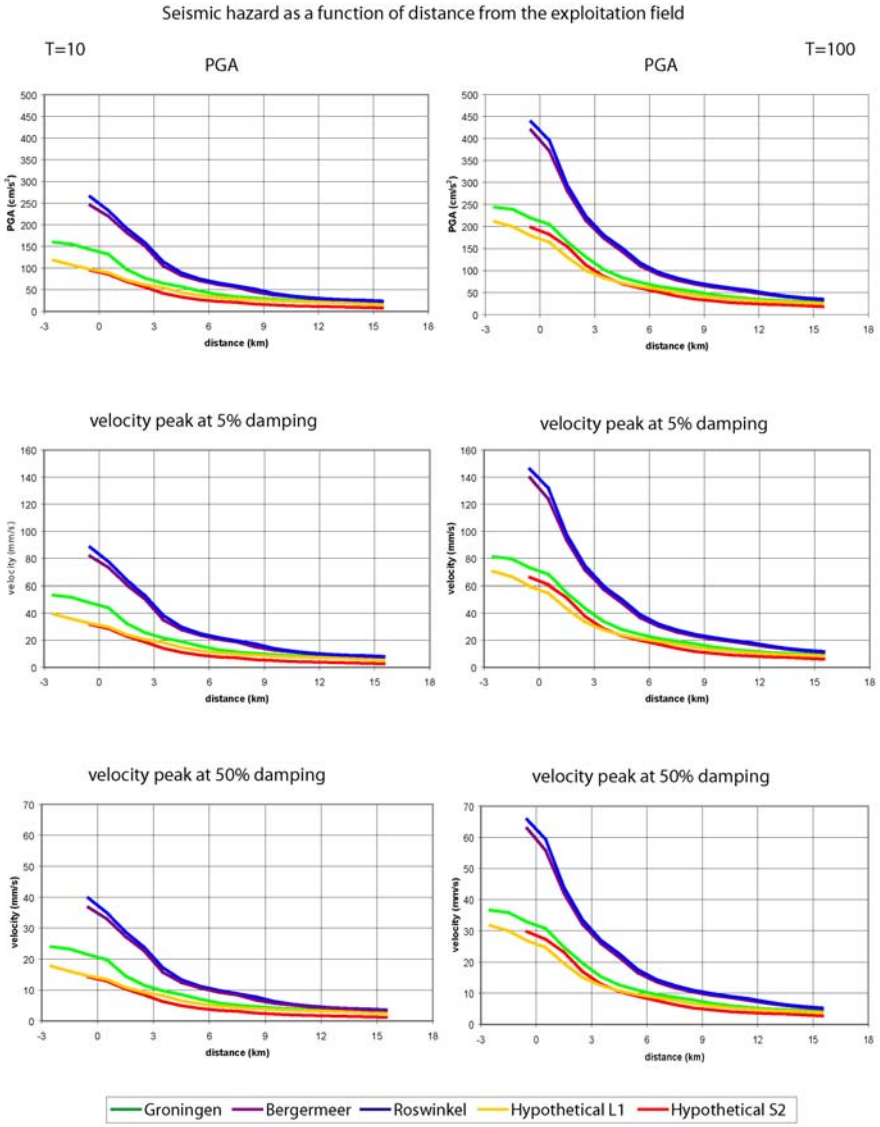

Figure 27. *Seismic hazard as a function of distance from the surface projection of the exploitation field. Five examples are shown: The Groningen, the Bergermeer and the Roswinkel field and two hypothetical fields, L1 and S2. From top to bottom are shown the PGA, velocity peak, V_{peak}, at 5% damping and at 50% damping respectively. The hazard is shown for two return periods, T=10 and T=100 years. These hazard curves have been used in the pragmatic approach to obtain seismic risk estimates*

6. Uncertainty analysis

6.1 Rate of seismicity

Stationary seismicity rate?
Our models assume a stationary seismicity rate. This is an obvious simplification: a) no seismicity will occur when no exploitation has been started, and b) seismicity rate changes are obvious at the beginning of the exploitation of the field and at the end of the production phase. Figure 5 suggests that it may take about two decades before induced events occur after the exploitation has been started. This is corroborated if we look at the individual fields where we have observed seismicity (Table 6). The one exception is the Appelscha field that showed seismic activity after just four years. Unfortunately, we are as yet unable to model these changes of the seismicity rate, because we lack a suitable physical or statistical model.

Table 6. *Gasfields, their production start and the first observed seismic event.*

Gasfield	Production start *)	First observed seismicity $M_L > 2.0$	M_L	Delay (years)	Comments
Roswinkel	1980	11-06-1992	2.7	12	
Sleen	1981	-	-	-	Stopped production
Bergermeer	1972	06-08-1994	3.0	22	
Bergen	1978	10-10-2001	2.7	23	
Groningen	1963	05-12-1991	2.4	28	
Eleveld	1975	26-12-1986	2.8	11	First event uncertain location
Annerveen	1973	16-08-1994	2.3	21	
Roden	1976	02-09-1996	2.1	20	
Dalen (Zechstein**?**)	1974	17-11-1996	2.2	22	Event association uncertain
Norg	1983	-	-	-	
Appelscha	1999	16-06-2003	2.3	4	
Emmen (Zechstein)	1977	15-02-1991	2.0	14	
Waalwijk	1991	None	-	-	2003: 12 years
Middelie (Zechstein**?**)	1975	01-12-1989	2.7	14	association uncertain.
Lacq (France)	1957	1969	3.0	12	First felt event Lahaie and Grasso (1999)

*) source NITG

Possible relations production and induced seismicity.
It is generally agreed that induced seismicity occurs on existing re-activated faults. Currently, at least two major hypotheses predict movement along pre-existing fault planes due to hydrocarbon exploitation (Segall et al. 1994; Zoback and Zinke, 2002):

a) Localized increased pore pressure due to water-flooding or injection, and
b) Poroelastic stress changes in the medium surrounding a compacting reservoir

On the one hand the last mechanism has been modeled assuming differential compaction for some gas (storage) fields in The Netherlands (Roest and Kuilman, 1993, 1994; Nagelhout and Roest, 1997) and seems to provide a probable model explaining the seismicity, specifically for the Eleveld field and Bergermeer field. This model suggests that reservoir geometry has a major significance in explaining the induced seismicity. This hypothesis of poroelastic stress changes seems also applicable on the Lacq gas field in France (Feignier and Grasso, 1990; Lahaie and Grasso, 1999), where they assume that production rate changes are causing the driving stress changes. On the other hand, so far no clear correlation between production rate and seismicity could be found for gasfields in The Netherlands.

No observed seismicity → no seismic hazard?
NITG (Scheffers, personal communication, 2003) observes that all earthquakes occur in 17 reservoirs located in the Perm group (Rotliegend: 13 reservoirs; Zechstein: 4 reservoirs). One reservoir with (significant) induced seismicity (Roswinkel) is situated in Trias. Alternatively, of all the reservoirs located in the non-Perm group only one, Roswinkel, has shown induced seismicity up till present. This observation seems to disagree with our highly simplified model of uniform spatial and Poisson temporal distribution. However, an explanation for this observation is as yet not available and it remains therefore difficult to model quantitatively in a seismic hazard analysis. At least two mechanical models exists that predict induced seismicity in and/or around hydrocarbon fields provided there are pre-existing faults. Therefore, we argue that there is a seismic hazard related to hydrocarbon

exploitation. It remains an open question if, for gasfields where no seismicity has been observed or where exploitations has not started yet, we should quantify this hazard more explicitly than as presented in De Crook et al. (1998).

6.2 Sensitivity study for Roswinkel

A sensitivity analysis using a limited logic tree has been made for the Roswinkel hazard analysis (section 5.2) in order to get some impressions of the influence of the different model and parameter assumptions. Different combinations of the parameters listed in Table 7 have been used to obtain the hazard curves as presented in Figure 28**.** Two extreme models and one average model have been highlighted. These results show the large range of uncertainties even with a relatively small range of model parameters. From the following sections we hope it will be clear that the uncertainties in the ground motion prediction equations or attenuation relations (i.e. σ) are probably the most significant. This conclusion corresponds with those of many other hazard studies (van Eck and Stoyanov, 1997).

Table 7. *Model parameters used for Roswinkel sensitivity study*

Seismicity models	1: N (M ≥ 1.5) = 8, b = 0.8
	2: N (M ≥ 1.5) = 2, b = 0.5
	3: N (M ≥ 1.5) = 2, b = 0.8
M_{max} parameter	3.5
	3.9
σ	0.2
	0.3
	0.4

6.3 Attenuation function and σ

The variations in hazard estimates due to different peak ground motion prediction equations are indicated in Figure 29. Although Campbell (1989) provided one of the few attenuation relation specifically estimated for small earthquakes it is inappropriate for our case of small and shallow earthquakes due to a significance depth dependence factor (see section 4.2). The Campbell (1997) and Dost et al. (2004) relations show small variations. As yet we have too little data to confirm which one is the most appropriate.

The variation introduced by the inherent uncertainty (σ) in the attenuation function for the Campbell (1997) relation is illustrated in Figure 30. Currently, we assume that the applied σ = 0.4 represents aleatory uncertainty, i.e. inherent to the unpredictability of the ground motion prediction equation, and cannot be reduced (Dost et al. 2004). However, the attenuation relation includes both a source mechanism and a site effect. The site effect can probably be more specific and the source mechanism seems to be consistent in some areas. Therefore, it may be possible to obtain more accurate ground motion prediction equations and thus a smaller variation, i.e. σ.

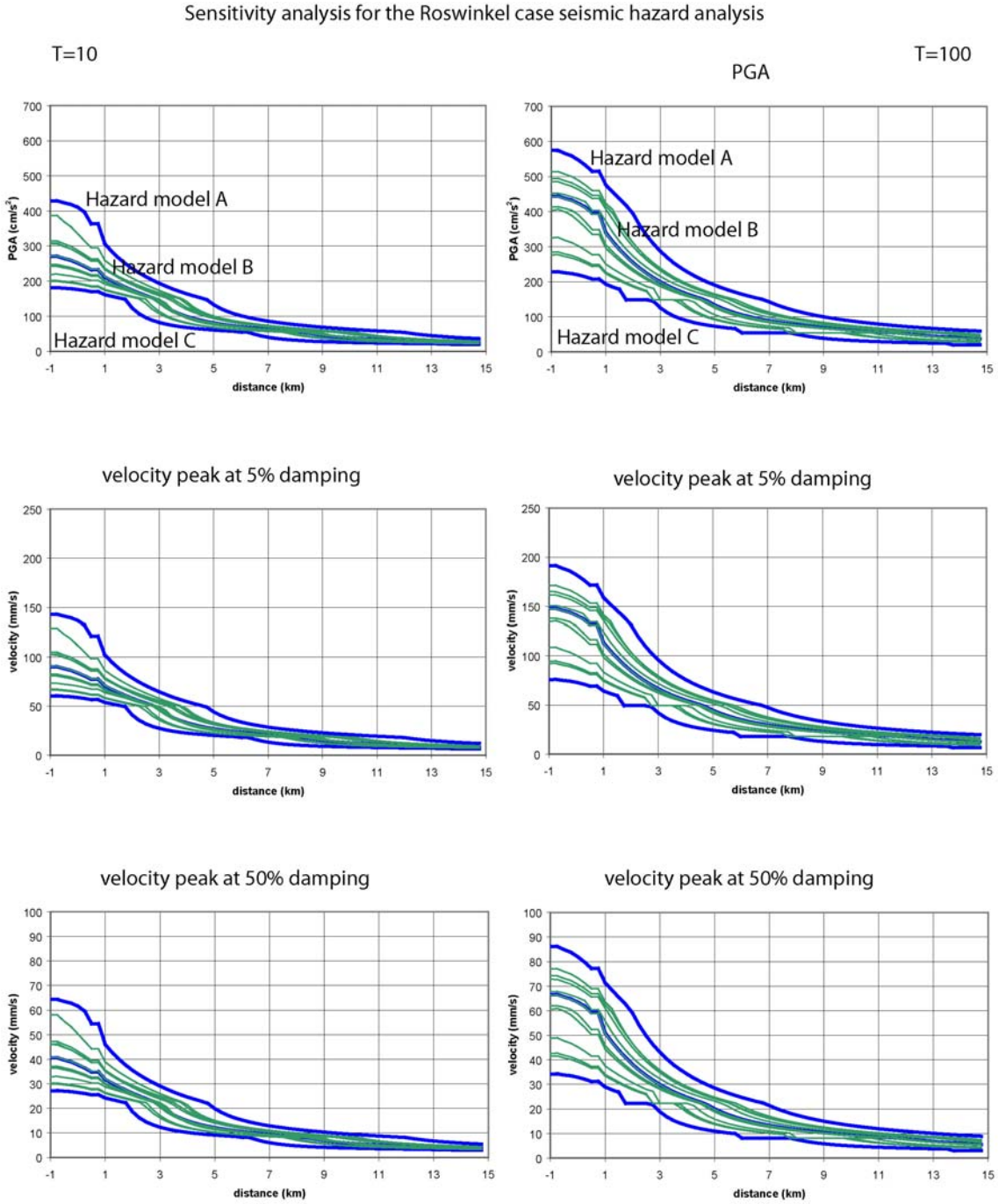

Figure 28. *Sensitivity analysis for the seismic hazard in the vicinity of the Roswinkel field for different model and parameter values. Left figures: hazard estimates for T=10. Right figures: hazard estimates for T=100.*
From top to bottom: the PGA, peak velocities for 5% and 50% respectively.
Two extreme models (A and C) and one average model (B) are indicated in blue. Other models are indicated in green.
Hazard model A (upper curve): seismicity model 1, i.e. N(M≥1.5)=8, b=0.8, M_{max} = 3.9 and σ = 0.4.
Hazard model B (middle curve): seismicity model 2, i.e. N(M≥1.5)=2, b=0.5, M_{max} = 3.5 and σ = 0.4.
Hazard model C (lower curve): seismicity model 2, i.e. N(M≥1.5)=2, b=0.5, M_{max} = 3.5 and σ = 0.2.

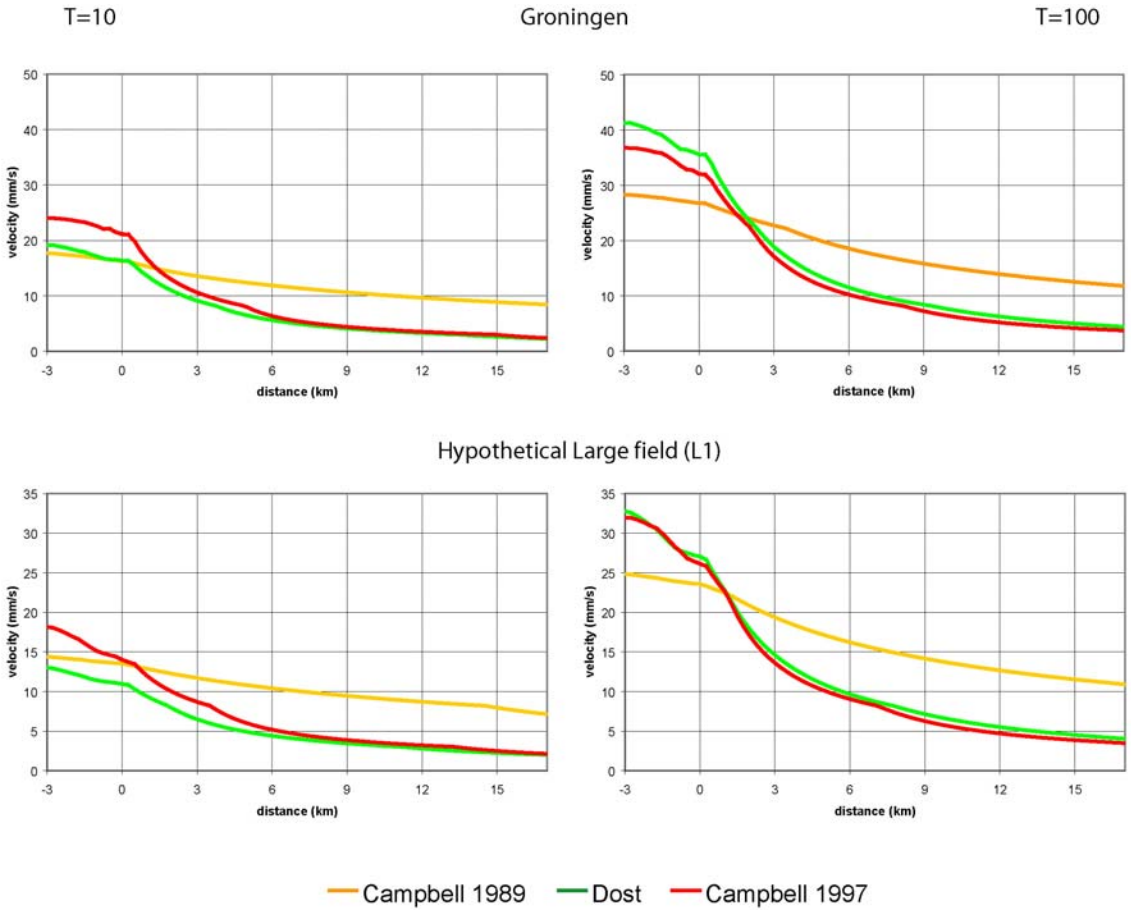

Figure 29. *Hazard curves for V_{max} for 50% damping obtained with different attenuation functions (see Figure 7). The curves refer to Campbell (1989), Campbell (1997) and Dost et al. (2004). Two cases are shown: The Groningen field and the hypothetical field. The comparison between Campbell (1997) and Dost et al. (2004) has been explained in detail in the original paper. The difference between Campbell (1989) and Campbell (1997) illustrates what possible differences can occur if attenuation functions are adapted without proper reference to local observed data.*

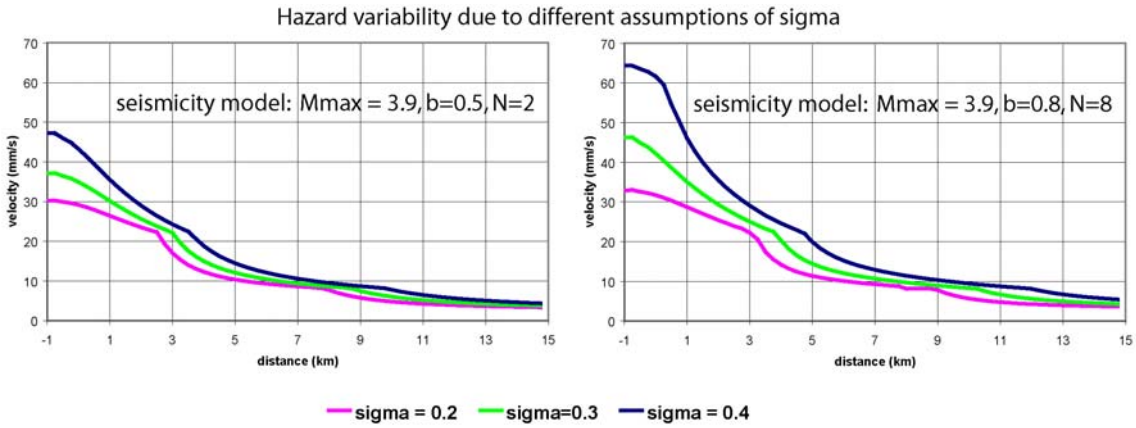

Figure 30. *Sensitivity analysis for variations in σ [0.2, 0.3 and 0.4 respectively], the standard deviation of ln (a_{max})as estimated with the attenuation function of Campbell (1997). Here we compare only the V_{max} at 50% damping. The left figure models the hazard in the Roswinkel field. When compared with Figure 28 it seems clear that this uncertainty provides the largest contribution to the uncertainties. The right figure models the hazard in the Groningen field.*

6.4 Maximum possible earthquake

The dependence of the hazard on variations in the M_{max} is shown in Figure 31. The hazard curves as proposed in this report are based on models in which we assume M_{max} = 3.5. Changing this to M_{max} = 3.9 will have little influence on the hazard estimates, as the probability of occurrence of these larger events is very small. This M_{max} effect seems consequently negligible compared with the uncertainties introduced by the ground motion prediction equations and other uncertainties.

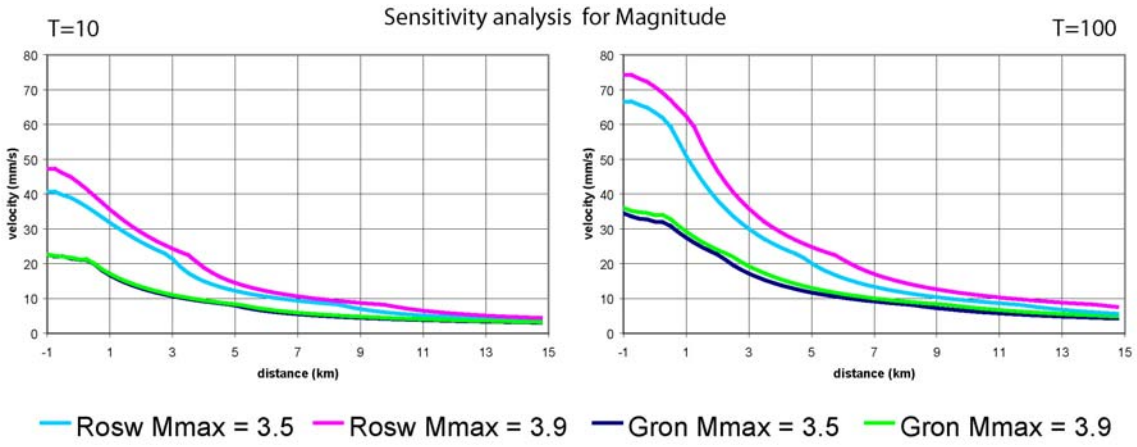

Figure 31. *Comparison of hazard curves as function of distance from the exploitation field as in Figure 27 for two different M_{max}, 3.5 and 3.9. Here we compare the V_{max} for 50% damping. The Groningen field case (left) and the Roswinkel field case (right) are shown. The maximum magnitude variation has minimal effect on the hazard and is practically negligible as compared to the uncertainties due to the attenuation variations (Figure 30).*

6.5 Seismic zonation

A systematic analysis with regard to different seismic zonation models is unrealistic. As yet we have observed too few seismic events to clearly characterize specific seismic active zones in or near an exploitation field. A possible exception may currently be the Groningen field. Here a possible concentration of seismicity seems to evolve, which may well be correlated with some existing faults systems (Figure 12). Although this is presently only a hypothesis to be tested, we can use this as a possible alternative source zonation model. Consequently, to give an impression of the associated uncertainty in the seismic hazard due to different zonation models we compared two seismicity distribution models: one in which the seismicity is uniformly distributed over the whole surface, as in our hazard models (section 5.4), and one in which seismicity is concentrated in four linear sources (a simplified fault model). The results, shown in Figure 32**,** indicate fairly large variations. Consequently, much may be gained by learning if specific faults have higher probabilities of seismic movements then others.

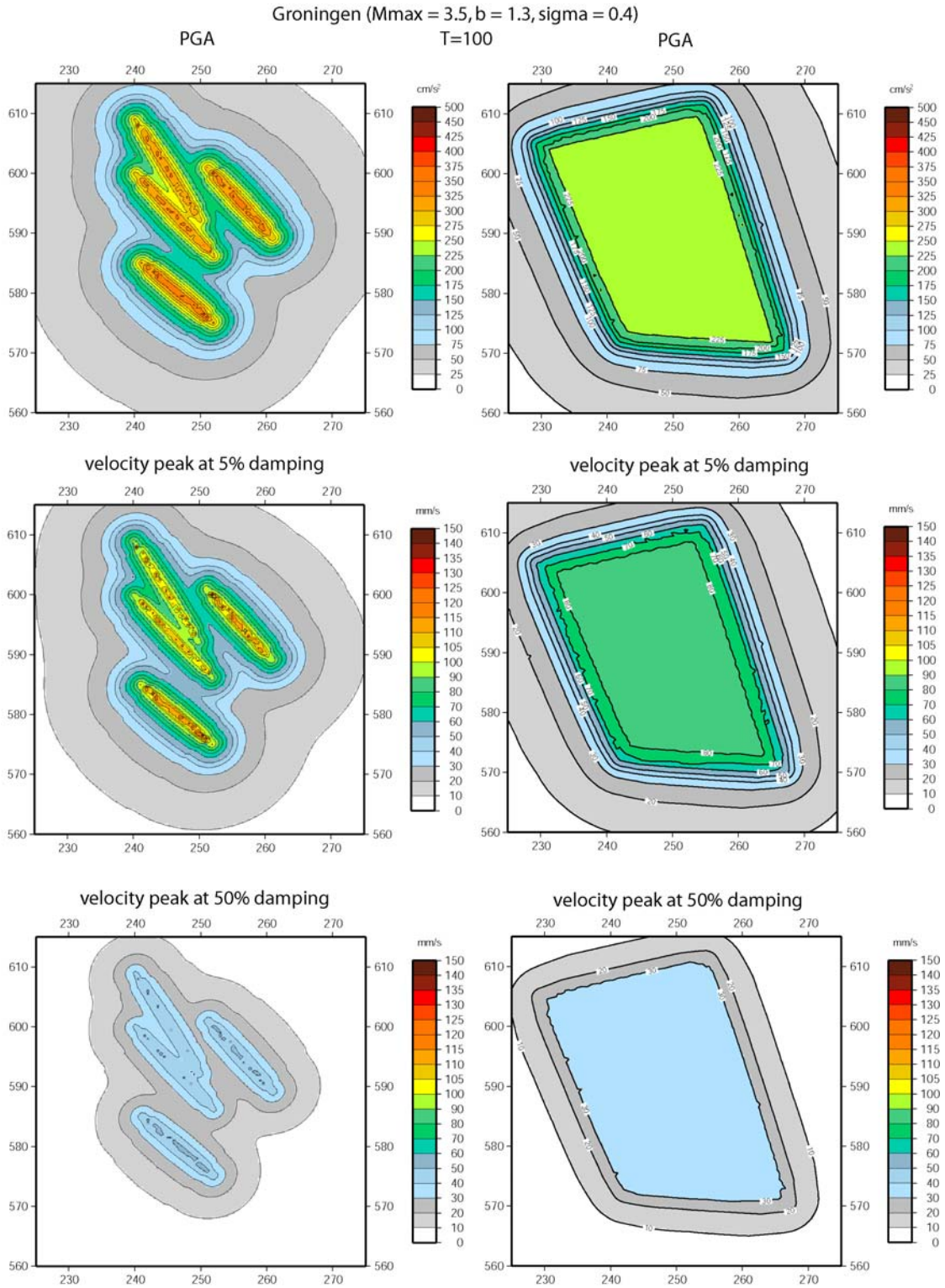

Figure 32. *Two source models used in a seismic hazard analysis for a schematic Groningen field and T=100. To the right the seismicity is assumed to be distributed homogeneously over the whole exploitation field. To the left the seismicity is assumed to be distributed over four main faults (here modeled as straight lines). The observed seismicity suggests some linear correlations that may be related to fault zones. This comparison gives an indication of the uncertainty due to the source modeling. In some areas the hazard increases in PGA from around 225 to 300-350 cm/sec^2. In other areas the hazard decreases in PGA from around 225 to about 100-125 cm/sec^2 and even lower. The x- and y-axis indicate distance in kilometers.*

6.6 Earthquake scenarios

An alternative way of looking at the hazard potential is to provide a scenario study, for example, a 'worst-case' scenario and a 'realistic' scenario. A 'worst-case' scenario could be an M = 3.9 event. Its probability of occurrence is very low. The 50% and 84% probability of exceedance of a specific ground motion as a function of epicentral distance is given in Figure 33. A 'realistic' scenario is an event with M ≥ 3.0, which may occur with a probability of 0.5 per year. Also for this case the 50% and 84% probability of exceedance of a specific ground motion as function of epicentral distance is given in Figure 15. This approach compares to a simplified version of the Safe Shutdown Earthquake (SSE) and Operation Based Earthquake (OBE) approach used for vulnerable structures like Nuclear Power Plants, Liquid Natural Gas or Oil storage plants, etc. (Reiter 1990).

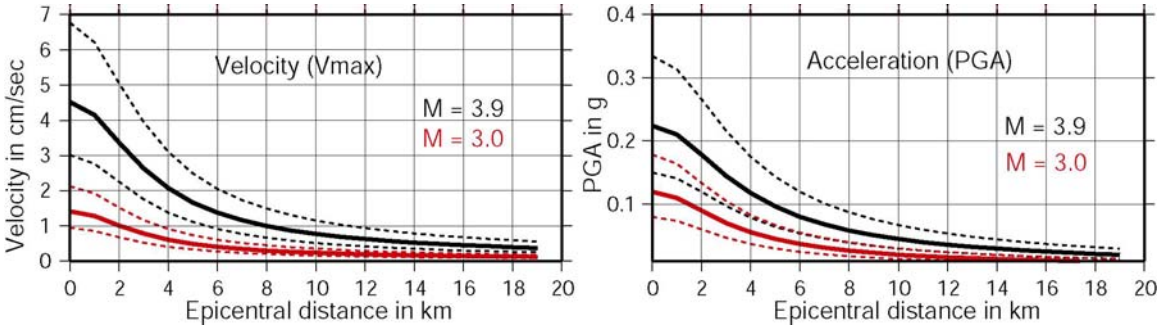

Figure 33. *The 16% probability (median - 1σ), 50% probability (median) and 84% probability (median + 1σ) of ground motion exceedance for the 'worst-case' scenario (black, M=3.9) and the 'realistic' scenario (red, M=3.0) for seismic hazard due to induced seismicity. In this case we have presented the hazard parameters PGA and V_{peak}.(50% damping).*

6.6.1 Earthquake scenario near Roswinkel

A scenario for the February 19, 1997 M = 3.4 induced event near Roswinkel can be directly related to the observed data. Our predicted PGV values are in Figure 34 compared with observed intensities from the macroseismic study by Dost and Haak (1997) for this event. The "observed" Intensities presented in Figure 35 are based on average values. An important conclusion is that the PGV/PGA - Intensity relations are clearly different from the ones used in California (Wald et al., 1999).

It is also clear from the macroseismic maps of the September 21, 1994 (Figure 23) and the February 19, 1997 (Figure 18) events that we observe fairly large local variations. A more appropriate Intensity – groundmotion relation deserves a systematic comparison involving both site response and focal mechanisms.

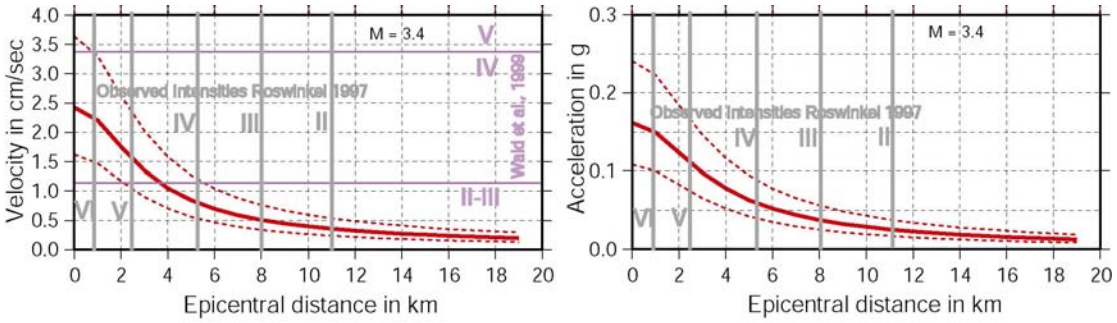

Figure 34*. Ground motion model (PGA and PGV) of Campbell (1997) and Intensity observations for the M=3.4 Roswinkel earthquake of 19 February 1997 (Dost and Haak, 1997). Also shown are the Intensity values as related to the PGV by Wald et al. (1999).*

Table 8. *Intensity versus ground motion for natural events.*

Intensity	I	II-III	IV	V	VI	VII	VIII	IX	X+
PGA %g *)	< 0.17	0.17-1.4	1.4-3.9	3.9-9.2	9.2-18	18-34	34-65	65-124	>124
PGA cm/sec^2 **)			<10	22	50	100			
PGV cm/sec *)	<0.1	0.1-1.1	1.1-3.4	2.3-8.1	8.1-16	16-31	31-60	60-116	>116

*) Wald et al. (1999) (used Modified Mercally scale)

**) De Crook (1996) seismic zoning map for The Netherlands conforming to Eurocode-8 (MSK-scale)

7. Discussion

7.1 Models and methodology

We propose to use the PSHA to obtain first-order hazard estimates due to induced earthquakes in The Netherlands. It provides hazard probabilities in terms of ground motion for specific sites. The obtained hazard estimates are easy to associate with engineering interpretations and further risk analysis, but require more effort to explain to the general public (Wang et al., 2003). A deterministic approach or earthquake scenarios, in which hazard is estimated for hypothetical events, may be easier to understand, but may become confusing when different hazard scenarios are, and need to be, considered.

The validity of the PSHA.
Statistical (extrapolation) methods as the PSHA have been and still are criticized as being inappropriate in cases where you have too little data (Castaños and Lomnitz, 2002; Krinitzky, 2002a, Wang et al., 2003). Lack of seismicity data is, as in many seismic hazard estimates, the limiting factor for the induced seismicity in the north of The Netherlands. However, if a quantitative seismic hazard estimate is required, then the PSHA is one of the best possible approaches available at the moment. If provided with a transparant seismic hazard model and a clear sensitivity analysis it should do the job: model the probable ground motion at a site due to the occurrence of earthquakes. Both aspects, transparency and a sensitivity analysis, have been considered in this study. However, verifying seismic hazard estimates, comparing earthquake scenarios with past cases, can make the model stronger. A tentative approach in this direction has been presented, but a more thorough verification is required.

Hazard and risk
The seismic hazard estimates presented in this report and complemented with the site response effect in Wassing et al. (2003, 2004) are put into context by TNO-bouw using damage estimates associated with the presented hazard. The result is a risk estimate with regard to possible damage to buildings, but provides too small a basis for a sensible cost-benefit analysis (see also Snieder and Van Eck, 1997 and RIVM, 2003). However, a simplified approach considering the social aspects of the risk should accompany a clear presentation and explanation of the obtained hazard estimates to the public.

No observed seismicity → No hazard?
For fields that have been in production for a long time and where no seismicity has been detected, we should make a clear difference between the statements: “There is no hazard” and “We don’t know the hazard”. For fields where no seismicity has been observed so far, the last statement is more appropriate. As explained above we know very little about the hazard in these cases and it remains difficult to assign a relevant PSHA model. For example, a model with uniform seismicity, as in the proposed hypothetical model would indeed predict some seismic hazard also for fields with no seismicity. However, a model that predicts more accurately the few large events, like in the Bergermeer field, could very well be more appropriate. However, assuming no hazard at all is difficult to maintain with the current knowledge that induced seismicity has the same driving mechanism as natural seismicity: stress build up and/or fault lubrication. Consequently, it is difficult to provide a well-motivated argument for a specific model that quantifies the hazard in these cases. It seems more appropriate in these cases to express the hazard in qualitative terms.

7.2 Ground acceleration versus ground velocity and Intensity

Small and shallow earthquakes generate fairly high PGA values as compared to those for large earthquakes rupturing the seismogenic zone of the crust. This is shown in our observations, but also in those of others elsewhere (Fletcher et al., 1983; McGarr and Bicknell, 1990; Ahorner, 1997 personal communication; Wu et al., 2003). However, the observed intensity, which is risk related, remains smaller than those compared with similar PGA values due to large earthquakes (see Figure 34). For example, PGA values larger than 0.2g are usually associated with damage in the case of large earthquakes (Martinez-Pereira and Bommer, 1998; Wald et al., 1999), while we observe for induced earthquakes much larger PGA values, but little damage. This seeming contradiction can be explained.
First, small shallow earthquakes cause short, but apparently large, acceleration pulses at the surface. Short strong accelerations cause much less damage than similar size accelerations with longer duration.
Second, Intensities are partly based on people perceptions (low intensities) and partly on damage (higher intensities). Low Intensity (< VI) values rely mostly on how people perceive the vibrations

caused by earthquakes. Experience from both Taiwan (Wu et al., 2003) and the US (Wald et al., 1999) show that this perception depends more on the PGA then on the PGV. On the other hand Schenk et al. (1990), Van Staalduinen and Smits (1993), Boatwright et al., (2001) and Wu et al. (2003) found that the peak velocity as presented above is a better indicator for damage and thus correlates better with the higher intensity values (> V).

Consequently, if damage aspects are of importance in a risk analysis the peak velocity (or PGV) seem to be more appropriate. If people's perception of the ground shaking is of concern in the risk analysis the PGA seems more appropriate. Both aspects are relevant for the induced seismicity in The Netherlands. A relation between PGA or PGV for shallow, small events and low intensity values still needs to be established.

For the damage aspect the international guidelines with respect to vibrations due to explosions (SBR, 2002), i.e. short duration, are therefore also defined in terms of velocity. Unfortunately, these international guidelines show a level of tolerance that is significantly different from country to country (Van Staalduinen and Geurts, 1998) unlike the European and American scale earthquake design criteria in the Eurocode-8 (CEN, 2002) and the NEHRP provisions (Borcherdt, 2002) .

7.3 Ground motion prediction equations

This study shows large uncertainties in the ground motion prediction relations for shallow and small earthquakes. By comparing international empirical attenuation relations with our limited acceleration database at the KNMI, we have been able to keep these uncertainties within reasonable bounds. This accelerometer data gathered in The Netherlands is unique for small and shallow earthquakes. Very little similar data is available elsewhere. But this data is crucial in putting constraints on the uncertainties in the ground motion prediction equations.
A regular update using additional accelerometer data from the KNMI network may further reduce these uncertainties. Such an update, combined with an extensive analysis of the observed earthquake mechanisms and the site response effects, will improve our attenuation relations and reduce the uncertainties. In our current study we lacked acceleration data for shallow and small events at distances beyond 3 km from the epicenter in order to establish reliable ground motion prediction equations for the north of The Netherlands.

7.4 Suggestions for further studies

Continuous monitoring of the seismicity and the ground motion .
Seismic hazard analysis is presently mainly based on observed induced seismicity. Causal relations between exploitation and induced seismicity can only be attempted if high quality observations of the induced events are available. Consequently, monitoring induced seismicity with high-quality instrumentation remains crucial both for a better understanding of the induced seismicity and verifying possible damage claims. Continuous and improved monitoring of the seismicity aimed at an optimal detection and location, and high-quality digital event registrations, is a minimum requirement. Strong motion instruments that measure the ground acceleration/velocity are indispensable here. Such measurements will provide better constraints on the expected hazard and provide the only physical measurements in case of legal disputes.

Earthquake mechanism studies.
The seismicity pattern as observed near Roswinkel up till now suggests an association with a number of faults on top of the reservoir (Figure 20). The often similar seismic signals suggest a preference for certain focal mechanisms. As shown in Figure 35 the S-wave amplitude is extremely dependent on this earthquake mechanism. Therefore, significant PGA values may be observed in one direction and much lower values in another azimuthal direction. Consequently, the ground motion, as observed at the surface, seems to depend strongly on the earthquake mechanisms. The observed mechanisms of events near Roswinkel seem fairly consistent. This deserves a systematic analysis.

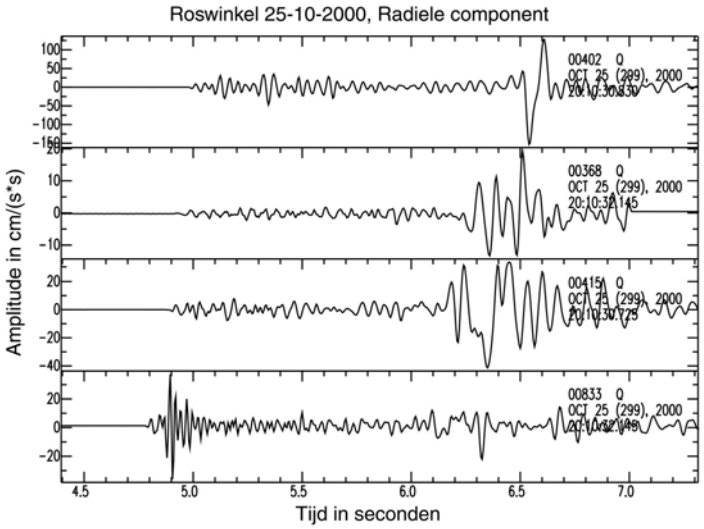

Figure 35*. The Roswinkel 25-10-2000 event (ML = 3.2) recorded by four accelerometers surrounding the epicenter. Only the radial components are shown. The P-wave and S-wave amplitudes are clearly dependent on the earthquake mechanism radiation patterns. This makes the records suitable for focal mechanism solutions. However, it also indicates the high variability of the ground motion acceleration due to the earthquake mechanism.*

Attenuation and site response.
Presently, the site response is mainly theoretical and lacks a quantitative uncertainty (Wassing et al., 2003, 2004) and the ground motion prediction equation is a general application. A systematic verification with all observed accelerations, Intensities and surface geology combined into one statistical model can most probably reduce and quantify the involved uncertainties. The KNMI is gathering an impressive database of ground motion data and observed Intensities. This will help obtaining an improved relation between ground velocity and observed intensity and enable interpreting older intensity datasets. New methods in site response estimation (Fäh et al., 2001; Scherbaum et al., 2003), combined with additional ground motion measurements, will provide an observational validation of possible site effects.

Microearthquake investigations.
Induced seismicity occurs in most exploitation fields (Zoback and Zinke, 2002; Phillips et al., 2000; Rutledge et al., 1998). Presently, we assume that the occurrence of microearthquakes is related to the occurrence of small, induced earthquakes that are felt at the surface. Yet, the existing monitoring network around the exploitation fields seldom observes events with $M_L < 0.0$. In fact the detection limit in the north of The Netherlands does not reach below $M_L = 0.5$. Only in some areas we may be able to locate events down to $M_L = 0.5$ (requiring detection by a minimum of three stations). However, a three weeks experiment near Roswinkel with three borehole seismometers at a depth of around 2 km shows the occurrence of a minimum of 39 microearthquakes down to a magnitude of M = -6 (Jupe et al., 2001). Although earthquake damage is probably only relevant for induced events with magnitude M_L larger then approximately 3.0, it seems very plausible that microearthquake investigations at depth could shed more light on the occurrence of relatively large induced events (for example, which faults are active, where and to what extent). It is therefore recommended to find methods to perform effective long-term microearthquake investigations.

Systematic parameter correlation study.
The causal relation between small, induced events and mechanical properties of the reservoir is presently unclear. There are a number of indications that there may be some statistical relations (Sheffers, 2003 personal communication; Feignier and Grasso, 1990). Tentative correlation studies have been performed for individual fields and showed little results (Van Eijs and Scheffers, 2000). However, thus far no systematic correlation study has been performed combining the extensive database of the exploitation companies and the observed seismicity. Assuming induced seismicity occurs in a gas field due to man made stress changes applied to existing faults, it remains to be explained why some gas fields do not display seismic events while other fields do. At least three questions needs to be answered:

a) When does seismicity start in a gasfield that is being exploited?
b) When is seismic movement preferred above aseismic movement?
c) What are the statistical probabilities of no occurrence of seismicity in a simple model?

Although this proposed correlation study may not provide adequate answers, especially as induced seismicity does not differ from natural seismicity in its unpredictability, it may provide some more insight in the driving mechanisms and possible constraints.

8. Conclusions

Long-term detailed monitoring in the north of The Netherlands has provided a unique and fairly good statistical description of induced seismicity due to hydrocarbon exploration in this region. Reducing the uncertainties in the hazard estimates require a continued and upgraded monitoring combined with a broadly oriented research effort.

In essence the conclusions as presented by De Crook et al. (1998) and Van Staalduinen and Geurts (1998) seem still valid. In general there exists a relation between exploitation and seismicity, but at present it is very difficult to quantify this for specific exploitation fields. However, the new Dutch mining legislation requires a more quantitative approach of the seismic hazard with the advantage that it, among other things, stimulates research to improve the seismic hazard estimates (Haak, 2000). In this report we conclude that seismic hazard analysis for induced seismicity due to hydrocarbon exploitation in The Netherlands still suffers from large uncertainties. Some of these uncertainties can be decreased significantly. In summary the major complications in this seismic hazard analysis are:

- We are as yet unable to make clear correlations between exploitation and induced seismicity causing damage. Since 1986 we have observed significant activity at some fields and no seismicity at other fields. Presently, we cannot find a satisfactory explanation.
- Induced earthquakes causing hazard are small and occur at a shallow depth. For these events we found from an extensive literature search that the relation between ground motion characteristics and risk is less well known. This complicates a pragmatic hazard analysis. In this report we present a first order approximation.
- For larger hydrocarbon exploitation fields with a long production period and no observed seismicity (M>1.5) it is as yet not possible to make a valuable quantitative hazard analysis.

Therefore we propose the following basic procedure:

- For exploitation fields that have shown significant seismicity the above proposed seismic hazard analysis is appropriate. Such fields are, for example, the Groningen field, the Roswinkel field and the Bergermeer field. In this report we present the procedure for such a hazard analysis.
- For large exploitation fields with a long production time and no observed seismicity (M>1.5) a quantitative seismic hazard analysis is presently unrealistic. For these fields induced seismicity cannot be excluded and only a tentative scenario can be provided. In this report we propose a procedure for such a hazard analysis based on such a tentative scenario as presented in section 5.1.
- Seismic hazard analysis with respect to hydrocarbon exploitation should be considered as a process undergoing continuous updating as new knowledge emerges. This requires however a continuous effort to improve monitoring and to do research into the relation between exploitation and induced seismicity. In this report we propose a number of concrete issues to consider for improved monitoring and future research.

Acknowledgements
We thank those who have contributed in the discussions, TPA and Tcbb members, Mirano Spalberg and those who have helped us obtain a fairly complete overview of the available reports, papers, data, etc. We thank TNO-NITG “Deep Underground” for supplying the relevant exploitation information required for parts of our work. We thank Julian Bommer for a concise review and initiating new interesting discussions.

References

Ahorner, L. and R. Pelzing, 1985. The source characteristics of the Liège earthquake on November 8, 1983, from digital recordings in West Germany. In: P. Melchior (ed), *Seismic activity in Western Europe*. D. Reidel, Dordrecht, 263-289.

Ambraseys, N.N., 1995. The prediction of earthquake peak ground acceleration in Europe. *Earthq. Eng. Struct. Dyn.*, **24**, 467-490.

Baranova, V., A. Mustaqeem and S. Bell, 1999. A model for induced seismicity caused by hydrocarbon production in the Western Canada Sedimentary Basin. *Can. J. Earth Sci*., **36**, 47-64.

Begeleidingscommissie Onderzoek Aardbevingen (BOA), 1993. *Eindrapport multidisciplinair onderzoek naar de relatie tussen gaswinning en aardbevingen in Noord-Nederland*. 76 pp.

Bender, B. and D.M. Perkins, 1987. SEISRISK III: A computer program for seismic hazard estimation. US Geological Survey. Bulletin 1772. Washington. 48 pp.

Boatwright, J., K. Thywissen and L.C. Seekins, 2001. Correlation of ground motion and Intensity for the 17 January 1994 Northridge, California, Earthquake. *Bull. Seismol. Soc. Am.*, **91**, 739-752.

Bommer, J.J., 2002. Deterministic vs. probabilistic seismic hazard assessment: an exaggerated and obstructive dichotomy. *J. Earthquake Engineering*, **6**, 43-73.

Bommer, J.J., 2003. Uncertainty about uncertainty in seismic hazard analysis. *Engineering Geology*, **70**, 165-168.

Borcherdt, R.D., 1994. Estimates of site-dependent response spectra for design (methodology and justification). Earthquake Spectra, **10**, 617-653.

Borcherdt, R.D., 2002. Empirical evidence for acceleration-dependent amplification factors. *Bull. Seismol. Soc. Am.*, **92**, 761-782.

Borcherdt, R.D., 2003. Erratum. *Earthquake Spectra*, **19**, 453-454.

Bungum, H., C.D. Lindholm, A. Dahle, G. Woo, F. Nadim, J.K. Holme, O.T.Gudmestad, T. Hagberg and K. Karthigeyan. New seismic zoning maps for Norway, the North Sea, and the United Kingdom. *Seismol. Res. Lett*., **71**, pp 687-697.

Campbell, K.W., 1989. The dependence of peak horizontal acceleration on magnitude, distance, and site effects for small magnitude earthquakes in California and Eastern North America. *Bull. Seismol. Soc. Am.*, **79**, 1311-1339.

Campbell, K.W., 1997. Empirical near-source attenuation relationships for horizontal and vertical components of Peak Ground Acceleration, Peak Ground Velocity, and Pseudo-absolute acceleration response spectra. *Seismol. Res. Lett*., **68**, 154-179.

Campbell, K.W., 2000. Erratum. "Empirical near-source attenuation relationships for horizontal and vertical components of Peak Ground Acceleration, Peak Ground Velocity, and Pseudo-absolute acceleration response spectra". *Seismol. Res. Lett*., **71**, 352-354.

Campbell, K.W., 2001. Erratum. "Empirical near-source attenuation relationships for horizontal and vertical components of Peak Ground Acceleration, Peak Ground Velocity, and Pseudo-absolute acceleration response spectra". *Seismol. Res. Lett*., **72**, 474.

Campbell, K.W., 2003. Chapter 5. Engineering models of strong ground motion. In: Earthquake Engineering handbook, W.-F. Chen and C. Scawthorn (eds), CRC Press, Boca Raton, FL, USA. pp 5-1 – 5-76.

Campbell, K.W. and Y. Bozorgnia, 2003. Updated Near-source Ground motion (attenuation) relations for horizontal and vertical components of peak ground acceleration response spectra. *Bull. Seismol. Soc. Am*., **93**, 314-331.

Castaños, H. and C.Lomnitz, 2002. PSHA: is it science? *Engineering Geology*, **66**, 315-317.

CEN, 2002. Eurocode 8: *Design of structures for earthquake resistance. Part 1: General rules, seismic actions and rules for buildings.* Draft No 5, prEN 1998-1:200x.

Chen, W.-F. And C. Scawthorn (editors), 2003. *Earthquake Engineering Handbook*. CRC Press LLC.

Cornell, C.A., 1968. Engineering seismic risk analysis. *Bull. Seismol. Soc. Am*., **58**, 1503-1606.

Cornell, C.A. and H.A. Mertz, 1975. Seismic risk analysis of Boston. *J. Structural Div*. **ST10**, 2027-2043.

Cypser, D.A. and S.D. Davis, 1998. Induced seismicity and the potential for liability under U.S. law. *Tectonophysics*, **289**, 239 – 255.

De Crook, Th., 1996. A seismic zoning map conforming to Eurocode 8, and practical earthquake parameter relations for The Netherlands. *Geologie en Mijnbouw*, **75**. 11-18.

De Crook, Th., B. Dost en H.W. Haak, 1995. Analyse van het seismisch risico in Noord-Nederland. KNMI Technisch Rapport TR-168., 30 pp.

De Crook, Th., H.W. Haak en B. Dost, 1998. Seismisch risico in Noord-Nederland. KNMI Technisch Rapport TR-205, 24 pp.

Dobry, R., R.D. Borcherdt, C.B. Crouse, I.M. Idriss, W.B. Joyner, G.R. Martin, M.S. Power, E.E. Rinne and R.B. Seed, 2000. New site coefficients and site classification system used in recent building seismic code provisions. *Earthquake Spectra*, **16**, 41- 67.

Dost, B., T. van Eck and H. Haak, 2004. Scaling peak ground acceleration and peak ground velocity recorded in The Netherlands. *Bolletino di Geofisica*, In print.

Dost, B. en H.W. Haak, 1997. Macroseismische waarnemingen Roswinkel19-2-1997. TR-199, 5 pp.

Dost, B. and H. W. Haak, 2004. Seismicity. In: Wong, Th.E., D.A.J. Batjes and J. de Jager (eds.) Geology of The Netherlands. *in print*.

Feignier, B. and J.R. Grasso, 1990. Seismicity induced by gas production: I. Correlation of focal mechanisms and dome structure. *Pure and Applied Geophysics*. **134**, 405-426.

Fletcher, J.B., J. Boatwright and W.B. Joyner, 1983. Depth dependence of source parameters at Monticello, South Carolina. *Bull. Seismol. Soc. Am.*, **73**, 1735 – 1751.

Frikken, H.W., 1999. Reservoir-geological aspects of productivity and connectivity of gasfiels in the Netherlands. Thesis TU Delft, 91 pp.

Fäh, D., F. Kind and D. Giardini, 2001. A theoretical investigation of average H/V ratios. *Geophys. J. Int.*, **145**, 535-549.

Grasso, J.R., 1992. Mechanics of seismic instabilities induced by recovery of hydrocarbons. *Pure Apppl. Geophys.*, **129**, 507-533.

Grasso, J.R., P. Volant and D. Fourmaintraux, 1994. Scaling of seismic response to hydrocarbon production: A tool to estimate both seismic hazard and reservoir behaviour over time. Eurorock 94 contribution. 8 pp.

Grasso, J.R. and D. Sornette, 1998. Testing self-organised criticality by induced seismicity. *J. Geophys. Res*., **103**, 29,965-29,987.

Grünthal, G. ed. 1998. European Macroseismic Scale 1998. Cahiers du Centre Européen de Géodynamique et de Séismologie, Conseil de L'Europe, 15, Luxembourg, 99 pp.

Grünthal, G. and R. Wahlström, 2001. Sensitivity of parameters for probabilistic seismic hazard analysis using a logic tree approach. *J. Earthq. Engineering*, **5**, 309-328.

Gupta, A.K., 1990. *Response Spectrum Method: In seismic Analysis and Design of Structures.* CRC Press. 170 pp.

Haak, H.W., 1994a. Seismische analyse van de aardbeving bij Alkmaar op 6 augustus 1994. KNMI Report TR-166, 17 pp.

Haak, H.W., 1994b. Seismische analyse van de aardbeving bij Alkmaar op 21 september 1994. KNMI Report TR-167, 21 pp.

Haak, H.W., 2000. Aardbevingen en mijnbouwkundige activiteiten. In: Technische Workshop "Geinduceerde Aardbevingen in Noord-Nederland", De Bilt 7 Nov 2000.

Haak, H.W. and T. de Crook, 1993. Seismische analyse van aardbevingen in Noord-Nederland. Raport KNMI, 38 pp.

Haak, H.W., B. Dost and F.W. Goutbeek, 2001. Seismische analyse van aardbevingen bij Alkmaar op 9 en 10 september en Bergen op Zee op 10 oktober 2001. KNMI Report TR-239, 24 pp.

Hanks, T.C. and H. Kanamori, 1979. A moment magnitude scale. *J. Geophys. Res*., **84**, 2348-2350.

Houtgast, G., 1992. *Aardbevingen in Nederland; catalogus van aardbevingen t/m mei 1992*. KNMI publication 179, 166 pp.

Jaynes, E.T., edited by G.L. Bretthorst, 2003. *Probability theory. The logic of science.* Cambridge University Press, 727 pp.

Jupe, A., S. Wilson, D. Raymer and R. Jones, 2001. Roswinkel (RSW-1) microseismic monitoring trial (August/September 2001). ABB Offshore systems Ltd Report for NAM. 33 pp. (confidential)

Kagan, Y.Y., 1993. Statistics of characteristic earthquakes. *Bull. Seismol. Soc. Am.*, **83**, pp 7-24.

Krinitzky, E.L., 2002a. Epistematic and aleatory uncertainty: a new shtick for probabilistic seismic hazard analysis. *Engineering Geology*, **66**, 157-159.

Krinitzky, E.L., 2002b. How to obtain earthquake ground motion for engineering design. *Engineering Geology*, **65**, 1-16.

Lahaie, F and J.R. Grasso, 1999. Loading rate impact on fracturing pattern: Lessons from hydrocarbon recovery, Lacq gas field, France. *J. Geophys. Res*., **104**, 17,941-17,954.

Logan, J.M. and J. Rudnicki, 1994. *A review of hydrocarbon – operations induced seismicity and its relevance to the Alkmaar PGI project*. Report to BP, 20 pp. (confidential)

Logan, J.M., N.G. Higgs and J.W. Rudnicki, 1997. Seismicity risk assessment of a possible gas storage project in the Bergermeer field, Bergen concession. Report to BP, 137 pp. (confidential)

Lomnitz, C., 1974. *Global tectonics and earthquake risk*. Elsevier, 320 pp.

Main, I., 1996. Statistical physics, seismogenesis and seismic hazard. *Rev. Geophysics*, **34**, 433-462.

Martinez-Pereira, A. and J.J. Bommer, 1998. What is near field? In: *Seismic Design Practise into the Next Century: Research and Application*. E.Booth (editor). Proceedings 6th SECED Conference on seismic design practice. Balkemade. 245-252.
McGarr, A. 1984. Scaling of ground motion parameters, state of stress, and focal depth. *J. Geophys. Res.*, **89**, 6969-6979.
McGarr, A. and J. Bicknell, 1990. Estimation of the near-fault ground motion of mining-induced tremors. In: *Rockbursts and seismicity in Mines*. Editor: Fairhurst. Balkema, pp 245 - 248.
McGuire, R.K., 1976. FORTRAN computer program for seismic risk analysis. Open-File Report 76-67, US Dep. Int, Geological Survey, 90 pp.
McGuire, R.K., 1978. FRISK computer program for seismic risk analysis. Open-File Report 78-1007, US Dep. Int., 71 pp.
Moser, T.J., T. van Eck and G. Nolet, 1992. Hypocenter determination in strongly heterogeneous earth models using the shortest path method. *J. Geophys. Res*., **97**, 6563-6572.
Mulders, F.M.M., 2003. *Modelling of stress development and fault slip in and around a producing gas reservoir*. Ph.D. Thesis TU Delft., 272 pp.
Nagelhout, A.C.G. and J.P.A. Roest, 1997. Investigating fault slip in a model of an underground gas storage facility. Int. J. Rock Mech. Min. Sci., **34**, 3-4.
Phillips, W.S., J.T. Rutledge, L.S. House and M. Fehler, 2000. Induced microearthquake patterns in hydrocarbon and geothermal reservoirs. *Pure Applied Geophysics*. *Submitted.*
Reiter, L., 1990. *Earthquake hazard analysis. Issues and insights*. Columbia University Press, New York, 254 pp.
Rice, J.A., 1995. *Mathematical statistics and data analysis*. Duxbury Press, 602 pp.
Rijkers, R., W. Apon and H. Pagnier, 1999. Studie aardbevingen Roswinkel. Deel A: Structureel-geologische kartering. TNO-rapport NITG 99-41-C, 31 pp.
RGD, 1995. Geologische Atlas van de Diepe Ondergrond van Nederland. Toelichting bij kaarblad III: Rottumeroog-Groningen. Rijks Geologische Dienst, 113 pp.
Richter, C. F., 1935. An instrumental earthquake magnitude scale. *Bull. Seismol. Soc. Am*., **25**, 1-32.
Rinne and R.B. Seed, 2000. New site coefficients and site classification system used in recent building seismic code provisions. *Earthquake Spectra*, **16**, 41 – 67.
RIVM, 2003. *Nuchter omgaan met risico's*. Milieu- en Natuurplanbureau (MNP) – RIVM. Rapport 251701047, 52 pp.
Roest, J.P.A. and W. Kuilman, 1993. Geomechanische analyse van de lichte aardschokken in het Eleveld reservoir. Report TU Delft 01/09/1993. 57 pp.
Roest, J.P.A. and W. Kuilman, 1994. Geomechanical analysis of small earthquakes at the Eleveld reservoir. *Eurorock '94 Proceedings* Balkema, p 972.
Rutledge, J.T., W.S. Phillips and B.K. Schuessler, 1998. Reservoir characterization using oil-production-induced microseismicity, Clinto Country, Kentucky. *Tectonophysics,* **289**, 129-152.
Sabetta, F. and A. Pugliese, 1987. Attenuation of peak horizontal acceleration and velocity from Italian strong-motion records. *Bull. Seismol. Soc. Am*., **77**, 1491-1513.
SBR, 2002. Trillingen: schade aan gebouwen; meet- en beoordelingsrichtlijnen, NEN, 34 pp.
Schenk, V., F. Mantlik, M.N. Zhishin and A.G. Timarkin, 1990. Relation between macroseismic intensity and instrumental parameters of strong ground motion: A statistical approach. *Natural Hazards*, **3**, 111-124.
Scherbaum, F., K.-G. Hinzen and M. Ohrnberger, 2003. Determination of shallow shear wave velocity profiles in the Cologne, Germany area using ambient vibrations. *Geophys. J. Int*., **152**, 597-612.
Schnabel, P.B., J Lysmer and H.B. Seed, 1972. SHAKE: A computer program for earthquake response analysisof horizontally layered sites. EERC Report 72-12, 88 pp.
Scholtz, C.H., 2002. The mechanics of earthquakes and faulting. 2nd edition. Cambridge Univ. Press, 471 pp.
Schroot, B.M., J.H.A. Bosch, H.S. Buitenkamp, J.H.J. Ebbing, G. de Lange, C. Lehnen, W. vander Linden and W. Roos, 2003. *Oorzaak schade aan gebouwen nabij Grou*, TNO-rapport NITG 03-062-B, 138 pp.
Segall, P., J-P Grasso and A. Mossop, 1994. Poroelastic stressing and induced seismicity near the Lacq gas field, southwestern France. *J. Geophys. Res*.**., 99**, 15,423 – 15.438.
Segall, P. and S.D. Fitzgerald, 1998. A note on induced stress changes in hydrocarbon and geothermal reservoirs. *Tectonophysics*, **289**, 117-128.
Snieder, R. and T. van Eck, 1997. Earthquake prediction: a political problem? *Geol. Rundsch*., 86, 446-463.

Staatsblad van het Koninkrijk der Nederlanden, 2002. 542. Wet van 31 oktober 2002, houdende regels met betrekking tot het onderzoek naar en het winnen van delfstoffen en met betrekking tot de mijnbouw verwante activiteiten (Mijnbouwwet).

Toro, G.R., N.A. Abrahamson and J.F. Schneider, 1997. Model of strong ground motion from earthquakes in central and eastern North America: Best estimates and uncertainties. *Seismol. Res. Lett.*, **68**, 41-57.

Van Eck, T. and T. Stoyanov, 1996. Seismotectonics and seismic hazard modelling for southern Bulgaria. *Tectonophysics*, **262**, 77 - 100

Van Eijs, 1999. Studie aardbevingen Roswinkel. Deel B: Geomechanisch onderzoek. TNO-Report NITG 99-8-C. 31 pp.

Van Eijs, R.M.H.E., B.C. Scheffers, 2000. *Shockgas; Aardbevingen als gevolg van gaswinning*. TNO-Report NITG 99-264-C, 22pp (confidential)

Van Staalduinen, P.C., 1995. Rekenmodel voor de bepaling van trillingssterkte. VROM Publicatiereeks Verstoringen 9/1995.

Van Staalduinen, P.C. and C.P.W.Geurts, 1998. *De relatie tussen schade aan gebouwen en lichte, ondiepe aardbevingen in Nederland: Inventarisatie*. TNO-bouw rapport 97-CON-R1523-1, 98 pp.

Wald, D.J., V. Quitoriano, T.H. Heaton and H. Kanamori, 1999. Relationships between Peak Ground Acceleration, Peak Ground Velocity, and Modified Mercalli Intensity in California. *Earthquake Spectra*, **15**, 557–564.

Wang, Z., E. W. Woolery, B. Shi and J.D. Kiefer, 2003. Communicating with uncertainty: A critical issue with probabilistic seismic hazard analysis. *EOS, Trans.,Am. Geophys. Union*, **84**, 501-508.

Wassing, B., D. Maljers, R. Westerhoff, A. Bosch and H. Weerts, 2003. *Seismisch hazard van geïnduceerde aardbevingen: Rapportage fase 1.* TNO-report NITG 03-185-C**, 77** pp.

Wassing, B., D. Maljers, A. Bosch, H. Weerts, A. Koopman, A. Dullemond and W. Roos, 2003. *Seismisch hazard van geïnduceerde aardbevingen: Rapportage fase 1*. TNO-report NITG 03-186-C**,** 31 pp

Wetmiller, R.J., 1986. Earthquakes near Rocky Mountain House, Alberta, and their relationship to gas production facilities. *Canadian J. Earth Sciences*, **23**, 172 – 181.

Wu, Yih-Min, Ta-Liang Teng, Tzay-Chyn Shin and Nai-Chi Hsiao, 2003. Relationship between Peak Ground Acceleration, Peak Ground Velocity, and Intensity in Taiwan. *Bull. Seismol. Soc. Am.*, **93**, 386-396.

Zoback, M.D. and J.C. Zinke, 2002. Production-induced Normal faulting in the Valhall and Ekofisk Oil fields. *Pure Applied Geophysics*, **159**, 403-420.

Appendices:

Appendix 1. Glossary of terms.
Appendix 2. Dost, B., T. van Eck and H. Haak, 2004. Scaling peak ground acceleration and peak ground velocity recorded in The Netherlands. *Bollettino di Geofisica*. (in print)
Appendix 3. Haak, H.W. and B. Dost, 2003. Detectiegrenzen voor aardbevingen in Nederland.
Appendix 4. Catalogue of induced earthquakes in the north of The Netherlands (1986-2003).

Appendix 1. Glossary of terms.

Aleatory uncertainty – Inherent uncertainty of the data used in the analysis. Generally accounts for the unpredictable nature of the parameters used in a specific model, like source, path and site response (Toro et al, 1997).

Attenuation relation – or ground motion prediction equation (Bommer, 2002). An equation that predicts a ground motion parameter value, for example, Peak Ground Acceleration (PGA) or Peak Ground Velocity (PGV), given the earthquake magnitude and the distance to the earthquake source. An attenuation relation is generally empirical and lacks both a well-defined physical model and dimensional consistency. An attenuation relation is often a best-fit model to the observed data and therefore includes a statistical description of the variability (aleatory uncertainty).

Epistimic uncertainty – Uncertainty due to incomplete knowledge of the models and the variability in the interpretation of the data (Toro et al, 1997).

Hazard – Refers to the frequency and severity of a threat inflicting losses on people, property, systems or functions.

Intensity – A measure of the effect, or the strength, of an earthquake hazard at a specific location, commonly measured on quantitative subjective scales such as the MSK (Medvedev-Sponheuer-Karnik) or the EMS (European Macroseismic Scale). Currently, the EMS is used as a standard in Europe (Grünthal, 1998).

Magnitude – An instrumental or seismological measure of an earthquake's size proportional to the logarithm of the amplitude or energy of ground motion. For earthquakes in The Netherlands we use two magnitude definitions: M_L – Richter magnitude as defined originally by Richter (1935) and M_w – Moment magnitude, where $M_w = ⅔ M_0 - 6$ (Hanks and Kanamori, 1979) and M_0 the seismic moment in Nm. For small (induced) earthquakes the differences are negligible.

Return Period – The reciprocal of the annual probability of occurrence (of an event). In seismic hazard analysis the event is often the exceedance of a certain ground motion level. In statistical descriptions of seismicity the event is an earthquake with magnitude larger then a certain value.

Response spectrum – A plot of undamped natural period or frequency vs. the maximum response of a viscously damped single-degree-of-freedom oscillator subjected to a specified ground motion time history at its base (Gupta, 1990).

Risk – The product of exposure, hazard and vulnerability.

Seismic hazard – The likelihood or probability of experiencing a specific ground shaking due to earthquakes at a specific site or over a region. The seismic hazard can, for example, be described as the probability that a specific Peak Ground Acceleration (PGA) or Peak Ground Velocity (PGV) will be exceeded at a specific site and within a specific time interval.

Seismic risk – The probability of expected damage or loss. This is usually the product of the seismic hazard and the vulnerability (and cost).

Scaling of peak ground acceleration and peak ground velocity recorded in the Netherlands

Bernard Dost, Torild van Eck and Hein Haak
KNMI, seismology section, P.O.Box 201, 3730AE De Bilt, the Netherlands

Abstract

Measured accelerations caused by induced and tectonic events in the Netherlands are available since 1997. Measured mean horizontal peak ground accelerations reach values up to 2.2 m/s^2 for an induced event of magnitude 3.4 at a hypocentral distance of 2.5 km and with a dominant frequency of 10 Hz. Measured mean peak horizontal ground velocities reach values up to 4.5 cm/s for a tectonic event of magnitude 3.9 at a hypocentral distance of 4.4 km. These high values are predicted by existing empirical relations for the scaling of peak ground accelerations and peak ground velocity. The best fit to the observations for magnitudes larger then 3.0, taking into account that underestimates should be avoided, is given by Campbell (1997). For the total magnitude range a new scaling relation for the Netherlands was estimated, based on the attenuation relation determined to calculate local magnitudes for induced events. These relations will be used in updates of seismic hazard studies for the Netherlands.

Introduction

Although the Netherlands is a low seismicity area, moderate earthquakes do occur and seismic hazard is an issue. The 1992 Roermond earthquake, M_L =5.8, caused damage to structures in the epicentral area (Berz, 1994), but, unfortunately, no accelerations were measures within a radius of 50 km from the epicentre (Camelbeeck et al., 1994). Since then accelerometers have been installed in the Netherlands and its surroundings to improve this situation. The presently existing seismic hazard map for the Netherlands of de Crook (1996) is based on expected peak intensities from possible tectonic earthquakes in the southern part of the country. The approximate conversion to peak ground acceleration (PGA), based on relations used in Germany and France, needs to be replaced by an attenuation relation based on measured accelerations.

Monitoring induced seismicity in the northern part of the Netherlands (Dost and Haak, 2003) received a high priority. Although the largest recorded induced event in that region had a magnitude of 3.5, damage is often reported for events of magnitude 3 and higher and for the largest events even intensity VI according to the European Macroseismic Scale (Gruenthal 1998) was reported. This is due to the fact that the depth of these events is usually around 2-3 km. Therefore, starting in 1996, an accelerometer network was built up that consists presently of 17 stations in the northern part of the country (Fig. 1). This network has by June 2003 recorded 60 triaxial accelerograms of seismic events.

In December 2000 a tectonic event occurred in the southern part of the Netherlands near the city of Voerendaal. This region experienced 15 years before a small earthquake swarm with small (M_L<3.1) and shallow (3-6 km) events. In anticipation of a new swarm, initially two and later three accelerometers were installed near Voerendaal.

The swarm that followed counted 139 events until the end of 2001 with a maximum magnitude of 3.9. Activity continues during 2002 and 2003, but with a much lower rate of occurrence. In summer 2002 an event of magnitude 4.9 occurred near Alsdorf in western Germany, only 20 km from Voerendaal. This event was recorded in all three accelerometer stations around Voerendaal. In total 66 triaxial accelerograms have been recorded.

The purpose of the present paper is to investigate the scaling of the measured horizontal peak ground accelerations (PGA) and derived peak ground velocity (PGV) values from small magnitude events. We compare this with existing empirical attenuation functions for small-magnitude earthquakes and extrapolations of existing empirical attenuation functions based on measured accelerations from larger earthquakes and at larger distances. Finally, we will compare attenuation functions derived from borehole seismometer data in the northern part of the Netherlands with the acceleration scaling.

Data

The accelerometers deployed are mainly SIG SMACH AC-23 sensors in combination with 16-bit SMACH SM-2-16 recorders. In 2002 also two Kinemetrics epi-sensors with ETNA data loggers were installed. But up to mid 2003, these did not record any acceleration as yet.

In the northern part of the Netherlands most accelerograms have been obtained from the region around the village of Roswinkel, situated in the northeastern part of the Netherlands and 22 events were recorded on one or more accelerometers in the period 1997-2003. The largest measured PGA is 215 cm/s^2 for the 1997 (February 19) M_L 3.4 event at a dominant frequency of 10 Hz. For these events two accelerometer stations are situated at a nearly constant hypocenter distance of 2.3-2.7 km. The high accelerations measured are not uncommon for a combination of low magnitude events and small distances. Hanks and Johnson (1976) reported PGA values of 100-200 cm/s^2 for a magnitude 3.2 event at a source-site distance of 10 km. Fletcher et al. (1983) show examples for induced seismicity near the Monticello dam in South Carolina, where PGA's in access of 200 cm/ s^2 are measured for events of magnitude 3.0 at a distance around 1 km.

In the southern part of the Netherlands 44 events near Voerendaal are recorded on one to three accelerometers. The largest event (M_L=3.9) in this cluster of events produced a PGA of 124 cm/s^2 at 4 km epicentral distance. The largest tectonic event, the event near Alsdorf, recorded by these accelerometers occurred at an epicentre distance of 18-20 km. This Alsdorf event displayed a longer duration and lower frequencies (around 1-2 Hz) as compared to the Voerendaal events.

The majority of the accelerometers are located in garages, cellars or small sheds connected to a one to two-story building. The instruments are anchored to the concrete floors. At one location, where the structure was larger than average, we observed anomalously low PGA's. To investigate the influence of the building, we carried out an experiment comparing the signal of the accelerometer in the building with one of an accelerometer outside in the free field. Results are shown in figure 3. Besides attenuating the higher frequencies, the building seems to introduce SV energy at the vertical component and at the same time reduce SV energy at the radial component. The PGA at

the radial component is reduced by a factor 2, which is considerable and explains partly the observed differences. A source radiation effect and possible site effects are other components.

In this paper the PGAs are defined as in Campbell (1997, 2003): the geometric mean of the peaks of the two horizontal components. The horizontal components are rotated to compare radial and transverse components for all events. Since some empirical relations use "recorded" PGAs, i.e. the largest recorded value, instead of an average value, such values have also been measured (see Table 1).

Waveform characteristics

Events around Roswinkel have a characteristic waveform shape. After instrument correction and conversion to displacement, a simple displacement pulse remains (Fig. 4). A remarkable feature of this displacement pulse is that the pulse duration seems to be stable at approximately 0.1 seconds over the recorded magnitude range of 0.8-3.4. For the larger events the waveform seems to become more complex. This pulse form is clearly visible in station ROS1 and ROS2, where most accelerations are measured. For the Voerendaal regions, this simple waveform has not been observed.

Scaling relations

We compared our data with four published empirical PGA relations and two empirical PGV relations. In addition an attenuation function, derived for local magnitude determination in the northern part of the Netherlands, is used as a basis to determine new regional scaling relations. The relations are shortly presented below.

Different types of empirical attenuation relations have been constructed over the years; see for a recent overview a special issue of Seismological Research Letters (Abrahamson and Shedlock, 1997). Few studies provide scaling relations for smaller earthquakes (e.g. Campbell, 1989; Ambraseys, 1995). We further selected scaling relations obtained by Campbell (1997, errata 2000, 2001) from near source data from shallow Crustal events, as in our case. Campbell uses a global dataset. Relations derived by Ambraseys (1995) are based on European events for a large range of magnitudes. A study by Sabetta and Pugliese (1987) focussing on Italian strong motion data has also been used for comparison. Both the Campbell (1997) and Sabetta and Pugliese (1987) relations are derived for magnitudes much larger than the events we show in this study. However, we are interested in how well these relations behave if extrapolated to the lower magnitudes.

Campbell (1989) derived an attenuation relationship for events in the (local) magnitude range $2.5 \le M_L \le 5.0$:

$$\ln A_h = -2.501 + 0.623 M_L - 1.0 \ln(R + 7.28) \qquad \textbf{1}$$

where A_h is the mean of the two horizontal components PGA in units of g (1g = 981 cm/s^2) and R the epicentral distance. The standard deviation σ in this relation is estimated at 0.506. The relation is based on 171 near source accelerograms mainly from events in California.

Campbell's (1997) attenuation relations, based on events in the (moment) magnitude range $4.7 \le M_W \le 8.0$, consist of a basic equation and additions for e.g.

different styles of faulting and local site conditions. For firm soil and strike-slip these additions are equal to zero and the relation becomes:

$$\ln A_h = -3.1512 + 0.904M - 1.328\ln\sqrt{r^2 + \{0.149e^{0.647M}\}^2} \quad \textbf{2}$$

where A_h is the mean horizontal PGA in units of g, M the moment magnitude and r the source-to-site distance. Source mechanisms determined in the southern part of the Netherlands are dominated by normal faulting, which is underrepresented in the Campbell 1997 relations. Normal faulting is also the main structural feature in the northern part of the country where induced seismicity dominates, although there are also indications for shallow dipping thrust events. It is originally suggested by Campbell (1997) to use an intermediate between strike-slip and thrust faulting for normal faulting. Later, in the first erratum (Campbell, 2000) the author recommends to use the strike-slip description instead and this is followed in the present paper. In a recent update of these relations by Campbell and Bozorgnia (2003) the new basic relation is slightly modified:

$$\ln A_h = -2.896 + 0.812M - 1.318\ln\sqrt{r^2 + \{0.187e^{0.616M}\}^2} \quad \textbf{3}$$

In their paper the authors also argue that normal faulting in extensional stress regimes have lower median predicted ground motion and can be modelled together with the strike-slip events. The standard deviation in the empirical relations is of considerable importance, especially if these relations are used in hazard estimates. These are explicitly mentioned in the aforementioned papers and are given as a function of horizontal PGA (Campbell, 1997):

$$for\ A_h < 0.068g : \sigma = 0.55$$
$$for\ 0.068g \le A_h \le 0.21g : \sigma = 0.173 - 0.140 * \ln A_h$$
$$for\ \ln A_h > 0.21g : \sigma = 0.39$$

Campbell and Bozorgnia (2003) give a similar relation with slightly adjusted parameter values.

From Ambraseys (1995) we selected a relation that includes the effect of focal depth and is based on data for a magnitude range of $2.0 \le M_S \le 7.3$. The dataset used consists of 1253 triaxial records:

$$\log(A_h) = -1.151 + 0.266M_S - 0.00022r - 1.024\log(r) \quad \textbf{4}$$

where A_h is the "recorded" horizontal PGA in units of g, not the geometric mean as used by Campbell. The distance r is defined as hypocentral distance. The magnitude is M_S, which for low magnitudes, is systematically lower as compared to M_L. The standard deviation $\sigma = 0.27$ on logarithmic unit, which is comparable to the values used by Campbell. When equation 4 is used for a fixed distance, investigating horizontal PGA as a function of magnitude, no "saturation" is build in for the higher magnitudes. This is one of the main differences between equations 3 and 4.

Sabetta and Pugliese (1987) determined an attenuation relation based on Italian strong motion data:

$$\log(A_h) = -1.562 + 0.306M - \log\sqrt{R^2 + 5.8^2} + 0.169S \quad \textbf{5}$$

As in equation 4, A_h is the "recorded" horizontal PGA in units of g. M=M_L for magnitudes less than 5.5, which is our range of interest. Distance R is defined as the closest distance to the surface projection of the fault. The factor S (either 1 or 0) takes the local site geology into account. In our application we are dealing with deep soil, which means that S=0.

Magnitudes of induced events in the Netherlands have been calibrated using a network of boreholes in the region (Dost and Haak, 2002). The sensor at a depth of 200m was used to simulate a Wood-Anderson instrument and an attenuation function was derived and magnitude determined by:

$$M_L = \log A_{wa} - \log A_0 = \log A_{wa} + 1.33\log(r) + 0.00139r + 0.924 \qquad \textbf{6}$$

where A_{wa} is the maximum averaged horizontal (displacement) amplitude of a simulated Wood-Anderson instrument in mm and r is the hypocentral distance. Due to an error in the sensitivity of the borehole sensor, the displacement values in equation 6 should be corrected by addition of a factor -0.50.

First, assuming a dominant frequency of 10 Hz for the S-pulse over the measured magnitude range, which has been observed for the induced events, a simple conversion from displacement to acceleration can be made and equation 6 can be re-written into the form:

$$\log(A_h) = -0.27 + M_L - 0.00139r - 1.33\log(r) \qquad \textbf{7}$$

In equation 7 the factor A_h is given in mm/s^2 and the free surface effect has not yet been taken into account. Adding a factor 2, we can use this equation to compare the acceleration scaling with the local attenuation derived from a different type of network/instrument. A difference in dominant frequency should show as a slope in the residues as a function of magnitude. If this is the case, we could look for a better fit.

In addition we considered two empirical relations for scaling the PGV and compare these relations to our dataset. Campbell (1997) gives one based on the PGA equations:

$$\begin{aligned} \ln V_h = {} & \ln A_h + 0.26 + 0.29M - 1.44\ln[r + 0.0203e^{0.958M}] + \\ & 1.89\ln[r + 0.361e^{0.576M}] + (0.0001 - 0.000565M)r \end{aligned} \qquad \textbf{8}$$

Again, this equation is shown without the terms for type of fault and soil and is based on the PGA as defined in equation 2. The parameter V_h is given in cm/s

Sabetta and Pugliese (1987) also give an equation for the attenuation of PGV:

$$\log(V_h) = -0.710 + 0.455M_L - \log\sqrt{(R^2 + 3.6^2)} + 0.133S \qquad \textbf{9}$$

where V_h in cm/s and the other parameters defined as in equation 5.

Finally, similar to equation 7, the relation for horizontal PGV for the northern part of the Netherlands becomes:

$$\log(V_h) = -2.07 + M_L - 0.00139r - 1.33\log(r) \qquad \textbf{10}$$

with V_h in cm/s.

Results

Since the available horizontal PGA and PGV measurements sample only a few points in distance (Table 1), we concentrate on the magnitude scaling. In order to compare the different empirical relations with the measurements, the differences between observations and model values are normalised by dividing the residual by the standard deviation of the model (see Campbell, 1997).

Since 1995 induced events near Roswinkel (Fig. 2a) are located using a borehole network in the northern part of the Netherlands (Fig. 1). As waveforms for the different events show a high waveform correlation, high precision relative locations could be estimated. These locations were related to absolute locations estimated on the basis of accelerometer data for events occurring since 1997. The depth of the events is assumed to be 2 km. A separate survey with a down hole seismic tool, carried out by contractors for the Nederlandse Aardolie Maatschappij (NAM) revealed a set of micro events at reservoir level that coincided with the locations of the larger events within an epicentral distance of less than 0.1 km and confirmed the depth of 2 km (with an error of 0.2 km). Therefore, the location of the events is assumed to be known with an accuracy that allows a comparison with empirical scaling functions.

In the series of tectonic events near Voerendaal, 44 events are recorded in the accelerometers deployed. Magnitude ranges from 1.1 to 3.9 at an hypocentral distance of approximately 4-6 km. Detailed locations are not yet available, but the locations for the larger events are fairly reliable (Fig. 2b). Therefore we restrict the current dataset to events of magnitude of 3.0 and larger in this study, resulting in a total of 6 triaxial recordings in two stations each.

In figure 5a the measured PGA's are shown as a function of magnitude and compared to the Campbell (1997) relation (equation 2), which gives a good overall fit to the data. For the Roswinkel events, recorded in stations ROS1 and ROS2, an average hypocentral distance of 2.5 km is assumed. ROS1 accelerations at the higher magnitudes ($M_L > 2.8$) fall within the predicted range, for the lower magnitudes equation 2 gives an overestimate. Measured PGAs do not (yet) show saturation. ROS2 shows a systematic lower PGA as compared to ROS1, which may be due to site effects and the influence of the source mechanism. For tectonic events we see, similar to the situation of induced events, an overestimate of the lower magnitudes and a better fit for the larger magnitudes. However, the fit starts to improve at much higher magnitudes ($M_L > 3.4$).

In figure 5b results of the normalised residual PGA is shown for all attenuation relations mentioned. All published relations, equations 1-5, show an overestimate of the PGA for magnitudes less than 2.0. At higher magnitudes, the Sabetta and Pugliese (1987) relation shows a serious underestimate of the PGA's. The Campbell 1989 relation shows an improvement over the 1997 relation for the lower magnitudes, $M_L < 2.5$, but not for the higher magnitudes and the relation of Ambraseys (1995) gives results comparable to Campbell (1997). Since Ambraseys model is based on M_S instead of M_L, the model by Campbell is to be preferred. The updated relation by Campbell and Bozorgnia (2003) provides an even larger overestimate of the PGA compared to the 1997 relation and is therefore not further pursued. It should be noted that in figure 5 both induced and tectonic events are mixed, although events with local magnitudes smaller than 3.0 are all induced.

PGV measurements, obtained after integration of the original accelerometer data, are shown in figure 6a and residuals with respect to equation 8 and 9 in figure 6b. The trend in the PGV values follows the empirical functions closely. Due to an increased standard deviation, peak velocities seem to fit better. However, one would expect an improved scaling for velocity due to the fact that source pulses in displacement are simple one-sided pulses, as also observed and discussed by Rovelli et al. (1991). Again, there is an indication for a systematic difference between the two stations ROS1 and ROS2.

Finally, we will discuss the results for the residual with respect to the attenuation relation based on the magnitude calibration for the northern part of the Netherlands (equation 7), which gives a good fit with a maximum deviation of ±1 σ, for 2.3 <M_L <3.9 (Fig. 7). At lower magnitudes the relation gives an underestimate, for higher magnitudes an overestimate. This is to be expected from the assumption of a dominant frequency of 10 Hz in the conversion from displacement to acceleration. In the comparison between the borehole amplitudes and the peak accelerations at the surface, we assume not only a factor 2 for the free surface effect, but also an additional factor 2 simulating an average site effect. Estimating the best fit by adapting the slope in the magnitude in equation 7 and adding a constant, gives the following equation:

$$\log(A_h) = -1.41 + 0.57M_L - 0.00139r - 1.33\log(r) \qquad \textbf{11}$$

with A_h in m/s^2. The fit to this equation, with an estimated σ =0.33, is shown in figure 7a.

Similar to the PGA's, we could modify the attenuation relation for PGV based on the attenuation curves for the northern part of the Netherlands. This leads to the equation:

$$\log(V_h) = -1.53 + 0.74M_L - 0.00139r - 1.33\log(r) \qquad \textbf{12}$$

with V_h in m/s. The fit to this equation, with also an estimated σ =0.33, is shown in figure 7b. Both equation 11 and 12 show the best overall fit to the total dataset and may be used in hazard studies in the region. However, these relations do not show a "flattening" of the PGA or PGV at the higher magnitudes, as is the case in Campbell's (1997) model. The standard deviation in equations 11 and 12 is rather high, 0.33 compared to a value of 0.27 in equation 4, but for a first estimate with a small dataset it is acceptable. Future accumulation of data is expected to lower the standard deviation.

Conclusion

The installation of an accelerometer network in the Netherlands at the end of 1996, coinciding with an increased activity of induced events and later followed by a swarm of shallow tectonic events gives the unique opportunity to study scaling of peak ground accelerations in the region. Since the distance to the source was less than 5 km for most events, scaling could be studied mainly as a function of magnitude. For small magnitudes (M_L <3.0) existing empirical relations overestimate the measured peak accelerations and peak velocities. For larger magnitudes (3.0 < M_L <5.0) existing relations like Campbell (1997) do predict the measurements well. However, applying the attenuation function derived for the northern part of the Netherlands to calculate local magnitudes and based on 200m deep borehole short period instruments, improves these existing relations. New attenuation relations for small magnitude events (1< M_L <5) could be derived for PGA and PGV in the Netherlands. Although currently the standard

deviations of these relations are high, they will be used in the analysis of seismic hazard in the country and are expected to improve the accuracy of the present hazard estimates.

Acknowledgements

We like to thank all people involved in the operation and maintenance of the accelerometer network. Constructive comments from Dario Slejko and two anonymous reviewers are greatly appreciated.

References

Abrahamson N.A. and Shedlock K.; 1997: *Overview*. Seism. Res. Lett., **68**, 9-23.

Ambraseys N. N.; 1995: *The prediction of earthquake peak ground acceleration in Europe*. Earthquake Engineering and structural Dynamics, **24**, 467-490.

Berz G.; 1994: *Assessment of the losses caused by the 1992 Roermond earthquake, the Netherlands (extended abstract)*. Geol. Mijnbouw, **73**, 281.

Camelbeeck T., van Eck T., Pelzing R., Ahorner L., Loohuis J., Haak H.W., Hoang-trong P. and Hollnack D.; 1994: *The 1992 Roermond earthquake, the Netherlands, and its aftershocks*. Geol. Mijnbouw, **73**, 181-197.

Campbell K.W.; 1989: *The dependence of peak horizontal acceleration on magnitude, distance, and site effects for small-magnitude earthquakes in California and eastern North America*. Bull. Seism. Soc. Am., **79**, 1311-1339.

Campbell K.W.; 1997: *Empirical Near-Source Attenuation Relationships for Horizontal and Vertical Components of Peak Ground Acceleration, Peak Ground Velocity, and Pseudo-Absolute Acceleration Response Spectra*. Seism. Res. Lett., **68**, 154-179.

Campbell, K. W.; 2000: *Erratum Empirical.*…Seism. Res. Lett., **71**, 352-354

Campbell, K. W.; 2001: *Erratum Empirical.*…, Seism. Res. Lett., **72**, 474

Campbell, K.W. and Bozorgnia Y.; 2003: *Updated Near-Source Ground Motion (Attenuation) Relations for the Horizontal and Vertical Components of Peak Ground Acceleration and Acceleration Response Spectra*. Bull. Seism. Soc. Am., **93**, 314-331.

De Crook T.; 1996: *A seismic zoning map conforming to Eurocode 8, and practical earthquake parameter relations for the Netherlands*. Geol. Mijnbouw, **75**, 11-18

Dost, B. and Haak H.W.; 2002: *A comprehensive description of the KNMI seismological instrumentation*. KNMI Technical Report, TR-245, 60 pp.

Dost, B. and Haak H.W.; 2003: *Seismicity*. In: Wong, Th. and J. de Jager (eds), Geology of the Netherlands, submitted.

Fletcher J.B., Boatwright J. and Joyner W.B.; 1983: *Depth dependence of source parameters at Monticello, South Carolina*. Bull. Seism. Soc. Am., **73**, 1735-1751.

Gruenthal, G. (ed); 1998: *European Macroseismic Scale*, Luxembourg, ISBN 2-87977-008-4, 99 pp.

Hanks, T.C. and Johnson D.A.; 1976: *Geophysical Assessment of Peak Accelerations*. Bull. Seism. Soc. Am., **66**, 959-968

Rovelli, A., Cocco M., Console R., Alessandrini B. and Mazza S.; 1991: *Ground motion waveforms and spectral scaling from close-distance accelerograms in a compressional regime area (Friuli, northeastern Italy)*. Bull. Seism. Soc. Am., **81**, 57-80

Sabetta, F., and Pugliese A.; 1987: *Attenuation of peak horizontal acceleration and velocity from Italian strong-motion records*. Bull. Seism. Soc. Am., **77**, 1491-1513

Table 1 Event list and measured PGA and PGV values

event time	station	R [km]	M_L	PGA [m/s^2] radial	PGA [m/s^2] transverse	PGA [m/s^2] average	PGV [cm/s] radial	PGV [cm/s] transverse	PGV [cm/s] average
970519_1543	ROS1	2.6	1.3	0.06	0..06	0.06	0.08	0.06	0.07
990312_1806	ROS1	2.6	1.3	0.07	0.08	0.08	0.09	0.07	0.08
990515_1928	ROS1	2.6	1.4	0.08	0.07	0.07	0.11	0.07	0.09
990317_2314	ROS1	2.7	1.5	0.16	0.16	0.16	0.23	0.15	0.18
970818_0442	ROS1	2.3	1.6	0.18	0.05	0.10	0.17	0.07	0.11
990514_1830	ROS1	2.6	1.7	0.14	0.15	0.14	0.23	0.14	0.18
970620_0045	ROS1	2.8	1.8	0.20	0.11	0.15	0.27	0.14	0.19
980128_2234	ROS1	2.3	2.0	0.28	0.14	0.20	0.39	0.19	0.27
970818_0517	ROS1	2.4	2.1	0.25	0.18	0.21	0.42	0.23	0.31
020214_1701	ROS1	2.3	2.1	0.46	0.41	0.43	0.68	0.37	0.50
970116_0012	ROS1	2.6	2.4	0.39	0.15	0.24	0.50	0.15	0.27
010428_2300	ROS1	2.4	2.4	0.42	0.52	0.47	0.55	0.41	0.47
980128_2133	ROS1	2.4	2.7	0.75	0.54	0.63	1.18	0.66	0.97
991231_1100	ROS1	2.4	2.8	1.23	0.72	0.95	1.83	0.73	1.16
001025_1810	ROS1	2.7	3.2	1.53	0.81	1.11	2.94	0.93	1.75
980714_1212	ROS1	2.7	3.3	2.81	0.87	1.58	4.89	1.18	2.41
970219_2153	ROS1	2.4	3.4	3.04	1.51	2.15	5.52	2.07	3.38
000327_1023	ROS2	2.3	0.8	0.02	0.02	0.02	0.02	0.02	0.02
021014_2345	ROS2	2.4	0.9	0.02	0.02	0.02	0.03	0.02	0.02
000107_1419	ROS2	2.3	1.1	0.04	0.02	0.03	0.05	0.02	0.03
990506_1813	ROS2	2.6	1.4	0.06	0.07	0.07	0.08	0.06	0.07
990515_1928	ROS2	2.5	1.4	0.06	0.05	0.05	0.06	0.05	0.05
021224_0257	ROS2	2.4	1.4	0.02	0.03	0.03	0.05	0.05	0.05
990317_2314	ROS2	2.3	1.5	0.13	0.07	0.10	0.15	0.08	0.11
970818_0442	ROS2	2.4	1.6	0.07	0.08	0.08	0.10	0.06	0.08
990514_1830	ROS2	2.5	1.7	0.10	0.06	0.08	0.13	0.06	0.09
980128_2234	ROS2	2.4	2.0	0.29	0.18	0.23	0.34	0.27	0.30
970818_0517	ROS2	2.5	2.1	0.20	0.15	0.17	0.36	0.19	0.26
020214_1701	ROS2	2.4	2.1	0.42	0.21	0.30	0.55	0.25	0.37
010428_2300	ROS2	2.4	2.4	0.16	0.08	0.12	0.33	0.10	0.18
980128_2133	ROS2	2.4	2.7	0.38	0.24	0.31	0.93	0.34	0.56
991231_1100	ROS2	2.5	2.8	0.56	1.13	0.80	2.21	0.76	1.28
001025_1810	ROS2	2.3	3.2	0.46	0.24	0.33	1.48	0.45	0.82
980714_1212	ROS2	2.4	3.3	0.91	0.58	0.73	1.88	0.59	1.05
010428_2300	ROS4	2.4	2.4	0.32	0.10	0.18	0.32	0.12	0.20
991231_1100	ROS4	2.3	2.8	0.51	0.27	0.37	0.66	0.53	0.59
001025_1810	ROS4	2.4	3.2	0.35	0.12	0.20	0.39	0.17	0.26
020214_1701	ROS5	2.1	2.1	0.07	0.05	0.06	0.10	0.07	0.08
010428_2300	ROS5	2.0	2.4	0.11	0.08	0.09	0.15	0.13	0.14
001025_1810	ROS5	2.0	3.2	0.22	0.50	0.33	0.30	0.65	0.44
021224_0257	ROS6	2.2	1.4	0.03	0.04	0.04	0.04	0.04	0.04
020214_1701	ROS6	2.1	2.1	0.21	0.29	0.25	0.25	0.44	0.33
010428_2300	ROS6	2.6	2.4	0.07	0.09	0.08	0.17	0.11	0.14
010623_0140	VOE1	4.4	3.9	1.18	1.80	1.46	3.24	6.23	4.48
010623_0153	VOE1	4.1	3.5	0.57	0.94	0.73	0.79	1.53	1.11
010623_0202	VOE1	4.0	3.2	0.28	0.42	0.34	0.41	0.95	0.63
010307_0917	VOE1	4.5	3.1	0.16	0.17	0.17	0.33	0.49	0.40
010307_1104	VOE1	4.5	3.1	0.52	0.18	0.31	0.74	0.57	0.65
010307_1029	VOE1	4.5	3.0	0.39	0.17	0.26	1.02	0.47	0.69
020722_0545	VOE1	23.2	4.9	0.52	0.23	0.35	3.44	1.45	2.23
010623_0140	VOE2	4.2	3.9	1.83	0.83	1.23	8.58	1.74	3.86
010623_0153	VOE2	3.9	3.5	0.25	0.33	0.29	1.06	0.98	1.02
010623_0202	VOE2	3.7	3.2	0.35	0.23	0.28	0.82	0.64	0.72
010307_0917	VOE2	4.3	3.1	0.17	0.15	0.16	0.64	0.54	0.58
010307_1104	VOE2	4.3	3.1	0.29	0.15	0.21	0.56	0.54	0.55
010307_1029	VOE2	4.2	3.0	0.19	0.15	0.17	0.54	0.49	0.52
020722_0545	VOE2	23.4	4.9	0.33	0.28	0.31	2.40	1.67	2.00

Figures

Figure 1. Overview of acceleration stations (black triangles) and other seismic stations (grey triangles) presently deployed by the KNMI in the Netherlands. Earthquake source regions (Voerendaal, Roswinkel and Alsdorf), mentioned in the text, are also shown.

Figure 2. Acceleration stations near Roswinkel (a) and Voerendaal (b). In (a) events are indicated with a circle; magnitudes varying from 0.8-3.4. The Roswinkel gasfield is indicated by a shaded contour. In (b) the largest events, magnitudes ≥ 3.0, near Voerendaal are shown. Main roads are indicated.

Figure 3. Accelerations for a Roswinkel event (31.12.1999) recorded inside an elongated building (2) and in the free field outside the building (1). From top to bottom, the vertical (Z), radial (R) and transverse (T) components are shown.

Figure 4. Radial displacement component of Roswinkel events recorded in station ROS1. Acceleration has been converted to displacement. From top to bottom magnitude increases from M_L= 1.1 to 3.4.

Figure 5. a] absolute and b] normalised scaling of PGA as a function of magnitude. Measurements are compared to a] Campbell (1997) and b] empirical relations mentioned in the text. In a] the solid line indicates the predicted mean value and the broken lines the mean + σ and the mean – σ predictions. The line colours refer to different source to site distances (see legend). In b] the y-axis indicates multiples of the standard deviations. ROS1 and ROS2 refer to accelerometer sites near Roswinkel (see text), VOE1 and VOE2 refer to accelerometer sites near Voerendaal (see text).

Figure 6. a] absolute and b] normalised scaling of PGV as a function of magnitude. Otherwise see description of figure 5.

Figure 7. Normalised scaling of a] PGA and b] PGV as a function of magnitude. Reference model is the model based on the attenuation function for the northern part of the Netherlands. The green symbols represent the fit to the model before adjustment of the magnitude dependence (equations 7 and 10), the red symbols after adjustment (equations 11 and 12).

Appendix 2. pre-print Bolletino di Geofisica teorica ed applicata, 2004

Labell

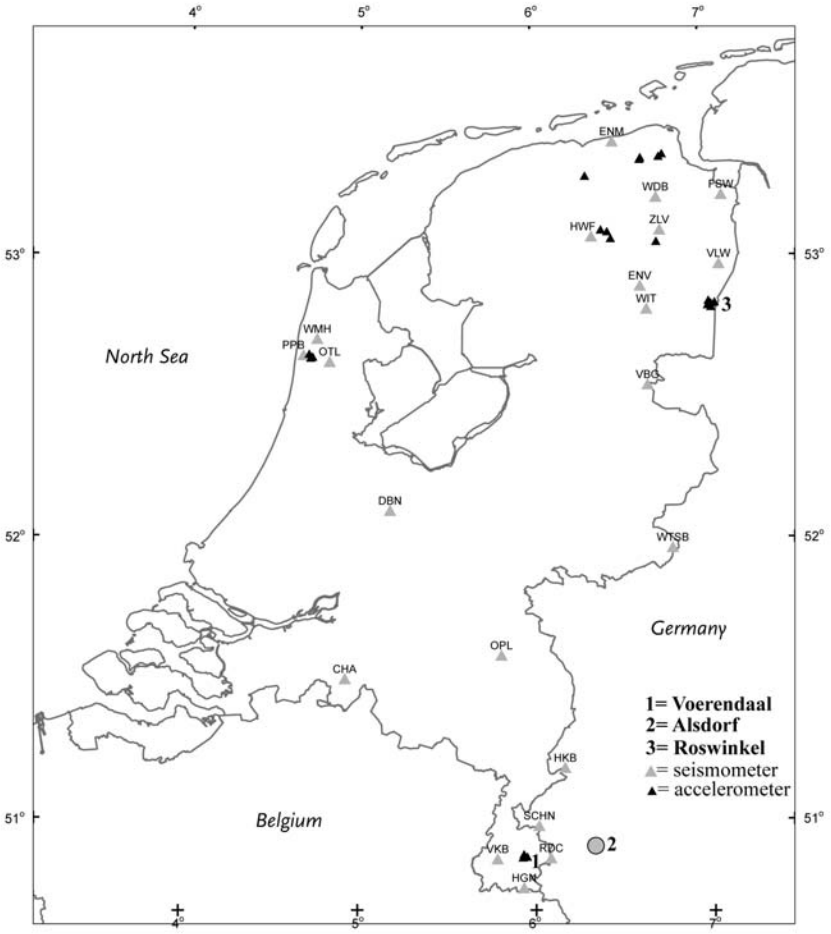

Figure 1

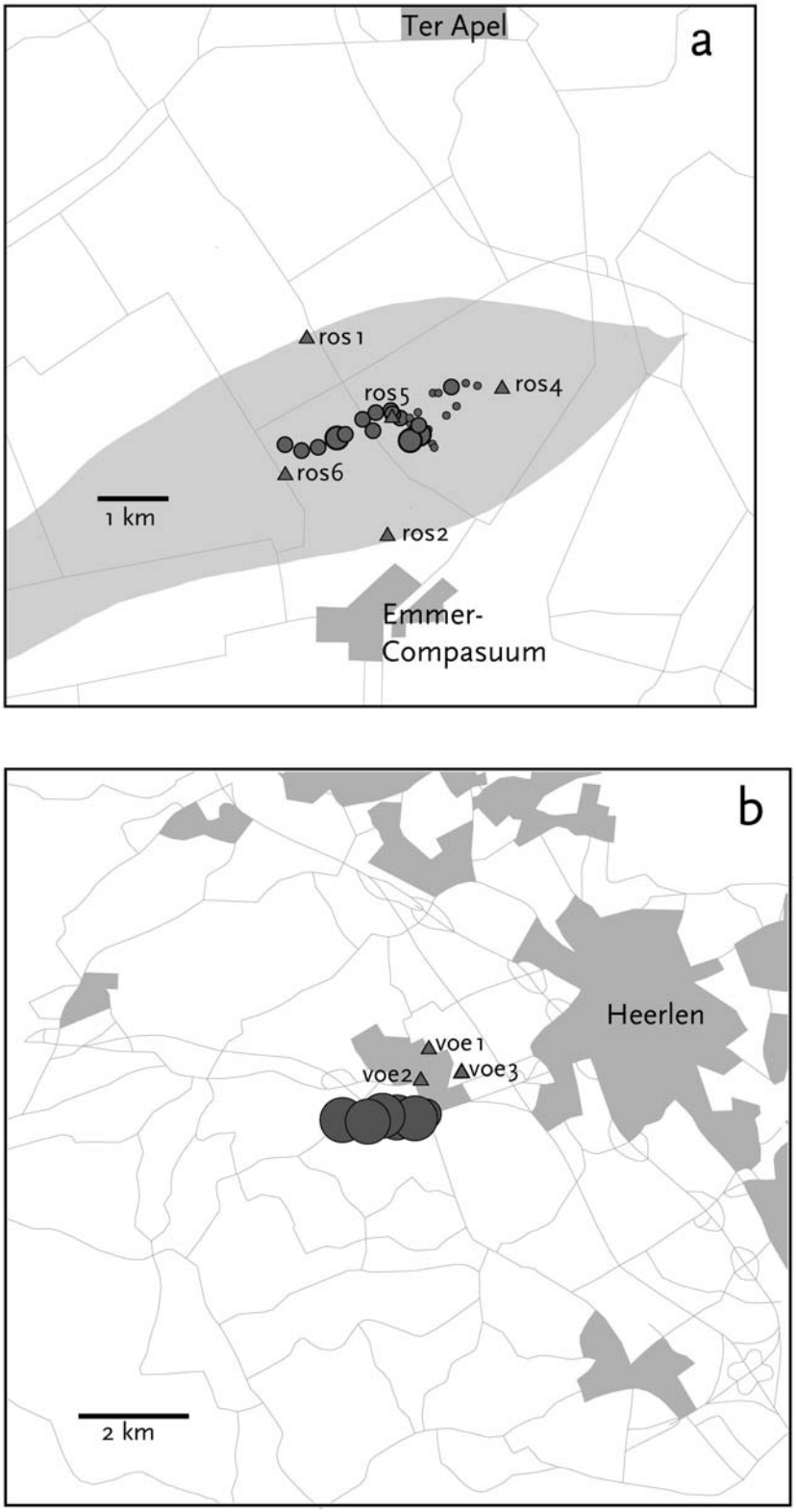
Ter Apel
a
ros1
ros5
ros4
ros6
1 km
ros2
Emmer-
Compasuum
b
Heerlen
voe1
voe2
voe3
2 km

Figure 2

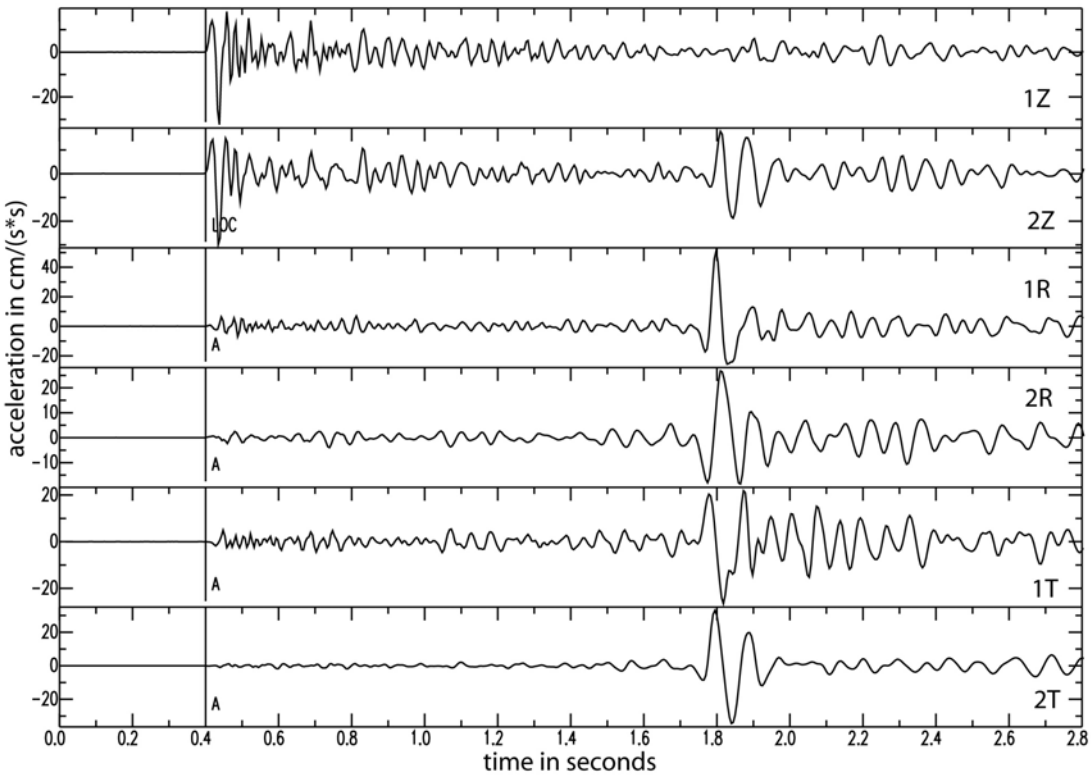

Figure 3

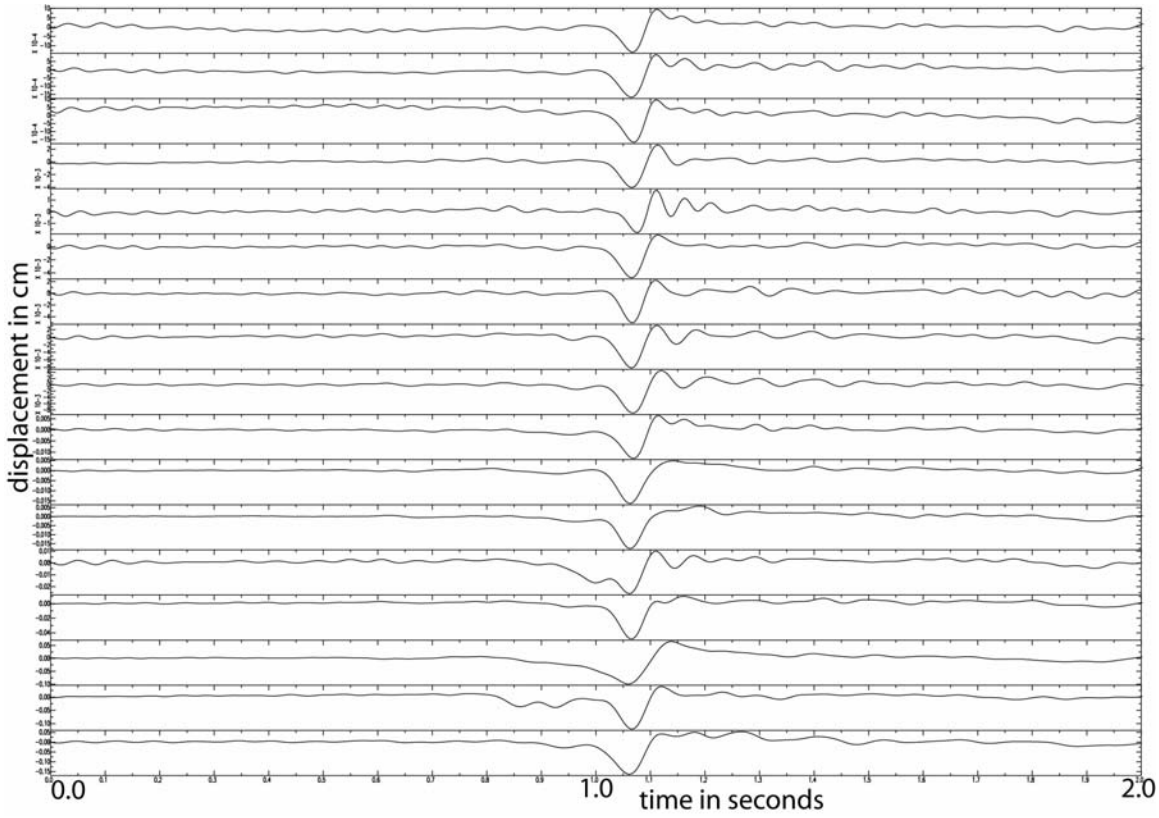

Figure 4

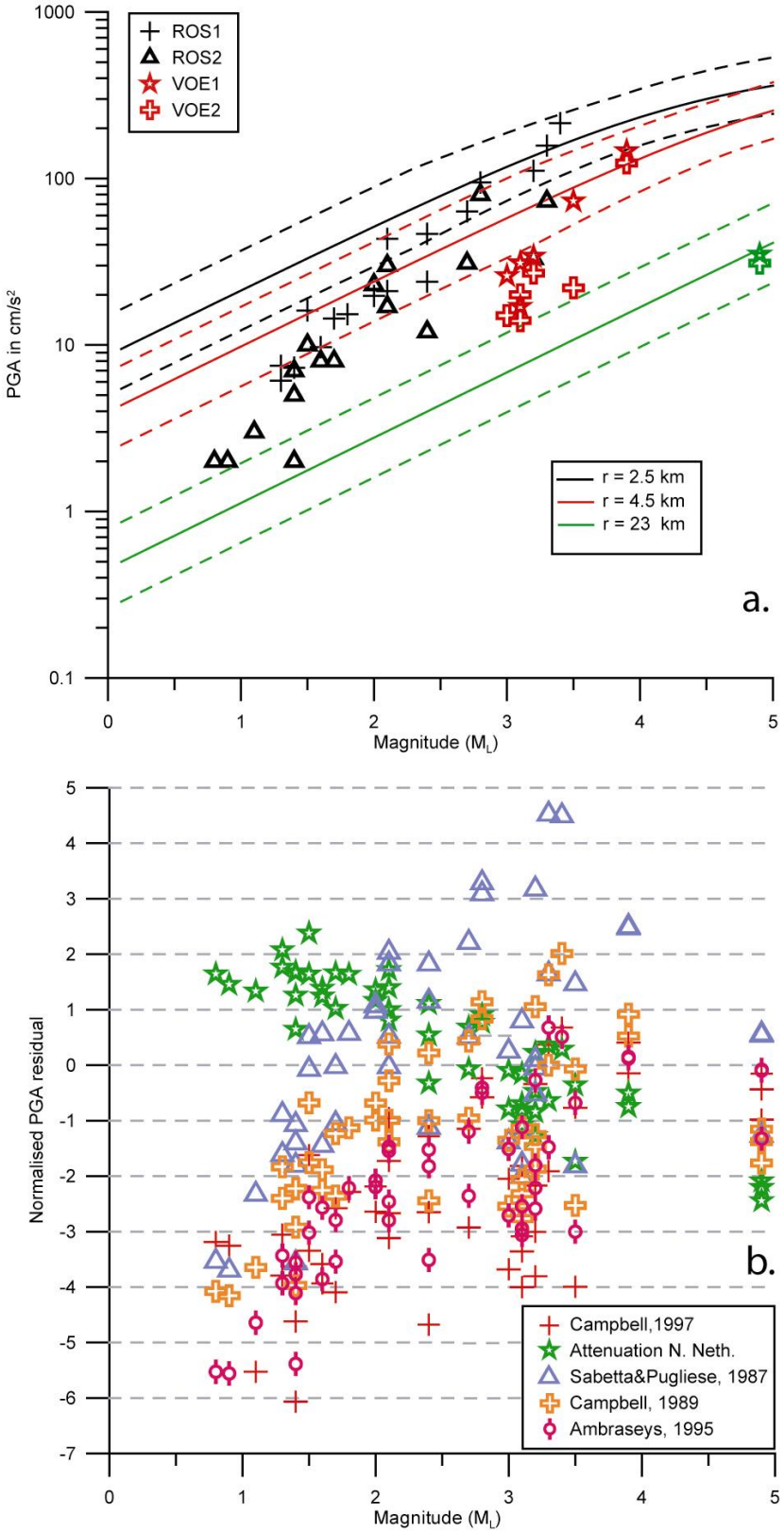
ROS1
ROS2
VOE1
VOE2
PGA in cm/s²
1000
100
10
1
0.1
r = 2.5 km
r = 4.5 km
r = 23 km
a.
0
1
2
3
4
5
Magnitude (M_L)
Normalised PGA residual
5
4
3
2
1
0
-1
-2
-3
-4
-5
-6
-7
b.
Campbell,1997
Attenuation N. Neth.
Sabetta&Pugliese, 1987
Campbell, 1989
Ambraseys, 1995
Magnitude (M_L)

Figure 5

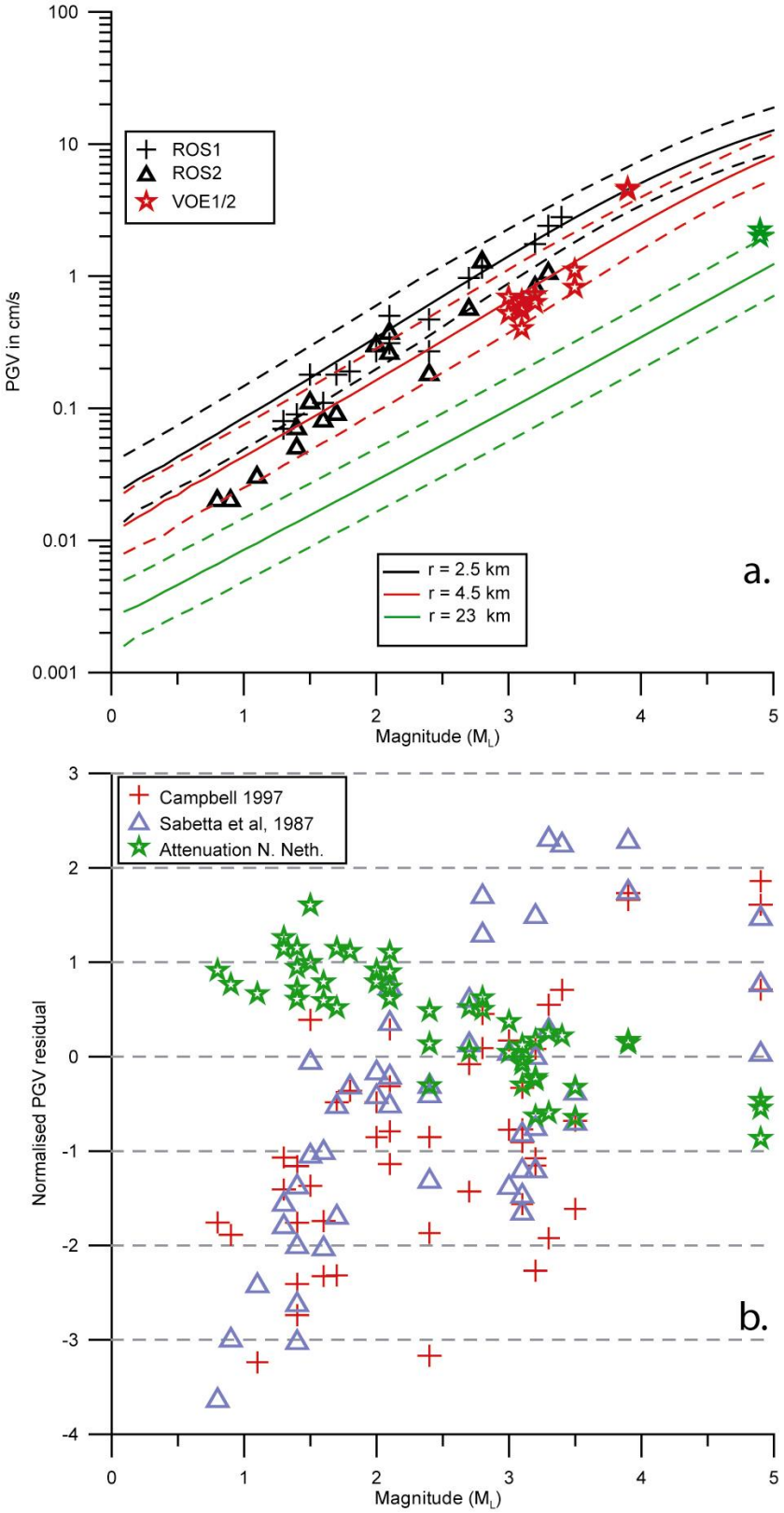
ROS1
ROS2
VOE1/2
r = 2.5 km
r = 4.5 km
r = 23 km
a.
PGV in cm/s
Magnitude (M_L)
Campbell 1997
Sabetta et al, 1987
Attenuation N. Neth.
b.
Normalised PGV residual
Magnitude (M_L)

Figure 6

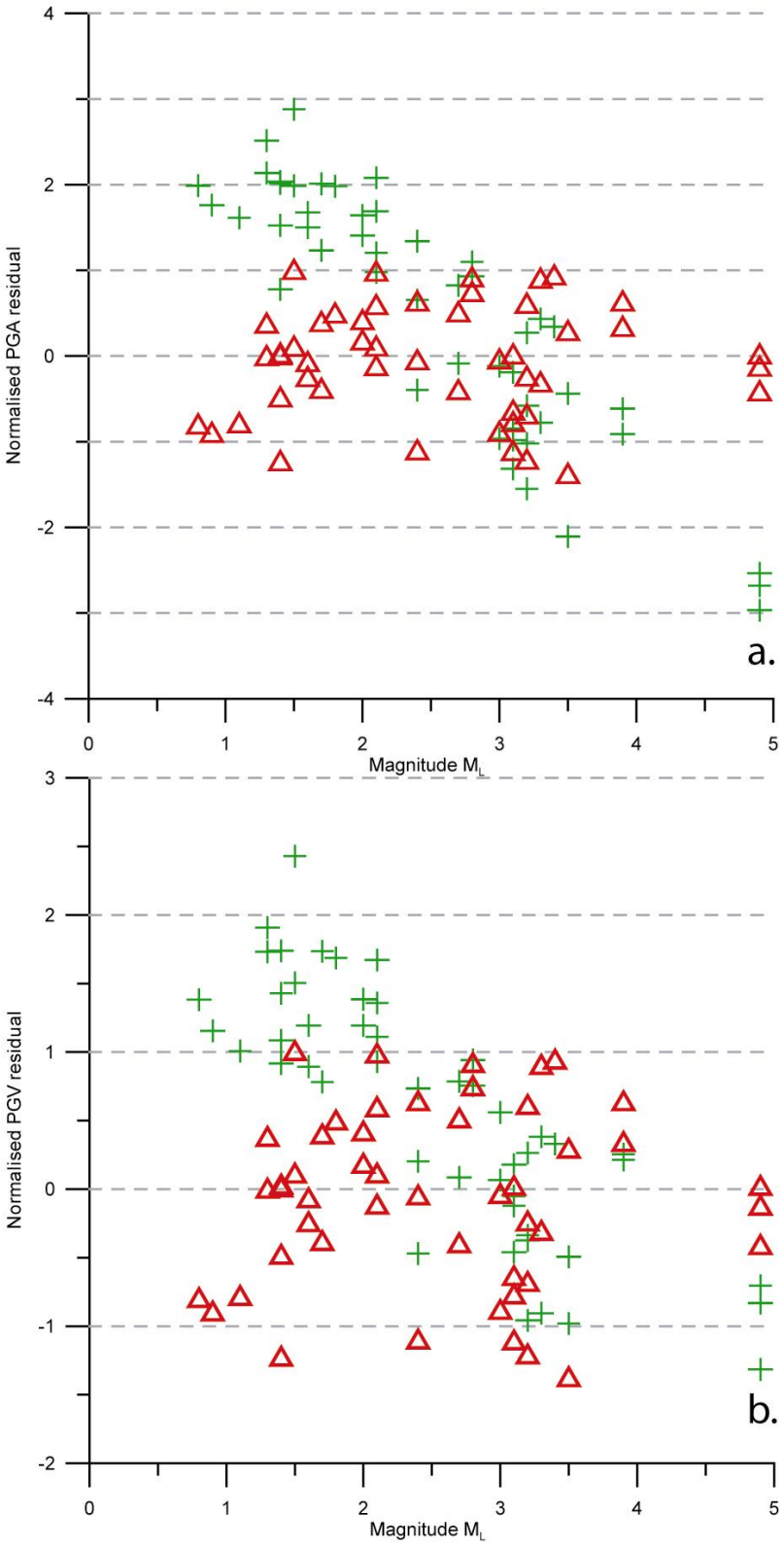
Normalised PGA residual
4
2
0
-2
-4
0
1
2
3
4
5
Magnitude M_L
a.
Normalised PGV residual
3
2
1
0
-1
-2
0
1
2
3
4
5
Magnitude M_L
b.

Figure 7

Detectiegrenzen voor aardbevingen in Nederland

Inleiding

De detecteerbaarheid van kleine aardbevingen in Nederland is van belang om het seismisch meetnet met voldoende capaciteit in te richten. Deze vraag komt met name aan de orde bij de detectie van kleine aardbevingen in Noord-Nederland. Als minimum voorwaarde kan daar gesteld worden dat wanneer een aardbeving door de bevolking wordt waargenomen, deze ook door instrumenten wordt geregistreerd. De grens waarmee aardbevingen in Noord-Nederland worden waargenomen door het algemene publiek is ongeveer 1,8 op de schaal van Richter. Uitzonderingen zijn waarnemingen van magnitude 1,6. In Zuid-Nederland is deze grens hoger omdat daar de bevingen over het algemeen een grotere diepte hebben, wat de waarneming niet bevorderd. In Zuid-Nederland blijkt de grens ongeveer 2,0 te zijn.

Grondslag van de berekening

In dit rapport worden twee kaarten gepresenteerd. Een kaart voor de detectie door één seismisch station, een andere kaart voor de detectie van een beving door drie stations. Wanneer een beving geregistreerd is door drie stations kan over het algemeen een epicentrum bepaald worden; de plaats aan het oppervlak waaronder de aardbeving heeft plaatsgevonden. Voor de bepaling van de diepte zijn over het algemeen meer gegevens nodig.

De berekening van de detectiegrenzen heeft plaatsgevonden onder aan aantal aannames omtrent het gemiddelde ruisniveau. Deze aannames zijn nodig om tot een begrijpelijk resultaat te komen. In principe is ieder seismisch station uniek en is ieder tijdsstip uniek voor wat betreft het ruisniveau van de grondbeweging, dat uiteindelijk de detecteerbaarheid bepaald. In de berekening is uitgegaan van een gemiddeld niveau van de bodemruis in twee groepen van seismische stations: oppervlakte stations en boorgat stations. Het bleek dat de verschillende aannames tot ongeveer dezelfde detecteerbaarheid leidden, omdat extra technische inspanningen zijn geleverd in gebieden die seismisch ongunstig waren. Dit maakt de kaarten eenvoudiger te interpreteren. Een complicatie is echter dat de variabiliteit van dag tot dag erg groot is. Dit betreft zowel dag/nacht verschillen als seizoensgebonden verschillen. Over het algemeen is een zomernacht het meest rustig, een winterdag laat de meeste ruis zien. Met name weer en wind veroorzaken grote verschillen in detecteerbaarheid van aardbevingen. Ook is de verstedelijking van grote invloed. Deze invloeden zijn groter in gebieden waar minder vast materiaal in de ondergrond aanwezig is; Noord-Holland, Groningen en Drenthe. De omstandigheden zijn het meest gunstig in Zuid-Limburg. De variabiliteit kan makkelijk een factor tussen 5 en 10 bedragen, hetgeen in het ongunstigste geval neerkomt op bijna een volle magnitude eenheid.

De eisen die aan de detecteerbaarheid gesteld worden gelden in sterkere mate voor de uiteindelijke analyse van de signalen. Wanneer het doel is een epicentrum te bepalen is het zaak de aankomsttijden van P- en S-golven zo nauwkeurig mogelijk te bepalen. De bodemruis maakt dit soms onmogelijk voor bevingen die net boven de detectiegrens uitkomen. De frequentie-inhoud van ruis en signalen is over het algemeen verschillend. Hiervan kan gebruik worden gemaakt om door filtering de grootste signaal/ruis verhouding te zoeken. Hiermee kan een zo scherp mogelijke inzet geconstrueerd worden. Wanneer ook de diepte van een beving moet worden bepaald geldt dit in versterkte mate. In de kaart voor de detectie door drie stations zijn echter deze overwegingen niet meegenomen omdat de kwantificering van de effecten nog te arbitrair is. De kaart is dus in dat opzicht een optimistische schatting van de mogelijkheid met drie stations een epicentrum te bepalen. Hier staat tegen over dat in veel

gevallen de bepaling van de richting van de seismische golven weer kan bijdragen aan de epicentrum bepaling van kleine bevingen.

In de berekening is uitgegaan van de attenuatie relatie, zoals met behulp van de boorgat stations voor Noord-Nederland bepaald is. Deze relatie is geldig voor de registraties van geophoons op een diepte van tenminste 200 meter. De respons wordt omgerekend naar die van een Wood-Anderson seismometer die vlak is voor bodembeweging voor periodes kleiner dan 1 seconde (frequenties groter dan 1 Hz). De magnitude-afstandsrelatie is:

$M_L(\Delta) = \log(Amp_{wa}) + 1{,}33 \log(\Delta) + 0{,}00139\ \Delta + 0{,}924$

Hierin is Δ de horizontale afstand in kilometers en Amp_{wa} de amplitude van het signaal in millimeters.

Voor de oppervlakte stations is de standaarduitdrukking voor de Richter magnitude aangehouden. Deze uitdrukking is strikt genomen van toepassing in Californië voor aardbevingen met een gemiddelde diepte van 15 kilometer, maar is ook voor het zuiden van Nederland goed bruikbaar. Oorspronkelijk zijn de correctie waarden voor de afstand in tabelvorm weergegeven. Een eenvoudige mathematische uitdrukking is:

$M_L(\Delta) = \log(Amp_{wa}) + 1{,}5 \log(\Delta)$

Deze eenvoudige uitdrukking is goed voor afstanden tot 200 kilometer, voor afstanden kleiner dan 5 kilometer wijkt de formule af. Dit is voor de bepaling van de detectiegrenzen van geen belang omdat magnitude nul als ondergrens gesteld is.
Voor de berekening van de kaarten zijn de ruisniveaus maatgevend voor de amplitudes. Er is uitgegaan van een signaal/ruis verhouding van 2. Een en ander komt neer op 0,02 mm voor Amp_{wa} van de boorgatseismometers in Noord-Nederland en 0,1 mm voor de andere stations.

Conclusie
Op de kaart van figuur 1 voor de detectie met één station is te zien dat de detecteerbaarheid overal in Nederland beter is dan magnitude 2. Voor de gebieden in Groningen en Drenthe waar gas gewonnen wordt, is de detectiegrens ongeveer 1,5 of beter. Dit geldt ook voor het gebied rond Alkmaar.
Op de kaart van figuur 2 is te zien dat wanneer drie stations de beving moeten detecteren er een tweedeling ontstaat. In Noord-Nederland lijken de contouren erg op die voor detectie met één station, ze zijn alleen wat kleiner. Dit is ook het geval voor Limburg. Met name Zuidwest Nederland, bijvoorbeeld Zeeland, is minder goed bedekt. In de figuren 3 en 4 zijn dezelfde kaarten weergegeven voor een signaal/ruis verhouding van 1. Met deze signaal/ruis verhouding kan alleen onder uitzonderlijk goede omstandigheden een conclusie omtrent het signaal getrokken worden. In figuur 5 zijn de locaties van de versnellingsmeters in Nederland weergegeven.
Samengevat kan gesteld worden dat met uitzondering van de provincie Zeeland het netwerk overal tenminste magnitude 2 kan detecteren zodat ook een epicentrum bepaald kan worden, en dat in een aantal geselecteerde gebieden de waarden verbeterd zijn met tenminste een halve magnitude waar boorgatseismometers zijn ingezet.

Hein Haak, Bernard Dost april 2003

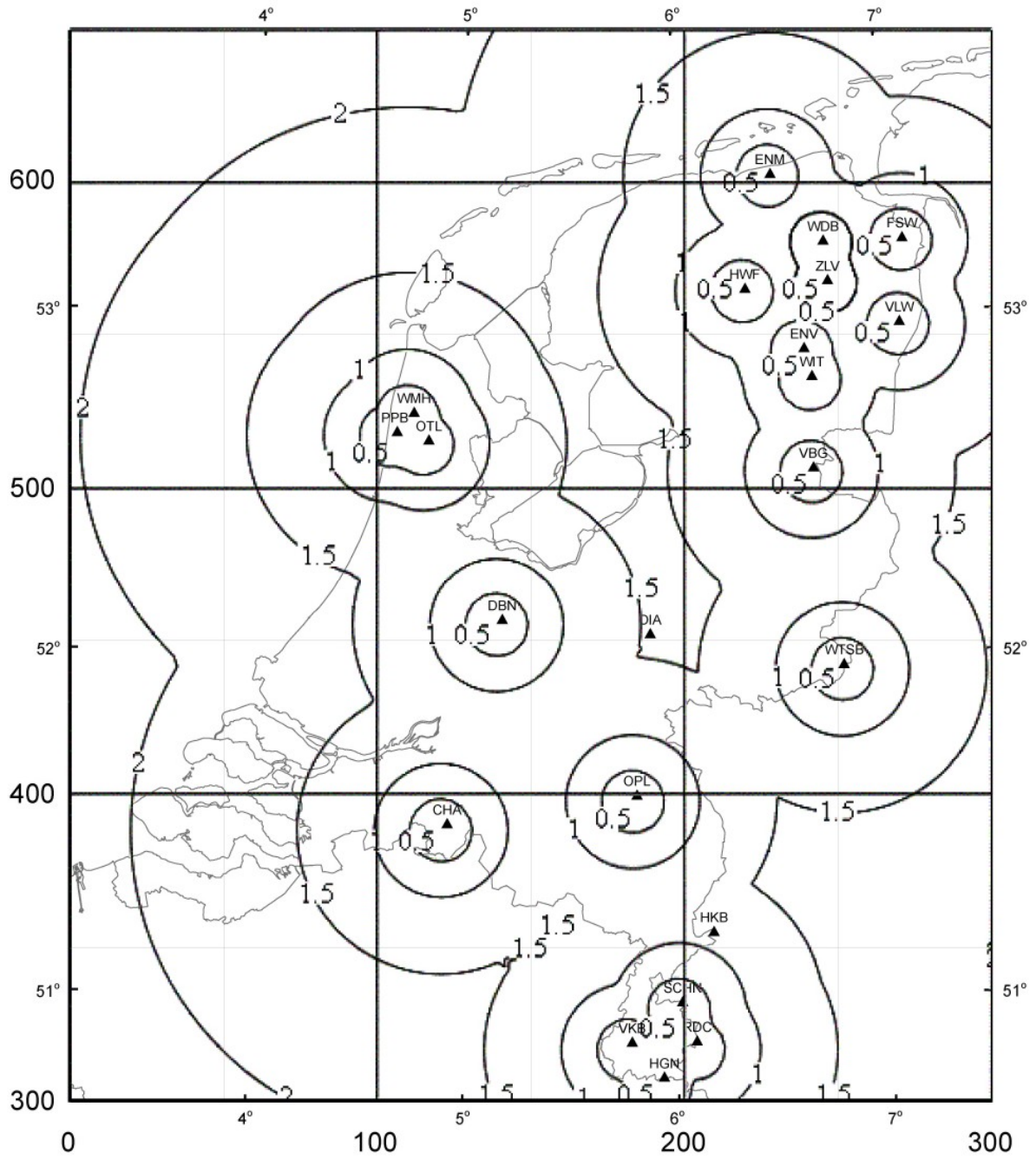

FD

Figuur 1
Detectiecapaciteit van Nederlandse seismische stations. De detectie vindt plaats door **één** station. De waarden bij de contouren zijn magnitudes. De assen zijn gegeven in Amersfoort coördinaten.

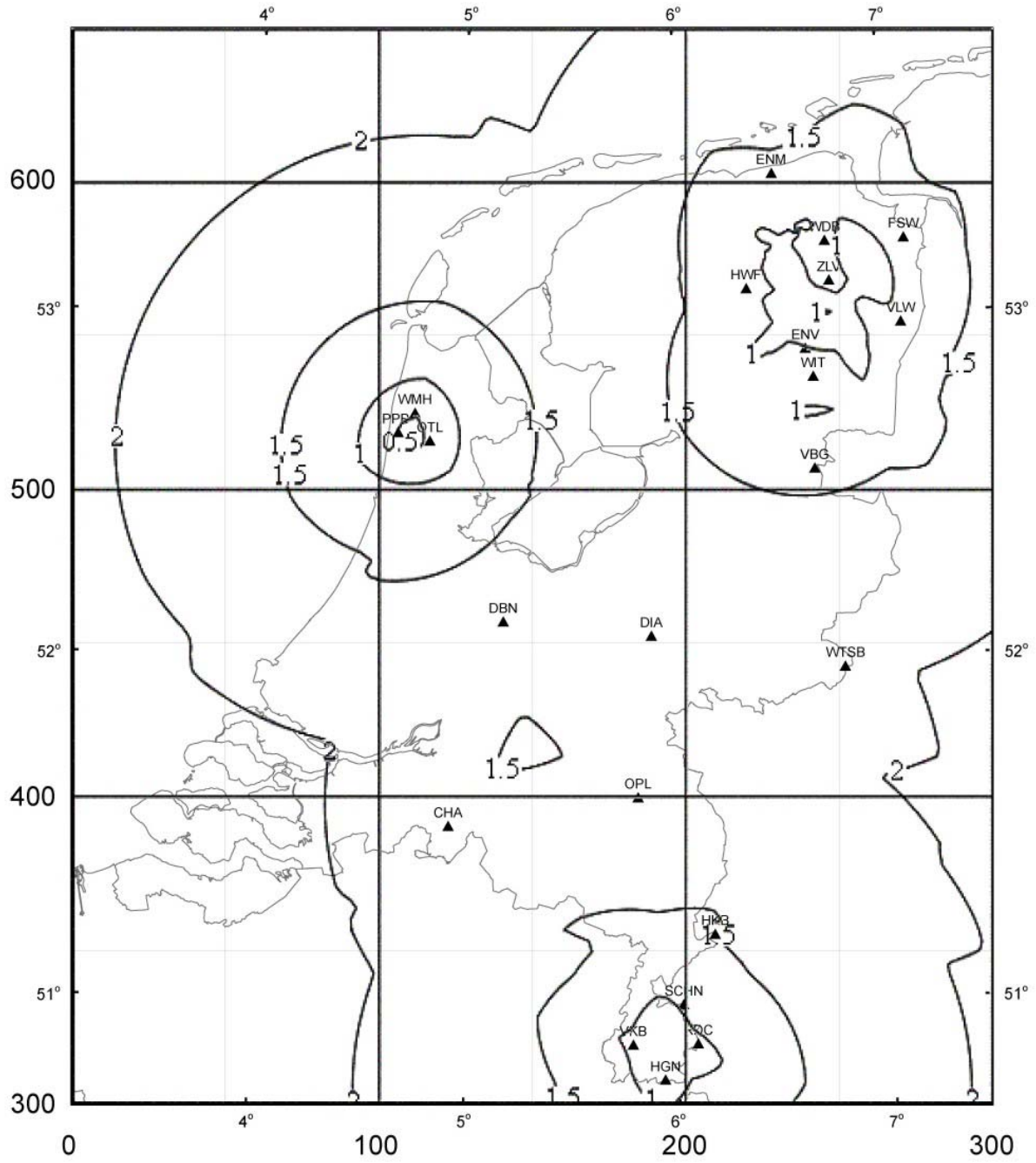

FH

Figuur 2
Detectiecapaciteit van Nederlandse seismische stations. De detectiewaarden zijn berekend voor detectie door **drie** stations. De waarden bij de contouren zijn magnitudes. De assen zijn gegeven in Amersfoort coördinaten.

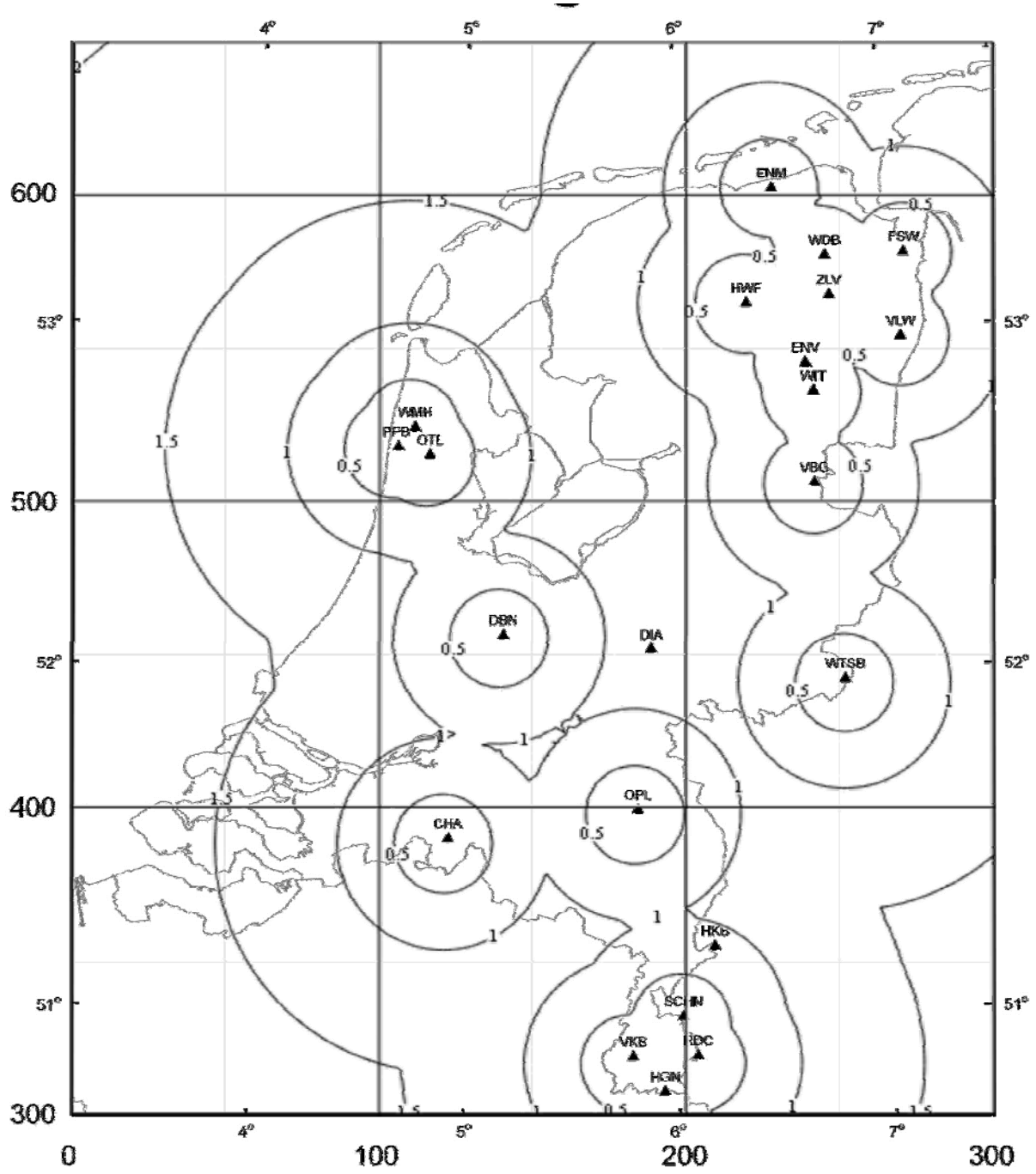

Figuur 3
Detectiecapaciteit van Nederlandse seismische stations voor een signaal/ruis verhouding van **1**. De detectie vindt plaats door **één** station. De waarden bij de contouren zijn magnitudes. De assen zijn gegeven in Amersfoort coördinaten..

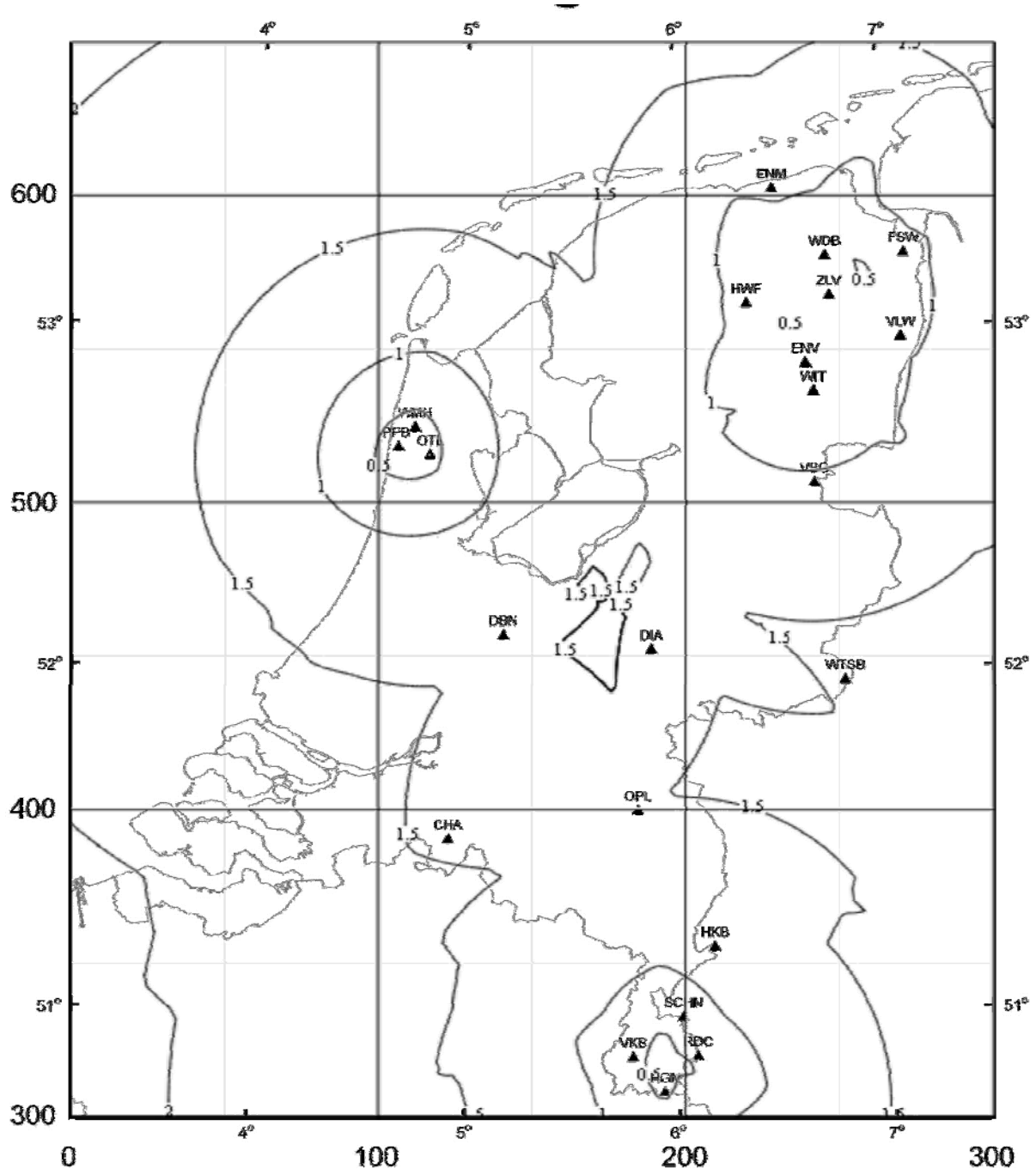

Figuur 4
Detectiecapaciteit van Nederlandse seismische stations voor een signaal/ruis verhouding van **1**. De detectiewaarden zijn berekend voor detectie door **drie** stations. De waarden bij de contouren zijn magnitudes. De assen zijn gegeven in Amersfoort coördinaten.

Appendix 3

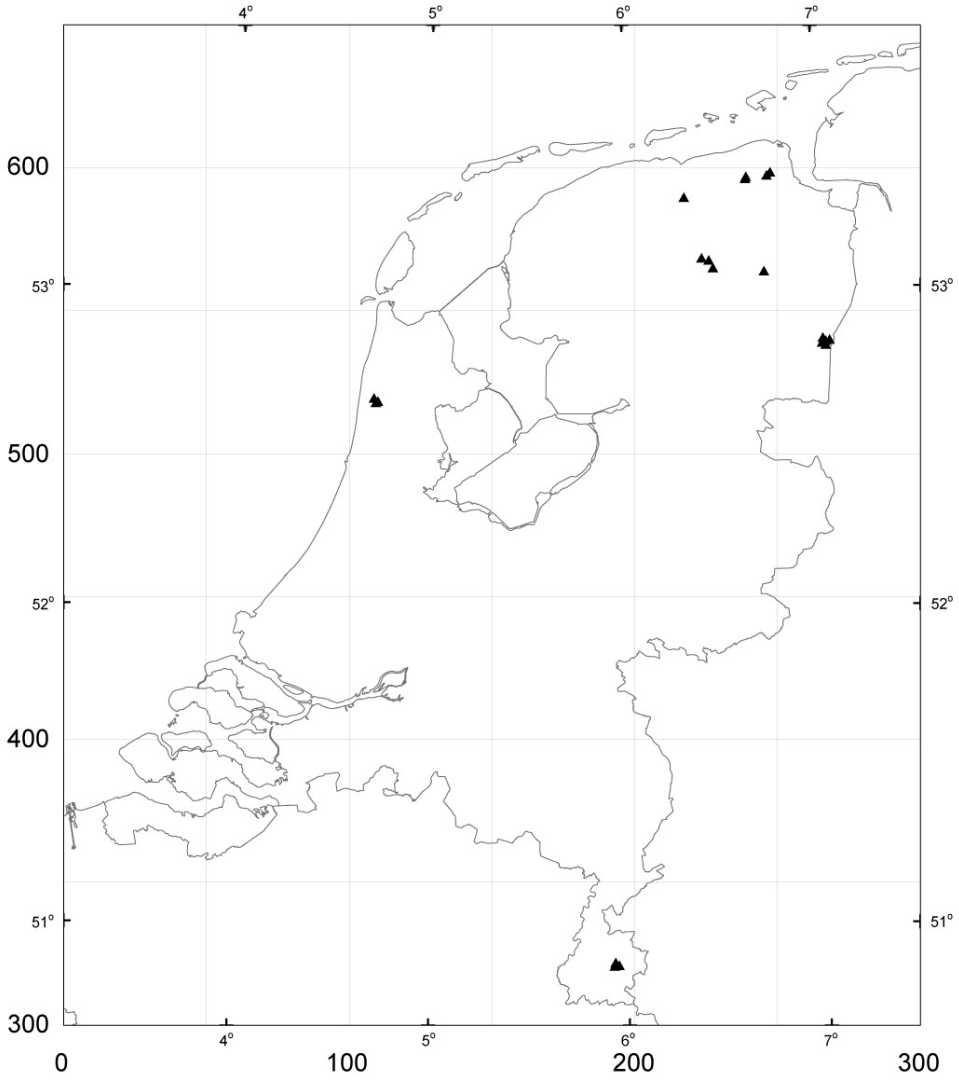

Figuur 5
Locaties van versnellingsmeters in Nederland.

Appendix 4. Geïnduceerde aardbevingen in Nederland

YYMMDD	TIME	LOCATION	LAT	LON	X_RD	Y_RD	INT	MAG.	DEPTH
19861226	074751.00	Assen	52.992	6.548	232,924	556,587	IV-V	2.8	1.0
19871214	204951.05	Hooghalen	52.928	6.552	233,266	549,537	IV	2.5	1.5
19891201	200914.35	Purmerend	52.529	4.971	126,697	504,593	V	2.7	1.2
19910215	021116.54	Emmen	52.771	6.914	257,992	532,491	III-I	2.2	3.0
19910425	102631.58	Geelbroek	52.952	6.575	234,788	552,218	III-I	2.6	3.0
19910808	040114.65	Eleveld	52.965	6.573	234,653	553,624	III-I	2.7	3.0
19911205	002456.74	Middelstum	53.358	6.657	239,503	597,465	III	2.4	3.0
19920523	152911.46	Geelbroek	52.953	6.572	234,563	552,325	III-I	2.6	3.0
19920524	180005.95	Geelbroek	52.957	6.562	233,885	552,685	II	1.6	3.0
19920611	170937.00	Roswinkel	52.831	7.032	265,802	539,341	3.5	2.7	1.5
19920722	232313.20	Eleveld	52.961	6.570	234,437	553,158	III	2.6	3.0
19921206	203432.01	Ten-Boer	53.320	6.740	245,107	593,338	1	1.3	3.0
19921211	130050.05	Slochteren	53.210	6.747	245,782	581,126	1	1.4	3.0
19930212	114600.76	Noordbroek	53.295	6.868	253,715	590,669	1	1.0	3.0
19930305	222725.22	Langelo	53.085	6.465	227,177	566,825	2.5	1.5	3.0
19930312	221241.52	Hoogezand	53.160	6.805	249,789	575,582	1	0.9	3.0
19930326	183421.16	Overschild	53.285	6.795	248,848	589,495	1	1.1	3.0
19930505	200832.79	Haren	53.177	6.685	241,729	577,378	1	1.5	3.0
19930514	193942.00	TenPost	53.305	6.793	248,692	591,773	1	1.1	3.0
19930627	020851.80	Bedum	53.317	6.650	239,118	592,839	1	1.4	3.0
19930627	025710.06	Stedum	53.315	6.660	239,788	592,647	1	1.0	3.0
19930710	002234.51	Appingedam	53.333	6.837	251,518	594,928	1	1.4	3.0
19930727	133918.07	Loppersum	53.336	6.808	249,625	595,169	1	0.8	3.0
19930823	005121.69	Nijenklooster	53.332	6.848	252,297	594,851	1	0.7	3.0
19930904	022450.15	Oldenzijl	53.363	6.765	246,682	598,117	1	1.4	3.0
19930922	173703.82	Middelstum	53.368	6.675	240,682	598,562	2.5	2.0	3.0
19930925	002133.46	Slochteren	53.208	6.812	250,129	580,932	1	0.9	3.0
19931123	123147.68	Slochteren	53.202	6.820	250,699	580,256	2.5	2.2	3.0
19931222	020442.79	TenPost	53.294	6.753	246,050	590,462	1	1.6	3.0
19940204	213238.91	Winneweer	53.306	6.777	247,581	591,790	1	1.3	3.0
19940205	151005.80	Roswinkel	52.833	7.045	266,672	539,583	4.5	2.9	1.5
19940228	210016.59	Garsthuizen	53.370	6.720	243,671	598,895	1	0.6	3.0
19940302	103638.08	Steendam	53.279	6.807	249,639	588,861	1	1.5	3.0
19940306	200231.23	Eenrum	53.323	6.805	249,431	593,774	1	1.0	3.0
19940314	093101.18	't-Zandt	53.345	6.808	249,605	596,207	1	1.3	3.0
19940314	223209.67	Westerbroek	53.170	6.747	245,866	576,693	1	1.1	3.0
19940324	052903.80	Delfzijl	53.316	6.962	259,885	593,193	1	0.8	3.0
19940404	184611.65	Steendam	53.275	6.828	251,094	588,389	1	1.3	3.0
19940507	200853.67	Kolham	53.194	6.798	249,269	579,374	1	1.0	3.0
19940510	013411.97	Hellum	53.226	6.835	251,646	583,021	1	0.8	3.0
19940605	021450.79	Weiwerd	53.295	6.950	259,159	590,784	1	1.0	3.0
19940606	040826.16	Achterdiep	53.156	6.823	251,022	575,217	1	1.0	3.0
19940608	222024.55	Garsthuizen	53.359	6.682	241,142	597,625	1	1.5	3.0
19940626	174438.88	DeKlip	53.335	6.852	252,512	595,171	1	1.0	3.0
19940627	205853.88	Uithuizermeeden	53.424	6.770	246,885	604,892	1	1.7	3.0
19940701	062742.61	Stedum	53.332	6.577	234,203	594,462	1	2.7	3.0
19940719	081729.67	't-Zandt	53.372	6.743	245,220	599,164	1	2.0	3.0
19940730	091820.78	Middelstum	53.351	6.628	237,609	596,616	4.5	2.7	1.0
19940730	095329.68	Middelstum,naschok	53.365	6.577	234,143	598,134	1	1.3	1.0
19940806	180219.20	Alkmaar	52.654	4.711	109,221	518,630	4.5	3.0	2.5
19940816	143739.85	Annen	53.061	6.698	242,855	564,487	4.5	2.3	3.0
19940907	220604.30	Warffum	53.402	6.575	233,964	602,231	1	1.4	3.0

YYMMDD	TIME	LOCATION	LAT	LON	X_RD	Y_RD	INT	MAG.	DEPTH
19940909	155654.38	Emmen	52.714	6.915	258,193	526,189	1	1.7	3.0
19940921	011258.13	Alkmaar	52.658	4.708	109,021	519,047	5	3.2	2.5
19941026	214101.83	Schildwolde	53.246	6.737	245,039	585,119	1	1.2	3.0
19950124	093839.19	Amsweer	53.316	6.897	255,555	593,044	1	1.3	3.0
19950131	194755.62	Annen	53.063	6.720	244,303	564,737	4	2.0	3.0
19950201	003132.00	Veendam	53.079	6.775	247,956	566,531	2	1.2	3.0
19950321	163744.34	Bierum	53.438	6.913	256,377	606,679	1	1.1	3.0
19950406	080343.45	Loppersum	53.360	6.680	241,030	597,677	1	2.0	3.0
19950426	173549.64	Zuidlaren	53.084	6.668	240,799	566,992	1	0.7	3.0
19950515	095239.35	Weiwerd	53.309	6.945	258,791	592,390	1	1.8	3.0
19950603	220638.51	Zevenhuizen	53.182	6.363	220,220	577,521	1	0.9	3.0
19950620	085940.10	Roswinkel	52.832	7.029	265,598	539,414	3	2.7	2.0
19950715	160539.14	Veenhuizen	53.207	6.823	250,911	580,817		1.0	3.0
19950721	232440.48	Meedhuizen	53.276	6.963	260,095	588,689	1	1.1	3.0
19950913	213436.83	Wirdumerdraai	53.335	6.728	244,299	594,974		1.1	3.0
19951018	003427.36	Altena	53.129	6.492	228,887	571,840		1.3	3.0
19951102	010700.71	Loppersum	53.352	6.718	243,598	596,835	2	1.6	3.0
19951104	055043.21	Uithuizerwad	53.470	6.722	243,577	609,986	1	1.8	3.0
19951120	022054.73	Steendam	53.315	6.762	246,561	592,809	1	1.1	3.0
19951224	132634.16	PolderWormer	52.511	4.847	118,279	502,595	1	2.3	3.0
19960212	140224.24	Schaaphok	53.256	6.767	247,021	586,231	1	0.9	3.0
19960224	033107.56	Emmen	52.761	6.908	257,635	531,315		1.8	3.0
19960225	135509.30	Roswinkel	52.838	7.062	267,805	540,166	1	0.9	1.5
19960229	080734.42	Eppenhuizen	53.343	6.640	238,401	595,721	1	2.0	3.0
19960306	092050.20	Roswinkel	52.838	7.062	267,805	540,166	2	1.6	1.5
19960312	005144.67	Eexterveen	53.064	6.790	248,994	564,882	2	1.1	3.0
19960312	121348.70	Roswinkel	52.838	7.059	267,631	540,117	4	2.6	2.0
19960312	183412.68	Schuilingsoord	53.072	6.653	239,817	565,676	1	0.8	3.0
19960314	222358.30	Roswinkel	52.838	7.064	267,947	540,136	1	1.1	2.0
19960316	041632.77	Appingedam	53.298	6.848	252,374	591,031	1	1.4	3.0
19960321	181901.80	Roswinkel	52.833	7.054	267,278	539,619	2	1.8	2.0
19960401	185345.19	Amen	52.940	6.608	237,052	550,845	1	0.6	3.0
19960401	232818.39	NieuwAnnerveen	53.067	6.790	248,986	565,289	1	0.1	3.0
19960409	135834.43	Spijkerboor	53.060	6.798	249,561	564,429	1	1.1	3.0
19960415	034131.20	Ten-Boer	53.289	6.688	241,727	589,862	1	0.9	3.0
19960417	190512.18	Holwierde	53.357	6.883	254,570	597,680	1	0.9	3.0
19960421	213602.32	Warffum	53.376	6.595	235,342	599,378	1	0.5	3.0
19960425	232220.44	Delfzijl	53.356	6.863	253,242	597,486	1	0.9	3.0
19960607	042056.64	Annerveenschekanaal	53.085	6.780	248,278	567,242	1	1.2	3.0
19960607	083407.01	Garrelsweer	53.309	6.778	247,685	592,143	1	1.3	3.0
19960607	145910.82	Annerveenschekanaal	53.082	6.832	251,744	567,013	1	0.7	3.0
19960616	025327.88	Eleveld	52.947	6.568	234,350	551,598	1	1.7	3.0
19960703	214007.16	Spijkerboor	53.053	6.803	249,911	563,693	1	0.8	3.0
19960804	004217.83	Wachtum	52.724	6.738	246,237	527,063	1	1.6	3.0
19960806	133827.76	Weerdinge	52.756	6.917	258,209	530,771	1	1.6	3.0
19960809	023145.71	Annen	53.057	6.688	242,193	564,031	1	0.3	3.0
19960809	063847.14	Oterdumerwarven	53.287	6.958	259,734	589,942	1	1.6	3.0
19960825	222411.14	Geelbroek	52.945	6.570	234,465	551,451	2	1.7	3.0
19960902	052051.92	Nieuw-Roden	53.147	6.422	224,175	573,700	3.5	2.1	3.0
19961016	050900.10	Amen	52.942	6.610	237,160	551,070	1	1.3	3.0
19961116	033349.87	't-Zandt	53.355	6.755	246,033	597,251	1	1.3	3.0
19961117	045952.05	Wachtum	52.724	6.732	245,787	527,055	3.5	2.2	3.0
19961130	202657.95	Leek	53.165	6.410	223,365	575,746	1	1.0	3.0
19961206	164648.00	Roswinkel	52.835	7.053	267,220	539,807	1	1.6	1.5

YYMMDD	TIME	LOCATION	LAT	LON	X_RD	Y_RD	INT	MAG.	DEPTH
19961216	160115.16	Annerveenschekanaal	53.072	6.815	250,651	565,823	1	0.5	3.0
19961216	160650.21	Annerveenschekanaal	53.078	6.822	251,085	566,481	1	-0.1	3.0
19961226	195205.57	Schaaphok	53.261	6.765	246,898	586,824	1	-0.2	3.0
19961228	005408.57	Winde	53.107	6.505	229,818	569,369	1	1.9	3.0
19961228	181652.79	Roswinkel	52.834	7.043	266,548	539,725	4.5	2.7	2.0
19961228	233946.90	Donderen	53.111	6.502	229,589	569,755	2	1.8	3.0
19970108	012054.49	Westeremden	53.338	6.713	243,294	595,288	1	1.5	3.0
19970114	211340.62	Geelbroek	52.943	6.577	234,917	551,199	1	0.7	3.0
19970116	001246.60	Roswinkel	52.835	7.046	266,708	539,807	4	2.4	2.0
19970124	040004.54	Annen	53.079	6.678	241,478	566,484	1	0.6	3.0
19970217	072055.23	Zijldijk	53.387	6.752	245,743	600,826	1	1.6	3.0
19970217	111600.47	Eleveld	52.948	6.568	234,349	551,691	1	1.2	3.0
19970219	215350.81	Roswinkel	52.832	7.038	266,230	539,495	6	3.4	2.0
19970226	193122.43	Coevorden	52.642	6.803	250,808	517,933	1	1.2	3.0
19970302	152532.54	Kommerzijl	53.289	6.265	213,502	589,361	1	1.3	3.0
19970308	142904.28	Zuidlaarderveen	53.107	6.815	250,575	569,680	1	-0.8	3.0
19970308	142916.94	Zuidlaarderveen	53.109	6.812	250,345	569,990	1	0.0	3.0
19970325	001307.74	Woudbloem	53.252	6.748	245,806	585,726	1	-0.2	3.0
19970401	003419.04	Emmen	52.768	6.873	255,255	532,137	1	1.4	3.0
19970409	222143.97	Noordbroek	53.200	6.865	253,708	580,187	1	0.5	3.0
19970417	202756.13	Roswinkel	52.800	7.027	265,510	535,839	1	0.8	2.0
19970429	181646.34	Schildwolde	53.249	6.803	249,482	585,519	1	1.4	3.0
19970504	024239.74	Weiwerd	53.300	6.930	257,813	591,386	1	1.1	3.0
19970504	042909.85	Kropswolde	53.144	6.737	245,252	573,770	1	0.8	3.0
19970519	154356.26	Roswinkel	52.836	7.053	267,227	539,911	1	1.3	2.0
19970606	193918.88	Opwierde	53.293	6.875	254,165	590,455	1	1.2	3.0
19970619	231925.56	't-Zandt	53.364	6.753	245,903	598,231	1	1.8	3.0
19970620	004538.55	Roswinkel	52.834	7.048	266,894	539,718	2	1.8	2.0
19970621	003033.08	Oud-Annerveen	53.094	6.752	246,361	568,207		1.9	3.5
19970709	062312.06	Roswinkel	52.833	7.053	267,234	539,596	1	1.2	2.0
19970717	025629.71	Oud-Annerveen	53.061	6.717	244,085	564,455	1	-0.7	3.0
19970723	064436.04	Lageland	53.247	6.753	246,150	585,195	1	1.2	3.0
19970818	044228.77	Roswinkel	52.834	7.050	267,006	539,739	2	1.6	2.0
19970818	051732.25	Roswinkel	52.834	7.050	267,006	539,721	3	2.1	2.0
19970822	102708.85	Spijkerboor	53.063	6.813	250,558	564,857	1	0.2	3.0
19970823	000156.53	Spijkerboor	53.063	6.813	250,558	564,857	1	0.6	3.0
19970823	193935.04	Lageland	53.239	6.683	241,494	584,256	1	1.6	3.0
19970913	213041.02	Wirdum	53.338	6.747	245,513	595,349	1	1.1	3.0
19970914	193902.65	Annen	53.046	6.740	245,681	562,796	1	0.4	3.0
19971101	225625.87	Zandeweer	53.427	6.705	242,558	605,164	1	1.4	3.0
19971103	181248.77	Donderen	53.108	6.513	230,374	569,489	1	1.4	3.0
19971104	195501.94	Wirdum	53.328	6.793	248,643	594,278	1	1.7	3.0
19971115	162232.14	Oud-Annerveen	53.104	6.822	251,026	569,429	1	0.3	3.0
19971120	173521.04	Slochteren	53.206	6.792	248,796	580,756	1	1.2	3.0
19971126	023537.01	Woudbloem	53.254	6.765	246,913	586,062	1	0.2	3.0
19971203	144719.71	Meedhuizen	53.279	6.897	255,641	588,947	1	1.8	3.0
19971203	150103.65	Siddeburen	53.244	6.858	253,164	585,000	1	1.3	3.0
19971207	070244.49	Zuidlaarderveen	53.075	6.702	243,051	566,012	1	0.3	3.0
19971223	062132.11	Termunterzijl	53.317	7.015	263,437	593,327	1	1.3	3.0
19980108	081145.26	Amen	52.937	6.597	236,272	550,573	1	1.2	3.0
19980122	103155.15	Geelbroek	52.984	6.547	232,828	555,728	1	1.1	3.5
19980128	213303.85	Roswinkel	52.833	7.040	266,336	539,539	5	2.7	2.0
19980128	223404.36	Roswinkel	52.833	7.038	266,201	539,583	3	2.0	2.0
19980131	083939.26	Woudbloem	53.237	6.745	245,615	584,053	1	0.7	3.0

YYMMDD	TIME	LOCATION	LAT	LON	X_RD	Y_RD	INT	MAG.	DEPTH
19980205	211149.34	Meedhuizen	53.291	6.935	258,169	590,317	1	1.1	3.0
19980215	072416.42	't-Zandt	53.356	6.773	247,251	597,367	3	2.6	3.0
19980329	060640.52	Westeremden	53.345	6.730	244,390	596,070	1	1.3	3.0
19980419	080012.08	Zeerijp	53.339	6.723	243,958	595,412	1	1.5	3.0
19980419	153235.72	Uithuizen	53.425	6.682	241,012	604,894	1	1.6	3.0
19980428	020225.27	Veendam	53.107	6.865	253,920	569,840	1	0.4	3.0
19980430	010841.72	Scharmer	53.197	6.707	243,138	579,574	1	0.9	3.0
19980518	220342.46	Oldenzijl	53.404	6.732	244,378	602,655	1	1.3	3.0
19980530	094315.14	Slochteren	53.204	6.777	247,800	580,422	1	0.9	3.0
19980714	121202.23	Roswinkel	52.833	7.053	267,235	539,540	5	3.3	2.0
19980814	192516.89	Froombosch	53.192	6.803	249,607	579,177		1.1	3.0
19980824	042858.00	Overschild	53.298	6.810	249,820	590,961	1	2.4	3.0
19980905	203611.24	Emmen	52.742	6.875	255,427	529,229	2.5	1.9	3.0
19981004	032832.97	Zeerijp	53.353	6.748	245,593	597,001	1	1.0	3.0
19981020	213205.00	Deurze	52.974	6.607	236,875	554,682	1	0.8	3.0
19981101	174829.50	Geelbroek	52.955	6.572	234,560	552,473	1	1.3	3.0
19981212	075139.52	Oldenzijl	53.392	6.698	242,186	601,261	1	2.0	3.0
19981226	234802.19	Slochteren	53.215	6.830	251,338	581,716	1	1.6	3.0
19990111	083609.14	Roswinkel	52.837	7.057	267,471	540,047	1	1.1	2.0
19990113	193637.03	Zeerijp	53.359	6.777	247,466	597,724	1	2.1	3.0
19990131	045300.59	Siddeburen	53.255	6.825	250,915	586,215	1	0.4	3.0
19990305	190040.23	Borgercompagnie	53.101	6.792	249,024	569,074	1	1.0	3.0
19990306	055639.96	Wirdum	53.325	6.778	247,651	593,906	1	1.6	3.0
19990312	180644.42	Roswinkel	52.833	7.052	267,111	539,571	1-2	1.3	2.0
19990317	231425.46	Roswinkel	52.832	7.052	267,124	539,482	1-2	1.5	2.0
19990421	105956.44	Appingedam	53.312	6.840	251,787	592,577	1	1.4	3.0
19990422	225802.90	Rottevalle	53.112	6.152	206,154	569,561	1	1.0	3.0
19990506	181356.37	Roswinkel	52.836	7.055	267,339	539,896	1-2	1.4	2.0
19990508	204018.93	Stedum	53.325	6.700	242,432	593,845	1	1.6	3.0
19990514	183020.73	Roswinkel	52.834	7.052	267,118	539,741	2	1.7	2.0
19990515	192830.37	Roswinkel	52.834	7.052	267,118	539,741	1-2	1.4	2.0
19990521	000938.86	Sappemeer	53.165	6.815	250,447	576,133	1	0.7	3.0
19990607	202031.38	Steenbergen	53.097	6.402	222,914	568,191	1	1.1	3.0
19990707	090311.36	Amen	52.950	6.627	238,264	552,071	1	1.3	3.0
19990810	232418.31	Garsthuizen	53.382	6.727	244,091	600,201	1	1.4	3.0
19990811	011800.96	Westeremden	53.346	6.702	242,500	596,202	1	0.7	3.0
19990907	171623.18	Eexterveen	53.170	6.802	249,544	576,708	1	1.5	3.0
19990907	194751.09	Eexterveen	53.057	6.813	250,572	564,189	1	0.5	3.0
19991018	185609.54	Schipborg	53.078	6.718	244,162	566,330	1	0.4	3.0
19991018	185755.40	Schuilingsoord	53.061	6.678	241,516	564,389	1	0.3	3.0
19991022	131916.77	Amen	52.941	6.592	235,929	550,994	1	1.7	3.0
19991208	053928.47	Achterdiep	53.179	6.802	249,524	577,729	1	0.2	3.0
19991209	093800.05	Schildwolde	53.247	6.803	249,487	585,241	1	1.1	3.0
19991209	095212.96	Achterdiep	53.184	6.797	249,179	578,242	1	1.0	3.0
19991210	061332.01	Achterdiep	53.175	6.792	248,865	577,215	1	1.4	3.0
19991220	122929.69	Westeremden	53.352	6.710	243,042	596,898	1	1.5	3.0
19991221	045237.74	Kolham	53.190	6.765	247,049	578,905	1	1.0	3.0
19991224	235241.12	Delfzijl	53.320	6.947	258,876	593,616	1	1.8	3.0
19991231	110055.32	Roswinkel	52.835	7.048	266,892	539,830	5	2.8	2.0
20000107	141906.76	Roswinkel	52.834	7.043	266,557	539,711	2	1.1	2.0
20000110	041807.46	Schipborg	53.077	6.655	239,920	566,197	1	0.6	3.0
20000212	194810.61	Appingedam	53.321	6.822	250,546	593,554	1	1.7	3.5
20000319	161336.08	Westeremden	53.343	6.698	242,285	595,827		1.6	3.0
20000327	102322.03	Roswinkel	52.835	7.045	266,667	539,825	1	0.8	2.0

YYMMDD	TIME	LOCATION	LAT	LON	X_RD	Y_RD	INT	MAG.	DEPTH
20000401	031351.38	Dalen	52.685	6.750	247,108	522,666		1.3	3.0
20000408	110729.68	Engelbert	53.223	6.663	240,192	582,396		1.1	3.0
20000408	211317.80	Godlinze	53.370	6.845	251,990	599,056		1.1	3.0
20000414	230747.79	Ten-Boer	53.308	6.772	247,243	592,006		1.2	3.0
20000516	011114.73	Garsthuizen	53.381	6.710	242,985	600,032		1.9	3.0
20000609	170347.28	Annerveenschekanaal	53.087	6.813	250,506	567,489	1	1.1	3.0
20000611	041220.13	Loppersum	53.348	6.763	246,602	596,483	2	2.0	3.0
20000612	154823.01	Loppersum	53.340	6.742	245,177	595,546	2	2.5	3.0
20000615	014224.95	Siddeburen	53.278	6.830	251,197	588,800	2	2.4	3.0
20000706	230956.72	Loppersum	53.340	6.752	245,843	595,559	1	1.2	3.0
20000710	150549.12	Vries	53.064	6.575	234,583	564,697		1.0	3.0
20000713	084152.43	Vries	53.079	6.565	233,886	566,299		1.1	3.0
20000716	013412.00	't-Zandt	53.367	6.782	247,783	598,565		1.5	3.0
20000922	170516.77	Annerveenschekanaal	53.076	6.820	250,978	566,256		1.0	3.0
20000922	205206.57	Annerveenschekanaal	53.081	6.772	247,728	566,786	2	2.2	3.5
20000923	034747.43	Annerveenschekanaal	53.081	6.788	248,845	566,771		1.0	2.7
20001025	181034.70	Roswinkel	52.832	7.052	267,125	539,463	5	3.2	2.3
20001112	021636.27	Deurze	52.977	6.608	236,981	555,054		0.3	3.0
20001223	052006.17	Borgercompagnie	53.108	6.812	250,348	569,842		0.4	3.0
20001226	163357.64	Meedhuizen	53.294	6.910	256,493	590,708		1.4	3.0
20010226	113907.31	Annerveenschekanaal	53.072	6.822	251,097	565,887		0.8	3.0
20010318	031420.70	Lageland	53.244	6.692	242,041	584,766		1.6	3.0
20010428	100008.29	Geelbroek	52.948	6.567	234,236	551,764		1.5	3.0
20010428	100055.51	Eleveld	52.959	6.575	234,776	552,978		1.1	3.0
20010428	230015.88	Roswinkel	52.833	7.053	267,233	539,633	4	2.4	2.1
20010517	074815.93	Hoornsedijk	53.173	6.612	236,835	576,828		1.4	3.0
20010610	033533.20	Annen	53.049	6.753	246,567	563,203		0.5	3.0
20010619	064955.57	Annerveenschekanaal	53.079	6.820	250,971	566,608		1.0	3.0
20010621	035049.03	Overschild	53.295	6.800	249,158	590,670		1.7	3.0
20010807	170901.50	Veendam	53.097	6.845	252,605	568,663		0.3	3.0
20010909	065812.64	Alkmaar	52.651	4.713	109,374	518,265	6	3.5	2.0
20010910	043015.35	Alkmaar	52.653	4.712	109,274	518,445	5	3.2	2.0
20011010	064109.36	Bergen-aan-Zee	52.682	4.648	105,011	521,739	3	2.7	2.9
20011010	140643.35	Schaaphok	53.239	6.763	246,834	584,355		1.0	3.0
20011010	140657.24	Schaaphok	53.240	6.763	246,832	584,429		0.8	3.0
20011204	190831.06	Woudbloem	53.204	6.785	248,355	580,507		0.2	3.0
20011204	190837.83	Woudbloem	53.204	6.785	248,355	580,507		0.0	3.0
20011204	223337.96	Woudbloem	53.210	6.743	245,560	581,085		1.0	3.0
20011211	151717.62	Slochteren	53.217	6.788	248,551	581,902		0.7	3.0
20011220	012542.98	Veendam	53.081	6.838	252,195	566,818		0.5	3.0
20011225	232809.44	Noordzee	53.487	6.718	243,320	611,874		1.3	0.0
20011226	123653.07	Eexterveen	53.057	6.805	250,015	564,104		-0.2	3.0
20020205	103039.74	Stedum	53.319	6.717	243,555	593,197		2.2	3.0
20020214	170104.74	Roswinkel	52.832	7.037	266,113	539,496	3	2.1	2.0
20020227	035214.03	Appingedam	53.337	6.825	250,732	595,339		1.1	3.0
20020317	011627.92	Donderen	53.094	6.543	232,409	567,908		0.4	3.0
20020414	011144.09	Annen	53.049	6.770	247,686	563,168		1.9	3.0
20020510	103348.95	Bierum	53.378	6.857	252,747	599,980		1.7	3.0
20020511	100723.22	Geelbroek	52.943	6.580	235,141	551,221		1.5	3.0
20020522	133813.04	Eleveld	52.956	6.585	235,453	552,655		1.0	3.0
20020628	030647.38	Smilde	52.968	6.450	226,363	553,848		1.8	3.0
20020718	053116.83	Froombosch	53.188	6.783	248,279	578,687		1.6	3.0
20020727	150108.63	Geelbroek	52.947	6.565	234,126	551,632		1.6	3.0
20020805	192810.16	Oudemolen	53.055	6.657	240,074	563,771		0.9	3.0

YYMMDD	TIME	LOCATION	LAT	LON	X_RD	Y_RD	INT	MAG.	DEPTH
20020829	211322.74	Luddeweer	53.247	6.747	245,705	585,205		0.0	3.0
20020905	000021.45	Mariënberg	52.508	6.563	234,809	502,735		0.9	3.0
20020906	060705.50	Veendam	53.112	6.842	252,347	570,365		0.6	3.0
20020922	071333.43	Annen	53.056	6.680	241,636	563,910		0.6	3.0
20020922	073013.81	Annen	53.035	6.638	238,885	561,486		0.5	3.0
20021012	023213.63	Veendam	53.107	6.815	250,575	569,680		0.9	3.0
20021014	234522.53	Roswinkel	52.834	7.045	266,670	539,694	1	0.9	2.0
20021019	180339.22	Spijkerboor	53.068	6.768	247,533	565,317		1.3	1.8
20021214	001324.62	Coevorden	52.677	6.832	252,648	521,865		1.4	3.0
20021216	122339.09	Zuidlaren	53.092	6.718	244,133	567,906		1.4	3.0
20021217	002318.74	Tjuchem	53.291	6.860	253,168	590,249		0.9	3.0
20021218	203109.15	Spitsbergen	53.175	6.847	252,540	577,380		0.8	3.0
20021224	025722.60	Roswinkel	52.833	7.042	266,449	539,522		1.4	2.0
20030101	191615.30	Loppersum	53.338	6.743	245,293	595,289		1.0	3.0
20030113	024545.50	Smilde	52.971	6.413	223,896	554,127		1.7	3.0
20030118	181243.32	Overschild	53.287	6.770	247,176	589,723		1.0	3.0
20030123	074616.66	Winneweer	53.307	6.752	245,912	591,906		1.6	3.0
20030130	002730.24	Leermens	53.342	6.795	248,723	595,875		1.5	3.0
20030131	152047.78	Denemarken	53.232	6.782	248,072	583,618		0.3	3.0
20030202	093223.69	Eleveld	52.950	6.588	235,688	552,009		2.0	3.0
20030206	192524.91	De-Paauwen	53.259	6.768	247,124	586,623		0.3	3.0
20030211	192949.56	Zeerijp	53.353	6.773	247,258	596,996		1.3	3.0
20030212	062220.02	De-Paauwen	53.262	6.812	250,009	586,995		0.8	3.0
20030214	065424.14	Rottevalle	53.146	6.122	204,107	573,360		1.8	3.0
20030228	215418.19	Westeremden	53.355	6.730	244,369	597,201		0.7	3.0
20030303	205121.89	Middelstum	53.360	6.662	239,809	597,730		2.2	3.0
20030306	201518.67	Hoogezand	53.141	6.753	246,374	573,419		0.9	3.0
20030309	053126.70	Kantens	53.372	6.640	238,344	598,984		1.1	3.0
20030323	160003.03	Emmapolder(Eemshaven)	53.457	6.783	247,698	608,673		1.5	3.0
20030329	210901.44	Harkstede	53.238	6.682	241,386	584,087		0.4	3.0
20030401	002552.09	Oldenklooster	53.364	6.852	252,448	598,342		0.3	3.0
20030402	201948.74	Loppersum	53.340	6.718	243,623	595,517		1.9	3.0
20030405	164948.33	Engelbert	53.209	6.630	237,991	580,874		0.3	3.0
20030406	000750.70	Overschild	53.272	6.795	248,877	588,012		0.1	3.0
20030406	005727.90	Ruiten	53.205	6.750	246,017	580,499		1.0	3.0
20030406	230204.37	Ruiten	53.206	6.763	246,904	580,683		0.7	3.0
20030416	162042.53	Overschild	53.281	6.775	247,522	589,079		0.7	3.0
20030418	235955.00	Schaaphok	53.238	6.753	246,168	584,250		0.0	3.0
20030420	001939.19	Schaaphok	53.247	6.750	245,928	585,172		0.1	3.0
20030428	215611.33	Ten-Boer	53.284	6.727	244,294	589,260		1.0	3.0
20030429	025504.92	Ten-Boer	53.284	6.730	244,516	589,283		1.3	3.0
20030514	205215.91	Siddeburen	53.254	6.865	253,587	586,121		0.8	3.0
20030514	222346.52	Siddeburen	53.257	6.847	252,357	586,411		0.8	3.0
20030521	045709.24	Annen	53.072	6.765	247,301	565,740		1.1	3.0
20030523	025950.86	Muntendam	53.084	6.823	251,182	567,207		0.6	3.0
20030531	231225.73	Siddeburen	53.247	6.875	254,270	585,374		0.8	3.0
20030603	161538.91	Stedum	53.337	6.683	241,299	595,104		1.5	3.0
20030606	142716.47	Harkstede	53.225	6.682	241,411	582,696		0.7	3.0
20030608	053047.24	Froombosch	53.192	6.788	248,605	579,139		1.0	3.0
20030608	081416.55	Woltersum	53.271	6.737	244,988	587,863		1.5	3.0
20030616	004417.12	Smilde	52.963	6.407	223,460	553,250		2.3	2.6
20030805	184508.49	Assen(Graswijk)	52.975	6.558	233,628	554,703		1.1	3.0
20030807	082421.12	Zeerijp	53.350	6.758	246,266	596,643		1.7	3.0
20030807	105639.85	Zeerijp	53.345	6.748	245,611	596,093		1.3	3.0

YYMMDD	TIME	LOCATION	LAT	LON	X_RD	Y_RD	INT	MAG.	DEPTH
20030820	084614.99	Veendam	53.106	6.815	250,575	569,661		0.5	3.0
20030825	042455.00	Kiel-Windeweer	53.108	6.792	249,010	569,779		0.7	3.0
20030825	100535.89	Kiel-Windeweer	53.108	6.795	249,233	569,784		0.9	3.0
20030922	175011.50	Uithuizen	53.395	6.688	241,514	601,638		2.4	3.0
20030927	135754.15	Westeremden	53.348	6.697	242,164	596,381		2.7	3.0
20031011	114408.34	Roswinkel	52.835	7.055	267,340	539,858		1.6	2.0
20031024	015241.16	Hoeksmeer	53.295	6.792	248,604	590,622	4.5	3.0	3.0
20031026	091700.14	Hoeksmeer	53.304	6.788	248,362	591,619		1.2	3.0
20031029	143009.26	Froombosch	53.192	6.783	248,271	579,114		1.0	3.0
20031110	002238.04	Stedum	53.335	6.702	242,524	594,923	4.5	3.0	3.0
20031110	024055.01	Westeremden	53.349	6.710	243,049	596,546		1.4	3.0
20031116	200411.48	Stedum	53.344	6.702	242,505	595,924		2.7	3.0
20031226	100958.93	Garrelsweer	53.320	6.802	249,216	593,380		1.4	3.0
20031226	170510.76	Spijkerboor	53.084	6.755	246,605	567,099		-0.6	3.0
20031228	042918.29	Spijkerboor	53.080	6.762	247,061	566,607		-0.3	3.0
20031229	130959.31	Delfzijl	53.343	6.938	258,266	596,144		1.5	3.0
20040112	010547.91	Kolham	53.188	6.745	245,718	578,638		1.6	3.0
20040124	135344.54	Woltersum	53.271	6.720	243,876	587,861		1.0	3.0
20040130	114740.99	Appingedam	53.314	6.868	253,671	592,821		1.2	3.0
20040307	071830.45	Veendam	53.103	6.845	252,592	569,312		0.2	3.0
20040308	014116.41	Meedhuizen	53.293	6.895	255,498	590,483		0.4	3.0
20040316	234941.24	Veendam	53.090	6.880	254,964	567,969		1.0	3.0
20040321	170544.58	Wagenborgen	53.255	6.918	257,142	586,344		1.4	3.0
20040326	023245.52	Steendam	53.273	6.862	253,321	588,231		0.5	3.0

YYMMDD - year, month, day
TIME - origin time (UT) Hour, minutes, seconds
LOCATION - location in nearest village or town,
LAT, LON - geopgraphical coordinates, latitude and longitude
X_RD, Y_RD - cartesian coordinates (RD system with Amersfoort as central point)
INT - Maximum observed Intensity
MAG - Richter Magnitude
DEPTH - Estimated depth in kilometers